

DEVELOPMENT OF HIGH-THROUGHPUT 3D NEURAL CELL CULTURE
PLATFORMS FOR MODELLING PARKINSON'S DISEASE

by

Kristin Robin Ko

Submitted in partial fulfilment of the requirements
for the degree of Master of Applied Science

at

Dalhousie University
Halifax, Nova Scotia
December 2017

© Copyright by Kristin Robin Ko, 2017

TABLE OF CONTENTS

LIST OF TABLES	vi
LIST OF FIGURES	vii
ABSTRACT	ix
LIST OF ABBREVIATIONS USED	x
ACKNOWLEDGEMENTS	xii
CHAPTER 1: INTRODUCTION	1
1.1. Traditional Preclinical Modelling Strategies	2
1.1.1. Animal Models.....	2
1.1.2. Two-Dimensional (2D) Cell Culture.....	3
1.2. Three-Dimensional (3D) Cell Culture	6
1.2.1. Explant Culture	7
1.2.2. Self-Assembling Aggregate Culture	8
1.2.3. Scaffold-Based Culture	11
1.2.4. Matrigel	14
1.3. Aqueous Two-Phase Systems (ATPSs).....	18
1.4. Parkinson’s Disease (PD).....	21
1.4.1. Etiology	22
1.4.2. Preclinical Modelling in PD.....	26
1.4.3. The SH-SY5Y Cell Line	28
1.4.4. The Lund Human Mesencephalic (LUHMES) Cell Line	32
1.5. Thesis Aims	33
1.5.1. Aim 1	34

1.5.2. Aim 2.....	34
1.5.3. Aim 3.....	34
CHAPTER 2: 3D CULTURE PLATFORM DEVELOPMENT	35
2.1. Rationale.....	35
2.2. Methodology.....	37
2.2.1. ATPS Polymer-Matrigel Compatibility Assessment	37
2.2.2. Matrigel Platform Characterization.....	38
2.2.3. Thickness Measurements	40
2.2.4. Area Measurements.....	42
2.3. Results	42
2.3.1. Common ATPS Polymers Interfere with Matrigel Gelation.....	42
2.3.2. Characterization of Matrigel-based 3D Platforms	46
2.4. Discussion.....	52
2.4.1. ATPS Polymers and Matrigel	52
2.4.2. The ATPS-Matrigel 3D Culture Method	54
2.4.3. The Matrigel-Only 3D Culture Method	57
CHAPTER 3: ASSESSMENT OF CELL CULTURE PLATFORMS	58
3.1. Rationale.....	58
3.2. Methodology.....	59
3.2.1. SH-SY5Y Cell Culture.....	59
3.2.2. PC-12 Cell Culture.....	60
3.2.3. SH-SY5Y Differentiation Protocols.....	60
3.2.4. Western Blotting	62

3.2.5. Immunocytochemistry.....	64
3.2.6. 2D Culture Method.....	65
3.2.7. ATPS-Matrigel 3D Culture Method.....	65
3.2.8. Kim et al. (2015) 3D Culture Method.....	66
3.2.9. Matrigel-Only 3D Culture Method.....	67
3.2.10. Cell Viability Assessment.....	67
3.3. Results.....	68
3.3.1. Assessment of DAergic Characteristics in SH-SY5Y Cells.....	68
3.3.2. ATPS-Matrigel 3D Culture of SH-SY5Y Cells.....	69
3.3.3. Comparison of Cell Culture Methodologies.....	73
3.3.4. The RA/TPA Differentiation Protocol.....	80
3.4. Discussion.....	82
3.4.1. ATPS-Matrigel 3D Culture vs. Matrigel-Only 3D Culture.....	82
3.4.2. The Kim et al. (2015) Method.....	84
CHAPTER 4: HIGH-THROUGHPUT NEUROTOXICITY ASSAYS	87
4.1. Rationale.....	87
4.2. Methodology.....	88
4.2.1. SH-SY5Y Neurotoxicity Assay.....	88
4.2.2. Cell Viability Assessment.....	92
4.2.3. LUHMES Cell Culture.....	93
4.2.4. LUHMES Neurotoxicity Assay.....	94
4.2.5. Statistical Analysis.....	96
4.3. Results.....	97

4.3.1. SH-SY5Y MPP+ Assay	97
4.3.2. SH-SY5Y Tn Assay	102
4.3.3. SH-SY5Y Epox Assay	104
4.3.4. LUHMES Cell Growth and Differentiation	107
4.3.5. Preliminary Responses of Differentiated LUHMES Cells to Neurotoxins	110
4.4. Discussion.....	114
4.4.1. Impact of Growth Environment on SH-SY5Y Responses to Neurotoxins	114
4.4.2. The Future with LUHMES Cells	118
CHAPTER 5: CONCLUSION.....	120
5.1. Statement of Contributions	122
5.2. Future Directions	123
BIBLIOGRAPHY	126
APPENDIX A: Cambridge University Press Copyright License.....	140

LIST OF TABLES

Table 1	Gel formation methods and corresponding bottom solution and top solution compositions.	39
Table 2	ATPS Polymer-Matrigel Compatibility.	43

LIST OF FIGURES

Figure 1	Cartoon representation of 2D, 3D, and native tissue growth environments.....	5
Figure 2	Hypothetical example of a binodal curve.	19
Figure 3	Cartoon representation of the ATPS-Matrigel 3D cell culture method in a high-throughput, 96-well plate format.	20
Figure 4	Examples of SH-SY5Y neuronal-like (N-type) and substrate adherent (S-type) cell populations.	29
Figure 5	Schematic of thickness measurement protocol.	41
Figure 6	Representative images of ATPS polymer effects on Matrigel stability and gel formation.	44
Figure 7	Characterization of bottom (B) dispensed into top (T) 3D Matrigel methods.	47
Figure 8	Characterization of top (T) dispensed onto bottom (B) 3D Matrigel methods.	51
Figure 9	SH-SY5Y differentiation protocols.	61
Figure 10	Preliminary assessment of DAergic and neuronal markers in SH-SY5Y cells.	69
Figure 11	ATPS-Matrigel 3D SH-SY5Y cell culture.....	71
Figure 12	Representative images (2X) of differentiation-induced contraction in C-AM-stained ATPS-Matrigel 3D cell cultures.	73
Figure 13	Representative images (10X) of undifferentiated SH-SY5Y cells grown under three growth conditions (2D, Kim et al. method, and Matrigel-only 3D method) on treated plates.	75
Figure 14	Representative images (10X) of RA/BDNF differentiated SH-SY5Y cells grown under three growth conditions (2D, Kim et al. method, and Matrigel-only 3D method) on treated plates.	77
Figure 15	Representative images (10X) of undifferentiated SH-SY5Y cells grown under three growth conditions (2D, Kim et al. method, and Matrigel-only 3D method) on untreated plates.	78

Figure 16	Representative images (10X) of RA/BDNF differentiated SH-SY5Y cells grown under three growth conditions (2D, Kim et al. method, and Matrigel-only 3D method) on untreated plates.	80
Figure 17	Representative images (10X) of RA/TPA differentiated SH-SY5Y cells grown under two growth conditions. 2D cultures were grown on treated plates and Matrigel-only 3D cultures were grown on untreated plates.....	81
Figure 18	Growth environment conditions for neurotoxicity assays.	89
Figure 19	SH-SY5Y growth and differentiation protocols for neurotoxicity assays.	90
Figure 20	Schematic of 96-well plate neurotoxin assay layout.....	91
Figure 21	LUHMES differentiation protocol for neurotoxicity assays.....	95
Figure 22	Schematic of 96-well plate neurotoxin assay layout for differentiated LUHMES cells.	96
Figure 23	MPP+ toxicity in undifferentiated and RA/BDNF differentiated SH-SY5Y cells grown under three growth conditions (2D, 2D-M, and 3D) after 48 h treatment.	99
Figure 24	Tn toxicity in undifferentiated and RA/BDNF differentiated SH-SY5Y cells grown under three growth conditions (2D, 2D-M, and 3D) after 48 h treatment.....	104
Figure 25	Epox toxicity in undifferentiated and RA/BDNF differentiated SH-SY5Y cells grown under three growth conditions (2D, 2D-M, and 3D) after 48 h treatment.	107
Figure 26	Gross morphological changes (2X) of C-AM-stained differentiated LUHMES cells in response to various growth conditions (2D, 2D-M, and 3D) and lower (initial seeding density: 1.6×10^4 cells/well) vs. higher (initial seeding density: 5×10^4 cells/well) cell densities.	109
Figure 27	Representative images (10X) of C-AM (green-live)/PI (red-dead)-stained differentiated LUHMES cells grown at an initial seeding density of 1.6×10^4 cells/well in response to LUHMES differentiation medium (CTRL) and MPP+ treatment.....	111
Figure 28	Representative images (10X) of C-AM (green-live)/PI (red-dead)-stained differentiated LUHMES cells grown at an initial seeding density of 1.6×10^4 cells/well in response to LUHMES differentiation medium (CTRL) and Epox (0.5 μ M) and Tn (0.1 μ g/ml) treatment.	113
Figure 29	Cartoon depiction of hypothetical RA/BDNF effects on TrkB expression in 2D- vs. 3D-grown SH-SY5Y cells.	117

ABSTRACT

The three-dimensional (3D) culture of neural cells in Matrigel, a thermoresponsive, self-assembling, extracellular matrix hydrogel, holds promise for modelling neurodegenerative disorders such as Parkinson's disease (PD). 3D cell culture has been proposed as a way to bridge the cell culture vs. tissue gap by providing more realistic mass transport, cell-cell interactions, and environmental cues compared to standard two-dimensional (2D) cell culture. However, air-liquid interfacial tension and evaporation can result in inconsistent 3D cultures at low volumes. Thick-layer hydrogels can counter these factors, but large diffusion distances, high cost, and incompatibility with standard imaging tools, plate readers, and assays limit their use. To address these limitations, two low cost, high-throughput, thin-layer, Matrigel-based, 3D cell culture techniques compatible with well-established equipment and commercially available materials were developed. The first technique involved using aqueous two-phase systems (ATPSs) to confine small volumes of Matrigel containing the model human neural cell line previously used in PD research, SH-SY5Y, into thin layers. Alternatively, the Matrigel-only 3D culture method involved dispensing cell-laden Matrigel directly into culture medium. Matrigel evaporation was eliminated in both the ATPS-Matrigel 3D culture and Matrigel-only 3D culture platforms, and small volumes could form thin gels. The ATPS-Matrigel 3D culture method provided viable cell cultures with excellent control over gel shape and thickness but was discovered to generate non-adherent cell cultures that would be more applicable towards contraction assay studies. Matrigel-only 3D culture produced thin gels also capable of supporting viable cell cultures but offered less control over gel shape and size. Nonetheless, the Matrigel-only 3D culture method provided a simpler protocol and adherent cultures. Thus, this platform was ultimately selected as the foundation for a potential 3D cell culture model to study PD and assess the impacts of 3D growth environment on SH-SY5Y cell growth, differentiation, and morphology. In 3D conditions, SH-SY5Y cells extended neurite-like processes in three-dimensions when differentiated with retinoic acid (RA) and brain-derived neurotrophic factor (BDNF) and contained purer neuronal phenotypes compared to alternative cell culture platforms (e.g., standard 2D cell culture). High-throughput neurotoxin assays using compounds previously used to model PD revealed that 3D-grown RA/BDNF-differentiated SH-SY5Y cells were more robust against neurotoxins compared to 2D-grown cells indicating that growth environment significantly impacted cell differentiation outcomes and behaviour. While these results suggested that RA/BDNF-differentiated SH-SY5Y cells do not provide an appropriate foundation for modelling PD, they also revealed the influence of 3D cell culture environment on cell growth and differentiation. As both 3D culture techniques are compatible with various cell types, alternative cell lines combined with these novel technologies may provide powerful new platforms to model PD in the lab and reveal information previously masked by standard 2D cell culture methods.

LIST OF ABBREVIATIONS USED

2D	Two-dimensional
2D-M	2D with Matrigel coat
3D	Three-dimensional
3D-T	3D-Treated
3D-UT	3D-Untreated
6-OHDA	6-hydroxydopamine
ABX	Antibiotic antimycotic solution
AD	Alzheimer's disease
ANOVA	Analysis of variance
ATPS	Aqueous two-phase system
BDNF	Brain-derived neurotrophic factor
bFGF	Basic fibroblast growth factor
BSA	Bovine serum albumin
C-AM	Calcein-AM
CRABP2	Cellular retinoic acid-binding protein-2
D10	Dextran 10 kDa
D150	Dextran 150 kDa
D500	Dextran 500 kDa
D70	Dextran 70 kDa
DA	Dopamine
DAT	Dopamine transporter
dbcAMP	Dibutyryl-cAMP
DEX	Dextran
dH ₂ O	Distilled Water
DMEM	Dulbecco's modified Eagle's medium
ECM	Extracellular matrix
Epox	Epoxomicin
ER	Endoplasmic reticulum
ESCs	Embryonic stem cells
FBS	Fetal bovine serum
FIB	Fibronectin
GDNF	Glial cell line-derived neurotrophic factor
HA	Hyaluronic acid
HPMC	Hydroxypropyl methylcellulose 4000 cps
HS	Horse serum
iPSCs	Induced pluripotent stem cells
L-DOPA	L-3,4-dihydroxyphenylalanine
LUHMES	Lund Human Mesencephalic
M/Air	Matrigel in air
M/HPMC	Matrigel in 0.5% HPMC
M/Medium	Matrigel in complete medium
M+D10/HPMC	Matrigel combined with 2.5% D10 in 0.5% HPMC
M+D10/Medium	Matrigel combined with 2.5% D10 in complete medium
MAO-B	Monoamine oxidase B

MPP+	1-methyl-4-phenylpyridinium
MPTP	1-methyl-4-phenyl-1,2,3,6-tetrahydropyridine
N-type	Neuronal-like
NF	Neurofilament
P35	Poly(ethylene glycol) 35 kDa
P8	Poly(ethylene glycol) 8 kDa
PBS	Phosphate buffered saline
PBST	PBS with Tween 20
PD	Parkinson's disease
PEG	Poly(ethylene glycol)
PEtOx	Poly(2-ethyl-2-oxazoline) 500 kDa
PF-127	Pluronic F-127
PI	Propidium iodide
PKC	Protein kinase C
PLO	Poly-L-ornithine
PVA	Poly(vinyl alcohol)
RA	Retinoic acid
RAR	Retinoic acid receptor
RGD	Arg-Gly-Asp
RLU	Relative light unit
ROS	Reactive oxygen species
RPMI	Roswell Park Memorial Institute
SB	Sample buffer
S-type	Substrate adherent
TBST	Tris-buffered saline with Tween 20
TH	Tyrosine hydroxylase
Tn	Tunicamycin
TPA	12-O-tetradecanoylphorbol-13-acetate
TrkB	Tyrosine kinase B
UV	Ultraviolet

ACKNOWLEDGEMENTS

I would like to thank my supervisor, Dr. John Frampton, for his excellent mentorship and support throughout my Master's program. You introduced me to the world of tissue engineering and gave me the freedom to pursue my own project. I am grateful for your optimism, encouragement, and constant flow of innovative ideas and energy. Seeing such passion for research is truly inspiring. Working with you has been an incredible journey, and your patient and thoughtful guidance has led me to grow significantly as a researcher and individual.

I would also like to thank my supervisory committee members: Dr. George Robertson, Dr. Brendan Leung, and Dr. Paul Gratzer. Your insightful feedback and advice were crucial towards the development of my thesis, and I have learned much from your expertise. Additionally, thank you, Dr. Robertson, for providing me access to PCR equipment. I would like to give thanks to my lab mates, past and present, who have provided such warm support and encouragement throughout the years: Alyne Teixeira, Angela Tsai, Leo Liu, Nicky Tam, Beatrice Chang, Mackenzie Ruthven, Hady Sarhan, and Connor Lamont. Our impromptu Costco trip, tea sessions, and lab outings will forever be in fond memory.

I am grateful to my dearest friends, Rishima Agarwal and Sarah McLeod, who stood by my side through thick and thin and through sickness and in health, who empathetically listened to my rants and raves when frustration got the better of me, who ran around three buildings looking for a new presentation location when I discovered my proposal was

booked to be held in a clinic simulation room, and who have been nothing but the kindest souls I have ever met. I can always count on you two to be there for me.

I would also like to thank Dr. Kazue Semba, Dr. Samuel Deurveilher, Joan Burns, and my undergraduate lab who provided access to Western blotting equipment used in this thesis. You all have remained steady supports throughout my progression as a scientist since I first came to your lab in 2010 and have continued to offer me advice throughout my Master's program. I would like to thank Shannon Hall for her friendship and for guiding me through the PCR process as well as Elizabeth Belland for her insight into PCR techniques.

I would like to thank my family who have supported me throughout my entire life. To my parents, Ruben Ko and Ruby Ko, I am truly grateful to you for your unconditional love and for everything that you have done for me. You raised me to become the person I am today and continue to care for my well-being. To my aunts, Alice King and Helen King, who remain my steadfast supports.

Finally, I would like to acknowledge the funding agencies and grants that supported this work: the Canadian Institutes of Health Research, the Nova Scotia Health Research Foundation, the Nova Scotia Provincial Government, the Canada Research Chairs Program, Canada Foundation for Innovation (Project #33533), the Natural Science and Engineering Research Council of Canada (RGPIN-2016-04298), and the Brain Repair Centre's Knowledge Translation Grant.

CHAPTER 1: INTRODUCTION

Neurological disorders account for approximately 12% of all deaths and impact nearly 1 billion people globally (1). With advancements in healthcare and technology increasingly promoting longer life expectancies and age-associated susceptibility to neurodegenerative diseases such as Alzheimer's (AD) and Parkinson's (PD), these numbers are projected to rise with time (1–3). As a result, considerable efforts and resources have been directed towards the study of the human nervous system. Neural imaging technologies and post-mortem organ donations have allowed us to investigate neural function and disease pathophysiology in actual human patients (4, 5). However, these techniques offer limited information about the molecular and cellular processes underlying disease pathogenesis. Alternatively, animal models and standard two-dimensional (2D) cell culture techniques provide manipulable living systems where certain features of disease can be modelled and isolated. These systems have been particularly useful for preclinical drug and neurotoxicological assessment in the laboratory. Once preclinical assessment generates promising therapeutic results, human clinical trials can proceed. Using the information gathered from these models, many novel therapeutics have emerged to prevent, halt, or potentially reverse neural damage. Between 2006-2015, 1304 promising treatments for neurological diseases were submitted for clinical assessment, the second highest number of drug submissions for a single disease category (6). Unfortunately, preclinical successes do not often translate to clinical success. The field of neurology has been reported to have one of the highest drug attrition rates (6). This disparity between preclinical laboratory

results and those observed in human patients reveal the limitations of our current preclinical modelling strategies.

1.1. Traditional Preclinical Modelling Strategies

1.1.1. Animal Models

The nervous system is an incredibly complex and challenging environment to model. In humans, the brain contains approximately 85 billion neurons and an equivalent number of non-neuronal cells (7). Interconnecting neural networks generate complex thought and control our bodies. In turn, changes in overall physiology (e.g., increasing aortic stiffness with age or modifications to gut microbiota) can influence nervous system function and health (8, 9). Despite significant scientific advancements over the past decade, we are not capable of fully recreating such intricate systems. Therefore, we have relied on animal models to offer insight into the complexities of intact living organisms. Using animal models, disease pathogenesis, behaviour, and drug efficacy can be assessed without requiring a human subject (10–13). Animal models also offer simpler, more controlled, and replicable systems for experimentation. For example, C57BL/6 is a common strain of laboratory mouse. This strain has been inbred to produce close genetic profiles useful for the development of transgenic mouse models. This avoids complications of genetic diversity and allows for closer inspection of specific details within a disorder.

However, due to species differences, many human neurological disorders are not easily replicable in standard laboratory animals. Mimicking disease neuropathology is particularly difficult when the full etiology of the disease is unknown. This is generally the

case for neurodegenerative disorders. In animal models, such pathologies must be artificially induced. Genetic manipulation or targeted cell death using toxins or physical damage are common techniques used to simulate certain neurological deficits (11–16). These models are informative and offer insight into the significance of genetic predispositions, protein function, cellular interactions, disease progression, and drug efficacy (11–15). However, physiological and pathological differences between animal models and humans can result in potentially unreliable information that may not translate well to the clinic (16–18). Therefore, alternative methods are essential to clarify and contextualize information obtained from animal models as well as minimize animal sacrifice. The most common preclinical supplement to *in vivo* animal work is traditional 2D cell culture.

1.1.2. Two-Dimensional (2D) Cell Culture

2D cell culture traditionally involves growing cells on treated plastic or glass surfaces. Sufficient nutrients, humidity, and CO₂ are provided to maintain cell viability. This technique offers a simplified model of living systems. Environmental cues and complex cellular interactions are stripped away to a minimum requirement for cell life. While removing information initially sounds counterintuitive, reducing complexity allows for greater control over the design and manipulation of the experimental system. Specific interactions and cellular behaviours can be further isolated and observed under highly regulated conditions.

Cells used in standard 2D culture can be obtained from several sources. Model cell lines are the most common and are typically derived from tumours. Cell lines can proliferate indefinitely and generate numerous identical samples for high-throughput analysis of genetically similar samples. Alternatively, primary cells offer disease-relevant models and are harvested directly from a source tissue. A substantial library of cell types and cell lines derived from humans and other species are commercially available and relatively easy to access. Compared to animal models, 2D cell culture offers the opportunity to examine human-derived cells and investigate disease pathologies from within the same species. In addition, with the rapid evolution of stem cell technologies, patient-derived *in vitro* modelling has emerged (19–21).

Due to the simplicity of this technique, 2D cell culture remains the gold standard for *in vitro* analysis of cellular interactions and behaviour in response to drug therapies. The minimalistic growth conditions offer relatively straightforward, low-cost, high-throughput, screening capabilities. However, 2D cell culture can suffer from its overly minimalistic methodology. Cells are not naturally accustomed to growing on plastic or glass. In typical 2D cell culture conditions, cells are directly exposed to a liquid medium that is changed every few days to remove waste and replenish nutrients (Figure 1). The shift between static and turbulent fluid motion against the cell body, while the other half of the cell remains adhered to a hard surface instead of a compliant extracellular matrix (ECM), generates highly unusual mass transport and environmental cues. Additionally, under 2D conditions, neighbouring cells are limited in their ability to form three-dimensional (3D) cell-cell interactions. All of these factors can have significant impacts on cellular morphology,

differentiation, function, behaviours, and responses to experimental treatments (22–25). For example, primary neural and astrocytic cell cultures have been shown to respond to substrate stiffness (22, 25, 26). Neurons have been noted to preferentially grow on softer substrates compared to astrocytes, which multiply and expand in stiffer environments (22). Puschmann et al. also observed that 2D growth conditions elevated markers of cellular stress and reactivity in astrocytes (25).

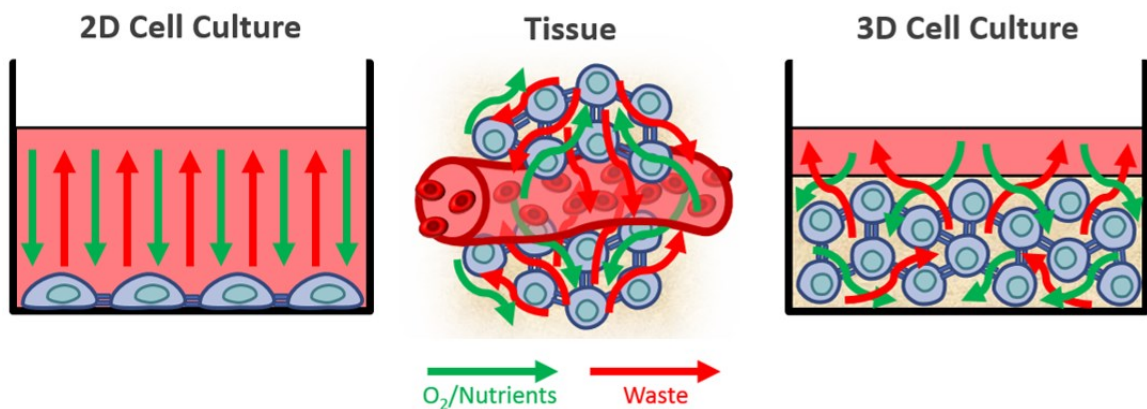


Figure 1 Cartoon representation of 2D, 3D, and native tissue growth environments.

Green arrows (\rightarrow) depict oxygen and nutrient flow while red arrows (\rightarrow) depict waste. 2D cell cultures are directly exposed to liquid medium while 3D cell culture attempts to mimic mass transport characteristics of native tissue.

With these limitations, pursuing novel techniques for *in vitro* modelling may be beneficial to supplement current 2D cell culture practices and obtain a clearer picture of neural cell behaviour. In recent years, more complex models of disease have emerged using microfluidic organ-on-a-chip technologies and have been used to mimic blood-brain barrier function *in vitro*, for example (27, 28). In these novel systems, cells can be organized and grown within microscale compartments and channels that offer defined spatiotemporal control over the microenvironment. While these technologies offer insight

into cellular and molecular mechanisms of disease and minimize reagent use due to their microscale requirements, they do not alone address the unnatural growth conditions of cells grown in 2D conditions. Therefore, the concept of building 3D cell culture models to better mimic native tissue has grown increasingly attractive (27, 29, 30).

1.2. Three-Dimensional (3D) Cell Culture

Alone, animal models and 2D cell culture offer limited portrayals of human neurological disease. Alternative techniques are becoming increasingly necessary to supplement information generated from these models. Many of these novel methods fall under the wide umbrella of 3D cell culture. 3D cell culture techniques aim to provide more representative neurological disease models in the laboratory. Many of these techniques attempt to provide natural environmental cues, mass transport, and 3D cell-cell and cell-ECM interactions (Figure 1). Neural cells grown in 3D culture conditions show different morphology (24, 25), improved differentiation into neuronal phenotypes (24), and minimization of spontaneous astrocyte reactivity (25) compared to 2D-grown cells. By bridging the gap between artificial *in vitro* models and native *in vivo* tissue, 3D cell culture has the potential to improve preclinical assessment of drug efficacy and neurotoxicology. In this section, I will briefly cover a small selection of the most popular 3D cell culture methods used in modelling the nervous system: explant culture, self-assembling aggregate culture, and scaffold-based culture.

1.2.1. Explant Culture

Commonly identified as organotypic slice culture, *ex vivo* modelling, or histoculture, explant culture involves growing a piece of animal or human tissue in the lab. Animal tissues are typically derived from healthy animals or genetically modified disease models (31–34). Explants from younger animals are preferred as these tissues are more robust and have been shown to survive for 15 weeks or more (32, 33). However, immature tissue can be a distant representation of certain neurodegenerative disease pathologies. Explants from older animals have been used in the past, but tissues are more sensitive and challenging to maintain (34, 35). For human explants, brain tissues are typically obtained from tumour biopsies or from epilepsy patients who undergo resective surgery to remove seizure epicentres (36–38).

Once the animal or human tissue has been retrieved, they are sectioned and can be grown on various platforms. These include in well-plates on membrane inserts (31–36), in microfluidic brain-on-a-chip devices (39), in suspension (40), or on gelatin-based sponge-gel matrices (38, 40, 41). Explants can be further processed to retrieve primary neural cell populations for other cell culture purposes (42, 43). However, leaving the ECM, vasculature, and existing circuitry intact offers opportunities for unique insight into neural cell growth and behaviour in their native tissue architecture, a key benefit of explant culture that we have not been able to fully mimic artificially.

Compared to animal models, explant culture offers greater control over the experimental environment and isolates areas of interest for further study. Small subsets of specialized

neuronal populations that cannot otherwise be harvested and propagated *in vitro* can be analysed using this technique (44). Explant culture also has potential to minimize animal sacrifice as multiple explants can originate from the same brain or spinal cord of a single animal (31). Furthermore, human-derived explant models avoid the limitations of species differences between humans and laboratory animal models.

Despite these advantages, explant culture can be time consuming, sensitive, and difficult to perform and maintain. Human explants can have high inter-specimen variability, and tissue quantity is limited. Targeting specific brain regions or neuronal populations is difficult as samples vary. Experiments rely on the availability of resective surgeries and close ties between research groups and surgical teams for successful transferal of viable tissues (37). As a result, most explant studies rely on animal models and experience similar limitations of species differences attributed to their source.

Explant culture should not be entirely discounted, however. In fact, the future of 3D cell culture may rely on this technique to validate and standardize the physiological relevancy of artificially engineered 3D tissue culture models. At present, explant culture offers a model we have yet to fully recapitulate and can be considered our current gold standard for 3D *in vitro* modelling.

1.2.2. Self-Assembling Aggregate Culture

Self-assembling aggregate culture is a category of techniques that encourage cells to spontaneously form 3D tissues without the presence of a scaffold to provide structural

support. Aggregate culture techniques include spheroids, organoids, neurospheres, microtissues, embryoid bodies, and “mini-brains”, colloquially (45). Neural aggregate cultures can be formed from neuroblastoma cell lines (46, 47), neural progenitor cells (48, 49), neural stem cells (50, 51), embryonic stem cells (ESCs) (52, 53), and induced pluripotent stem cells (iPSCs) (54, 55) through various methods. These include the use of ultra-low attachment plates (46, 47, 55), concave microwells (48, 49), hanging drop techniques (51), uniform mechanical agitation (e.g., bioreactors or rotary orbital shaking) (50, 56), and aqueous two-phase systems (ATPSs) (57–59).

ATPS methods use two immiscible water-based solutions to confine cells within small spaces and induce aggregation. ATPS-based techniques represent novel strategies for microtissue fabrication and have yet to be applied towards neural aggregate formation. However, ATPSs show promise as useful tools for the field of 3D neural tissue engineering. I will discuss ATPSs in more detail in section 1.3. Ultimately, all techniques promoting aggregate formation aim to increase cell-cell interaction and limit cell adhesion to a stiff substrate. When successful, tight 3D colonies are formed. Depending on the method used to generate aggregates, some may offer improved control over microtissue structure and size over others. For example, bioreactors and low-attachment plates can generate multiple aggregates in one vessel, but offer limited control over the size of each construct. In contrast, isolating small cell colonies with defined seeding densities using ATPS techniques and/or in separate microwells offers more control over aggregate formation.

With the range of neural cell sources available and advancements in stem cell technologies, aggregate culture has emerged as an exciting field for neural tissue engineering. The close, compact structure of aggregates can be considered an appropriate model of native brain tissue (60). Complex self-assembled structures mimicking premature fetal corticogenesis have been fabricated using commercially available low-binding plates to promote stem cell aggregation (52, 61). iPSCs from AD patients have been used to develop 3D neural microtissues to assess AD candidate drugs (55). Aggregate technology has also been applied towards studying the impacts of the Zika virus on neural development and microencephaly (62).

Despite these discoveries and relatively simple and scalable protocols for microtissue fabrication, these methodologies have yet to be well established within the general scientific community due to several limitations. Firstly, aggregate formation using stem cell sources can be significantly impacted by culture conditions such as cell density, passage number, and changes to media composition (63). Batch-to-batch differences have been observed in cellular composition as a result of these confounding factors (63). This can limit the reproducibility of aggregate cultures. Furthermore, aggregates are limited in terms of their ability to expand. Aggregates that grow too large can form necrotic cores. The lack of vasculature results in poor diffusion of oxygen, nutrients, and waste at the centre of the structure. Additionally, not all cell types spontaneously aggregate (27, 58). This factor limits the usage of alternative cell sources. Therefore, in cases where aggregate culture is unfeasible, a scaffold is necessary to provide a viable 3D environment.

1.2.3. Scaffold-Based Culture

Scaffold-based cell cultures take advantage of synthetic and/or natural biomaterials to provide 3D structural support for cultured cells. Porous sponge-like constructs, electrospun fibre networks, and hydrogels are some examples of cell culture scaffolds. For sponges and fibre networks, cell seeding can only occur after the scaffold is fabricated. Cells are added on top of the solid construct to form 3D cultures. Alternatively, hydrogels offer a cells-embedded-in-gel option. Cells can be seeded within hydrogels by providing the appropriate crosslinker to stimulate the hydrogel solution to assemble around the cells and form the necessary scaffolding for 3D growth.

Scaffold-based techniques are unique from aggregate culture in that they allow 3D environments to be designed rather than spontaneously formed by cells. However, many factors must be considered when crafting an appropriate scaffolding system to best model the environment of a chosen organ. The ideal 3D neural culture scaffolding should account for the stiffness of the native tissue, provide sufficient porosity for nutrient and oxygen exchange, and potentially mimic environmental and architectural cues such as ECM alignment if modelling the peripheral nervous system (64). Furthermore, if a polymerization reaction is required to form a 3D scaffold, crosslinkers such as chemical agents and extended ultraviolet (UV) photopolymerization must be assessed to determine impacts on cell viability (64). The degree of difficulty in fabricating the scaffold and its scalability for high-throughput testing for pharmaceutical development purposes should also be considered. With each material offering advantages and limitations towards their

use in modelling select systems, an appropriate scaffolding substrate must be chosen with these factors in mind.

Synthetic biomaterials that have been used in the past for 3D cell culture include, but are not limited to, poly(ethylene glycol) (PEG) (65–67), polystyrene (68), polycaprolactone (69), and graphene (70). These materials offer finer control over the tissue architecture. Porosity, scaffold orientation, mechanical stiffness, and electrical conduction can be readily manipulated and reproduced with minimal batch-to-batch variation. However, as these materials require more complex fabrication and functionalization steps, they can be expensive to produce and are not as readily accessible for high-throughput cell culture. Additionally, due to their synthetic origins, many of these materials do not have endogenous characteristics of native ECM.

Natural biomaterials are an alternative option to synthetic biomaterials and encompass any product isolated from natural sources. In contrast to synthetic biomaterials, natural biomaterials have higher risk of batch-to-batch variance. However, preparation steps are reduced leading to simpler protocols. Commercialized products are readily available and relatively standardized to minimize variance. As natural biomaterials can vary wildly in characteristics and capabilities, this category can be further divided into non-ECM-based materials and ECM-based materials. Non-ECM-based materials include alginate (24, 71), chitosan (72), agarose (73), and silk (74). Since many of these materials do not contain endogenous cellular adhesion motifs, they require further modification to promote cell infiltration and expansion. Some investigators have functionalized these platforms by

adding Arg-Gly-Asp (RGD) sequences, ECM components, or polyamino acid coatings to improve cellular attachment (24, 71, 72). Without such modifications, cell viability can be significantly impaired (73).

Common ECM-based materials include hyaluronic acid (HA) (23, 75, 76), collagen (23, 74, 76–78), basement membrane extracts (67, 79–81), and decellularized matrices (82). Decellularized matrices are materials that originate from harvested tissues stripped of all cells using several chemical washing steps to leave behind the ECM architecture. Residual detergents from decellularization processes may have an impact on cell growth, but this can be dependent on the protocol used (83). Decellularization technology has potential to offer the closest mimic of native neural tissue. While human neural tissue is limited, decellularized nerve and brain tissue can be obtained from laboratory animals. As other commercial ECM-based materials are commonly derived from rodent and bovine tissues, decellularization remains a promising technique for generating materials for 3D neural cell culture. However, while a single animal can provide multiple samples, scalability comparable to standard 2D cell culture performed in the pharmaceutical industry is challenging.

Unfortunately, most laboratories are not well equipped to handle more complex 3D tissue models. However, most are well-accustomed to liquid handling equipment and liquid-based culture assays. Therefore, hydrogel techniques may offer the most accessible high-throughput platform for 3D scaffold-based cell culture. While non-ECM-based materials such as agarose and alginate can serve as hydrogel platforms, their lack of cell attachment

sites limits their use. Alternatively, HA is a particularly attractive material as it constitutes the majority of ECM within the brain and can readily form a hydrogel when crosslinked (60). However, HA has poor cell attachment and suffers from similar limitations to non-ECM-based materials. HA requires the addition of polyamino acids or other ECM supplements such as collagen and laminin to support cell survival (23, 75, 76). This aspect of HA is compatible with its understood role within the adult brain ECM architecture. After development and maturation, the neural network consists of highly organized cellular interactions that are plastic but well regulated (60). An environment that promotes excessive cellular migration, proliferation, and random synaptogenesis is not ideal for the mature brain. Therefore, HA coupled with lecticans and tenascins within perineural nets control cell attachment and regulate the neural environment (60, 84).

Alternatively, hydrogels of type I collagen and Matrigel (a common ECM extract containing type IV collagen and laminin) are particularly prevalent in scaffold-based 3D culture due to their commercial availability, ease of handling, and endogenous cell adhesion motifs. However, cell survival and differentiation within type I collagen have been observed to produce poorer cell responses compared to Matrigel in studies using neural stem cells (85) and muscle progenitor cells (86).

1.2.4. Matrigel

Matrigel is a basement membrane extract from Engelbreth-Holm-Swarm mouse sarcoma cells. It has been used extensively in the field of oncology to study tumour cell infiltration and promote aggregate formation (87). Matrigel is a thermoresponsive, commercially

available, ECM-based hydrogel that self-assembles into an optically-clear scaffold at temperatures above 10 °C. As this material does not require any other crosslinking agent or chemical other than a minor temperature change to induce gelation and encapsulation of cells, Matrigel is relatively easy to use with minimal negative impact on cell growth. Each batch of Matrigel contains a mix of ECM proteins including ~60% laminin, ~30% type IV collagen, ~8% entactin, heparan sulfate, and other growth factors (although growth-factor reduced Matrigel can be purchased). While not a direct mimic of adult ECM in the brain, laminin has been noted to promote neurite outgrowth and is an important ECM protein during early neural development (88). Thus far, Matrigel has shown promising results as a 3D culture platform for modelling AD (79, 80). Investigators observed hallmark increases in amyloid beta and phosphorylated tau aggregation in a familial AD model grown under Matrigel-based 3D cell culture conditions (79). A microfluidic device called the “OrganoPlate” has also been developed using Matrigel as a 3D scaffold for iPSC-derived neural cell cultures (81).

While such advancements are exciting, hydrogel systems such as Matrigel are not commonly used platforms for neural cell culture. Like other 3D cell culture systems, hydrogel techniques are more difficult to perform compared to traditional 2D cell culture. 3D cell cultures also have limited compatibility with standard high-throughput equipment, assays, and imaging platforms. Despite the simplicity of Matrigel systems, the challenges involved in assessing 3D cell cultures and limitations in liquid handling impede their general use. Evaporation and air-liquid interfacial tension prevent effective handling of small volumes, so thick gels must be created. However, thicker gels are problematic

because they use additional material and have large diffusion distances. While large diffusion gradients may model features such as stroke, cardiac ischemia, and the formation of necrotic cores in tumours, they are not ideal for generating viable models of neural tissues. Neural tissues remain highly vascularised in the brain in many neurodegenerative diseases. Permeable transwell inserts can address issues with diffusion, but adding this step further complicates the 3D cell culture methodology and reduces high-throughput capabilities.

Attempts have been made to circumvent these limitations and generate thin-layer cultures using small volumes of Matrigel. The Whitesides group made use of chromatography paper to absorb 2-4 μl of cell-laden Matrigel prior to gelation (89, 90). The chromatography paper provided structural support for the spot of gel, and printed wax borders minimized leaching into adjacent cultures. After incubation at 37 °C, the technique produced thin cultures (200 μm) of cardiomyocytes and cardiac fibroblasts seeded in densities ranging from 2×10^4 to 1×10^5 cells/spot. However, the investigators noted that visualization of cells through chromatography paper was challenging and evaporation remained a high risk. This technique is unique in that chromatography papers filled with Matrigel spots could be stacked and split as desired for the study of ischemic gradients, for example. However, the protocol is difficult to perform and assess on a larger scale.

In 2015, Kim et al. detailed a novel “thin-layer” 3D cell culture method (80). Matrigel was diluted past the manufacturer’s recommended gelling point to generate a thin protein coating around cells (80). Evidently, the coating was sufficient to produce a thin gel around

the seeded cells. Cells were then grown and differentiated over a period of 2-12 weeks and were observed to form thin-layer 3D cultures ranging from 100-300 μm in thickness. This technique is promising due to its minimization of evaporation effects, interfacial tension, and material usage. Additionally, the thin-layer structure was compatible with standard liquid handling tools and could be assessed by immunocytochemistry. The investigators observed their model display key pathologies observed in AD (79, 80). However, while assessing this technique, I realized that their thin-layer 3D methodology did not appear to promote a cells-embedded-in-gel model as described in their protocol. Firstly, treated 96-well plates were used. The treated coating on culture vessels ordinarily promotes cellular adherence to the hard, plastic substrate. This feature is contrary to the goal of 3D neural cell culture, which would ideally mimic the softer tissue environment of the brain. Combined with the 2-12-week growth period and a seeding density of 2×10^6 cells/ml (79) to 1×10^7 cells/ml (80), cells may have been forced to grow as a tight stack. These growth conditions would certainly differ from a cells-embedded-in-gel model, which the investigators also assessed and termed as “thick-layer” 3D cultures. These thick-layer cultures used concentrated Matrigel and transwell inserts to accommodate for diffusion limitations. Ultimately, the thin-layer and thick-layer methodologies would provide dissimilar environmental cues that may impact cellular behaviour and differentiation depending on the chosen platform. The high seeding density would also not be ideal for high-throughput assay analysis. To address some of these initial concerns, I decided to replicate the thin-layer 3D culture protocol detailed by Kim et al. (2015) (80) and determine if this platform could sustain a lower cell seeding density. I also considered creating my own novel methodology for thin-layer 3D neural cell culture using Matrigel. To do so, I

investigated the use of ATPSs to shape small volumes of Matrigel to form thin-layer cultures in a 96-well plate format.

1.3. Aqueous Two-Phase Systems (ATPSs)

As previously described, ATPSs consist of two immiscible polymer-polymer or polymer-salt water-based solutions that phase-separate above critical concentrations. Factors that influence phase separation include temperature, molecular weight, ionic content, polarity, viscosity, etc. (91). Critical concentrations are typically determined by turbidimetric titration or cloud point method (91). These methods assess the point at which two solutions switch from miscibility to immiscibility or vice versa. Critical points are then plotted as a binodal curve on a phase diagram that delineates the concentrations of each solution required to form two phases (Figure 2). The ability of ATPSs to phase-separate offers unique utility in the separation of different compounds under aqueous conditions. Successes in ATPS-facilitated 3D aggregate culture have revealed the potential of ATPSs for use in 3D cell culture and tissue engineering applications (57–59). As ATPSs provide a unique platform for the precise manipulation of liquids, this technology has revealed intriguing applications beyond aggregate culture.

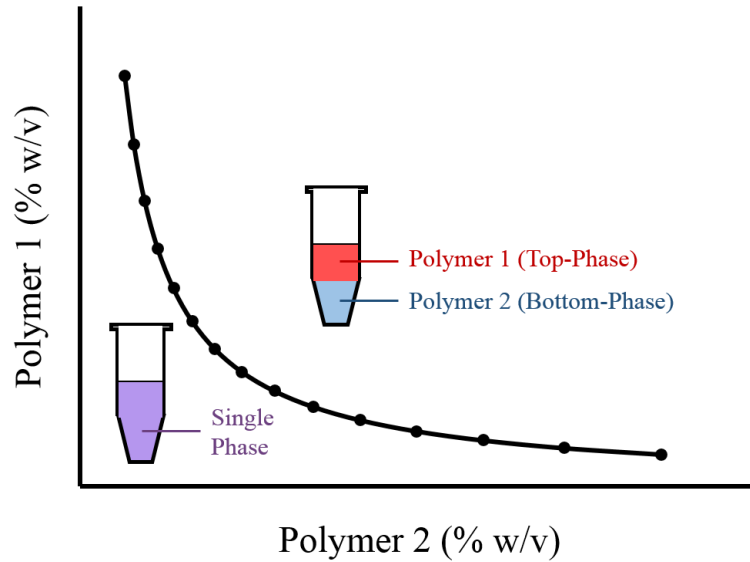


Figure 2 Hypothetical example of a binodal curve.

Black circles (•) indicate hypothetical critical points determined via turbidimetric titration. Two known concentrations (% w/v) of polymer 1 (red) and polymer 2 (blue) are combined to form an ATPS. The solution is gradually diluted with a solvent until the concentrations of each polymer can no longer maintain a stable ATPS, and a single phase (purple) is formed. The process is repeated to generate the rest of the points on the curve. Concentrations of polymer 1 and polymer 2 that lie above the binodal curve are predicted to form stable ATPSs, while concentrations that lie below the curve are expected to form a single-phase solution.

Moraes et al. demonstrated that by combining type I collagen with a bottom-phase-forming polymer, smaller volumes of hydrogel-forming solution could be used (92). The top-phase solution essentially formed a barrier that isolated the bottom-phase collagen solution from air and replaced the former air-liquid interface with that of a liquid-liquid interface prior to gelation. Evaporation was eliminated, and interfacial tension was significantly reduced. Volumes as low as 0.25-10 μl of cell-laden type I collagen were used to form microscale 3D cell cultures (92). Leung et al. further optimized this technique for liquid handling robotics and developed a high-throughput 3D breast cancer model using flat-bottomed 384-well plates (93).

Since ATPSs could provide a liquid-liquid interface for type I collagen, a similar strategy could be applied to Matrigel to form thin-layer cultures (Figure 2). I selected a 96-well plate format to take advantage of standard plate reader settings and common multichannel liquid handling tools for future high-throughput applications. To minimize cellular adherence to the plastic, untreated plates were used. The bottom-phase-forming solution would contain cell-laden Matrigel while the top-phase-forming solution containing culture medium would act as the protective barrier between the cell-laden Matrigel and air.

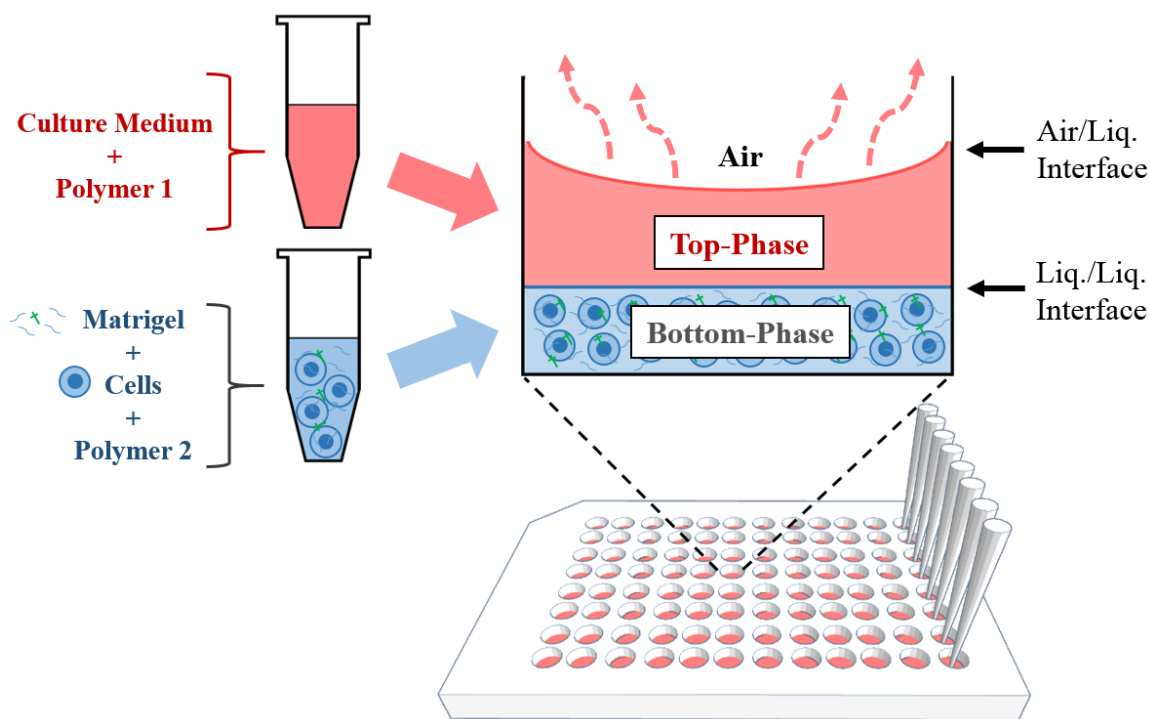


Figure 3 Cartoon representation of the ATPS-Matrigel 3D cell culture method in a high-throughput, 96-well plate format.

The presence of the top-phase solution effectively isolates the cell-laden Matrigel-bottom-phase solution from air to eliminate evaporation and reduce air-liquid interfacial tension.

By developing and optimizing a novel, thin-layer, hydrogel technique, I hypothesized that this system would address some of the limitations suspected in the Kim et al. methodology. Additionally, the new 3D culture technique would provide an improved 3D modelling platform compatible with high-throughput technologies and assays. As recent efforts in 3D neural cell culture have provided novel information previously undetected in animal and 2D cell culture models of AD (79), I considered whether other neurodegenerative diseases such as PD could be similarly modelled.

1.4. Parkinson's Disease (PD)

PD is the second most common neurodegenerative disorder after AD, impacting 0.2-0.3% of the world's population with prevalence rising with age (1, 94). PD is most notable for its gradual degradation of motor control. Key symptoms for a diagnosis of PD include bradykinesia (i.e., slow movement) with rigidity and/or resting tremor (95). Throughout progression of the disease, common nonmotor symptoms that can arise include sleep dysfunction, autonomic dysfunction (e.g., orthostatic hypotension, constipation, and urinary dysfunction), hyposmia, and psychiatric dysfunction (e.g., depression, anxiety, and hallucinations) (95). Cognitive impairments and dementia can also occur but typically appear during late stage PD (96). Both environmental factors and genetics appear to play roles in PD onset. For example, men are more likely to be diagnosed with PD than women (94, 96). Lower prevalence of PD has been observed in Asia compared to North America, Europe, and Australia (94). Pesticide exposure and the consumption of dairy products have been linked to greater incidence rates for PD, while caffeine and smoking have been associated with decreased risks (97). The impacts of geographical location, ethnicity,

lifestyle, sex, and genetics have offered hints towards the underlying etiology of PD. However, we remain far from understanding the complexities of this disease.

1.4.1. Etiology

PD is characterized by the substantial loss of dopaminergic (DAergic) neurons in the pars compacta region of the substantia nigra. These neurons are involved in sending projections to the striatum. Here, DA is released at the synapse and activates the DA receptors, D1 and D2, which correspond to the direct and indirect pathways of movement, respectively. The direct pathway promotes movement when DA is present, and the indirect pathway inhibits movement when DA is not present. In the direct pathway, release of DA at the striatum leads to increased excitatory thalamic output towards the motor cortex through a series of synaptic relays. Conversely, activation of D2 receptors in the indirect pathway results in decreased inhibition of the thalamus, which can then be free to send more excitatory signals to the motor cortex. The net result of these pathways when DA is released at the striatum is the promotion of movement. When DAergic neurons degenerate, the supply of DA is reduced, and the direct pathway weakens. The indirect pathway, however, strengthens inhibition on the thalamus and key motor symptoms of PD appear (96). Since the brain is plastic enough to accommodate losses in DAergic neuronal populations during early stages of the disease, by the time PD is diagnosed, many are already lost (98).

Current Treatments for PD

Having been discovered many decades ago, levodopa remains the gold standard treatment for PD motor symptoms. Levodopa, or L-3,4-dihydroxyphenylalanine (L-DOPA), is a

precursor to DA. It is endogenously catalysed by tyrosine hydroxylase (TH) from L-tyrosine, which is the rate-limiting step in catecholamine production (99). When given to patients, L-DOPA can pass through the blood-brain barrier and enter surviving DAergic neurons. L-DOPA bypasses the rate-limiting step and is immediately converted into DA to increase overall DA output. Despite potential side effects such as dyskinesia and DA dysregulation with long term use, L-DOPA remains the most efficacious treatment above alternatives such as DA agonists and monoamine oxidase B (MAO-B; an enzyme that can degrade DA) inhibitors (100). However, L-DOPA, like all other PD treatments, have only shown limited to moderate success in addressing the symptoms of PD. None have yet been successful in preventing or suspending PD's degenerative progress due to our lack of understanding of its etiology. Substantial research has been done to investigate the pathophysiology of PD with considerable attention having been focused on abnormalities in α -synuclein expression.

Lewy Bodies & Abnormalities in α -synuclein Expression in PD

The other main hallmark of PD is the aberrant deposition of oligomerized α -synuclein within the cytoplasm of neurons (96). The accumulation of α -synuclein deposits then aggregate to form insoluble structures called Lewy bodies or Lewy neurites (96). While initially assumed to be pathogenic, post-mortem assessment has suggested that DAergic neurons die before such aggregates appear (98). Thus, there is debate as to whether Lewy bodies innately impact disease progression or is more of a compensatory storage response to soluble toxic aggregates of α -synuclein (101). Older but otherwise healthy brains with no history of neurodegenerative disease have been found to express Lewy bodies as well,

suggesting a more benign impact of these features on brain function (102). Nonetheless, the comorbid spread of Lewy bodies and progressive deterioration of DAergic neurons has led to the suspicion that α -synuclein aggregation underlies PD pathology (96, 98).

Overexpression, misfolding, and dysfunction within proteolytic pathways, such as the ubiquitin-proteasome and autophagic-lysosomal systems, have been observed to lead to pathological accumulation of α -synuclein (96, 103). Rare duplications or point mutations (e.g., A53T or A30P) of the α -synuclein gene, SNCA, result in elevated levels and/or aggregation of α -synuclein and have been implicated in variations of familial PD (104, 105). Theories regarding the prion-like capabilities of misfolded α -synuclein to spread into other cells and act as seeds for new aggregates have also been postulated (96). Alternatively, genes such as PARK2 and PARK9, for example, are involved in ubiquitination and lysosomal autophagy, respectively, and when mutated have been held responsible for several cases of early-onset PD (101). While the ubiquitin-proteasome pathway has a role in degrading α -synuclein, past research has pointed towards a greater contribution of the autophagic-lysosomal pathway to PD pathology (96, 106). In the case of lysosomal dysfunction, unfolded/misfolded proteins end up accumulating in the endoplasmic reticulum (ER) leading to disruption of ER homeostasis, ER stress and eventual cell death (107, 108). Due to the complexities of these systems, the role of α -synuclein and how it may impact the brain remains unclear.

Other Factors Involved in PD Neurodegeneration

Why DAergic neurons of the substantia nigra selectively die in PD is also not completely understood. It has been proposed that their complex morphology, long (up to ~4.5 m), unmyelinated axons, an estimated ~1-2.4 million synapses at the striatum, and elevated basal mitochondria activity generates high amounts of reactive oxygen species (ROS) (109, 110). These features render these neurons particularly sensitive to oxidative and metabolic stressors (110).

The concept of mitochondrial dysfunction playing an important role in PD initially arose in 1983, when Langston et al. encountered four cases of illicit drug use leading to sudden onset of PD symptoms (111). The drug that the individuals had taken was 1-methyl-4-phenyl-1,2,3,6-tetrahydropyridine (MPTP), which had been marketed as the new “synthetic heroin” at the time (111). This compound was found to cause irreparable and targeted DAergic cell death in the substantia nigra. MPTP is a lipophilic compound that alone is not toxic. However, due to its lipophilicity, MPTP can easily pass through the blood-brain barrier. Once inside the central nervous system, MPTP can be metabolized by MAO-B into its toxic form, 1-methyl-4-phenylpyridinium (MPP+) (112). MPP+ can then enter DAergic neurons through the DA transporter (DAT), the reuptake mechanism for endogenous DA (112, 113). Inside the cell, MPP+ inhibits complex I of the mitochondrial electron transport chain leading to decreased ATP production, increased ROS production, and cell death (112, 114, 115). MPTP has been used across many different animal models and cell types and lines to reproduce PD neuropathology.

Past cell culture and animal work have also noted the impacts of DA and its metabolites on neuronal cell viability (116). Mosharov et al. observed that the presence of α -synuclein elevates L-DOPA induced DAergic neurotoxicity, suggesting the interplay between these factors may further selectively predispose DAergic neurons to die (116). On a side note, the observation of L-DOPA-induced neuronal death has led some to question the long-term prognosis of this treatment. However, no clear evidence has been found that L-DOPA aggravates PD progression in patients, and cell culture and animal model work have shown mixed results (117, 118).

Ultimately, it is well accepted that multiple factors play a role in PD. Impacts of neuroinflammation, oxidative stress, mitochondrial dysfunction, ER stress, and proteasome dysfunction likely have complementary exacerbating effects and are mutually impacted by dysregulation within any of these systems (96). Parsing the roles of these systems in PD using laboratory models will be key to better understanding disease progression and to developing novel therapeutic targets.

1.4.2. Preclinical Modelling in PD

Investigations into genetic factors that lead to familial PD have offered useful insights into the various mechanisms behind PD neuropathology. Our growing understanding of some of these genes have generated several methods for modelling PD. Common manipulations that have been done in both animal models and cell culture include altering expression of SNCA, PARK2, and other genes associated with familial PD (119–121). Alternatively, PD modelling has been accomplished using neurotoxins (e.g., MPTP, 6-hydroxydopamine [6-

OHDA], etc.) and pesticides (e.g., rotenone, paraquat, etc.) that have previously been noted to promote selective degeneration of DAergic neurons and induce symptoms of PD in humans and animal models (120). Due to the rapid onset of motor symptoms, neurotoxin/pesticide-based animal models are typically faster to produce compared to their transgenic counterparts, which has led to their popularity in PD research. In cell culture, toxins have been used as a method to test the efficacy of promising neuroprotective therapies and identify key cellular interactions involved in DAergic cell death (122, 123). However, most of these studies have used standard 2D cell culture practices to generate their results.

As previously discussed in section 1.1.2., 2D cell culture environments have been associated with alterations to cell behaviour, morphology, differentiation, etc. What impacts may these changes in cell behaviour impart to these experimental findings? Would neurotoxicological results differ when growth conditions are altered to better match native 3D tissue environments? Limited work has been done in this area with most preferring the simplicity of 2D cell culture systems over more cumbersome and unfamiliar 3D cell culture protocols. In this work, I will be presenting simple 3D cell culture methodologies that can easily be adapted for high-throughput screening of neurotoxins with future promise as a 3D modelling technology for drug assessment. I hypothesized that the 3D culture environment would have an impact on cellular response to neurotoxins when compared to standard 2D and cell culture methods. To test this hypothesis, I analysed the responses of two commercially available cell lines that have been previously used to assess PD

neuropathology under 2D and 3D culture conditions: the SH-SY5Y cell line and the Lund human mesencephalic (LUHMES) cell line.

1.4.3. The SH-SY5Y Cell Line

Established in the 1970s, the SH-SY5Y cell line is a derivation of the SH-N-SH cell line, which was obtained from a bone marrow biopsy of a 4-year-old female neuroblastoma patient (124). Interestingly, the cells can switch between adherent and non-adherent behaviours. While both are viable, adherent cells are more commonly used because they are easier to manage (125). The SH-N-SH cell line possesses two morphologically and biochemically different cell populations: an immature neuronal-like (N-type) phenotype and a substrate-adherent (S-type) epithelial-like phenotype (126). SH-SY5Y cells were originally cloned to isolate more of the N-type cells, although S-type cells remain within this cell line (Figure 4). SH-SY5Y N-type cells were observed to express TH and dopamine- β -hydroxylase (an enzyme that converts DA into norepinephrine) activity leading to its consideration as a catecholaminergic cell line (124, 126). DAT and various neuronal markers have been identified in these cells as well (122, 127). However, since these cells are cancerous, inherent genetic mutations could interfere with modelling pathways associated with PD. While it can be argued that we still do not fully understand PD pathology or the internal mechanisms within the SH-SY5Y cell line, whole genome sequencing has revealed that genes previously associated with PD remain intact within SH-SY5Y cultures and are useful for study as PD models (128). Since its discovery, SH-SY5Y has been widely used as a model cell line in PD and has also been applied to AD research due to the presence of tau proteins (128–130).

SH-SY5Y Cell Differentiation

While the majority of research using SH-SY5Y have left the cells undifferentiated, various methods have been developed to direct these cells towards more mature neuronal phenotypes (130, 131). Differentiation of SH-SY5Y cells removes them from the cell cycle, halts proliferation, and induces biochemical changes within the cells that result in neurite extension, cell spreading, and increased expression of neuronal markers (Figure 4b) (131). Retinoic acid (RA) is the most commonly used protocol to differentiate SH-SY5Y cells followed by two other methods: the sequential treatment of RA then 12-O-tetradecanoylphorbol-13-acetate (RA/TPA) or RA then brain-derived neurotrophic factor (RA/BDNF) (130).

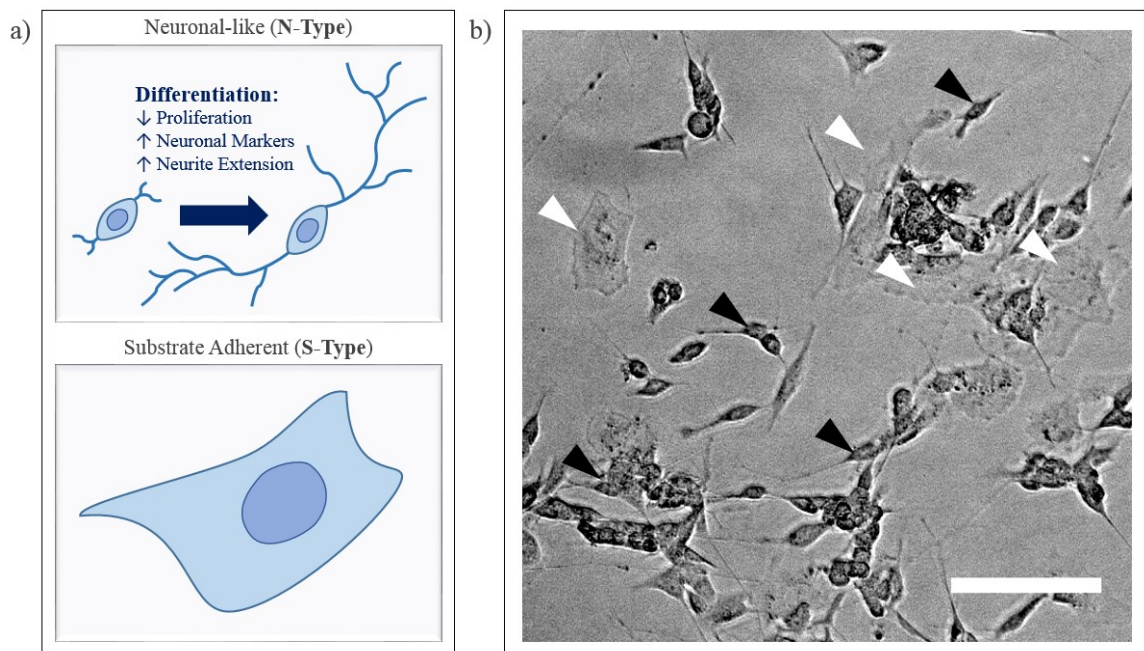


Figure 4 Examples of SH-SY5Y neuronal-like (N-type) and substrate adherent (S-type) cell populations.

a) Cartoon representation of cell types. b) Representative brightfield image (10X) of N-type (►) and S-type (▷) cells after 1 day of RA-only treatment grown in standard 2D cell culture conditions (cell culture methodology described in section 3.2.1.). Scale bar = 100 μ m.

RA is a derivative of vitamin A and has been shown to be crucial in embryogenesis and development (132). As a small, lipophilic molecule, RA can easily pass into the cell where it can bind to cellular retinoic acid-binding protein-2 (CRABP2). CRABP2 then takes RA into the nucleus to activate retinoic acid receptors (RARs) that mediate differentiation (132). It has been proposed that RARs influence microRNA activity, which can act to modify transcriptional expression and DNA methylation leading to downstream pathways that downregulate proliferation and promote differentiation (133–135). TPA is a phorbol ester and acts as a protein kinase C (PKC) activator (136). TPA treatment has been observed to lead to downstream increases in RAR β expression and alone can promote differentiation in neuroblastoma cells (136, 137). Finally, BDNF is a neurotrophic factor that promotes survival and differentiation during neuronal development. BDNF and its main receptor, tyrosine kinase B (TrkB), are involved in activating multiple intracellular signalling cascades that mediate axonal extension and synapse formation (138). Initial RA differentiation over 5 days in culture has been shown to maximally increase TrkB expression in SH-SY5Y cells (139). Following BDNF administration in serum-free medium, cells continue to grow and become reliant on BDNF to survive (139). This scenario mimics neurons during development where limited amounts of neurotrophic factors dictate neuronal population size (139).

While alternative differentiation protocols are available, they have not been commonly used or defined (130). Unfortunately, the literature and conclusions surrounding frequently used SH-SY5Y differentiation protocols are mixed as well (130). Some have concluded that RA-only differentiation generates a DAergic phenotype (140), while others have noted

greater cholinergic characteristics (*141*). RA-only treatment has been observed to elevate sensitivity to 6-OHDA, a commonly used DAergic neurotoxin that induces oxidative stress (*142*). However, another study observed that RA-only differentiation conferred resistance to both 6-OHDA and MPP+ instead (*122*). Furthermore, while 5-10 μ M of MPP+ may be sufficient to significantly reduce primary mouse DAergic cell populations (<50% cell viability) in culture after 24 h (*143*), 1 mM MPP+ barely induces SH-SY5Y cell death (>85% cell viability) (*122*). However, it is interesting to note that human DAergic neurons derived from ESCs (*144*) and iPSCs (*145, 146*) generally require 0.5-1 mM to promote significant reductions in cell viability (<50%) following 24 h of MPP+ exposure.

The other two commonly used differentiation protocols are less defined. RA/TPA treatment has also been shown to elevate DAergic characteristics. Cells differentiated using this method have greater sensitivity to MPP+ compared to RA-only and TPA-only differentiation protocols (*127, 147, 148*). RA/BDNF, on the other hand, has been observed to express neuronal markers and generate purer N-type cell populations (*139*). However, past investigation into the impacts of RA/BDNF on neuronal phenotype are inconclusive. One group observed elevated TH and DAT expression, DA reuptake, and DA release with potassium stimulation following RA/BDNF differentiation suggesting a DAergic phenotype (*149*). Another group did not find any change in TH expression and instead suggested that RA/BDNF differentiation induces a cholinergic phenotype (*150*). To date, none have tested RA/BDNF differentiated SH-SY5Y cells against PD neurotoxins such as MPP+.

Selection of the SH-SY5Y Cell Line

Despite a lack of consensus amongst those who have attempted to characterize this cell line, SH-SY5Y has remained an attractive choice due to its commercial availability, cost effectiveness, suitability for stable transfection, human origins, and simple growth protocols. Its long history of use in cell culture modelling has made it a very cell line. Thus far, a few groups have attempted to grow SH-SY5Y cells in 3D conditions with promising results (151–153). Additional research will need to be done to better understand the complex characteristics of SH-SY5Y cells and the impacts of growth environment on responses to experimental manipulation. I selected this cell line for most of my experiments due to its history in PD research, availability, ease of use, and unique characteristics. The dual populations (N-type and S-type) could prove useful for identifying the impacts of 3D growth environment on SH-SY5Y phenotype selection.

1.4.4. The Lund Human Mesencephalic (LUHMES) Cell Line

The LUHMES cell line was developed in 2002 and prepared from 8-week-old human embryonic ventral mesencephalic tissue obtained from Lund University (154). The human mesencephalic cells were immortalized with a v-myc retroviral vector that promotes v-myc overexpression in the absence of tetracycline (154). Therefore, the addition of tetracycline and other factors silence v-myc, inhibit proliferation, and promote differentiation. LUHMES cells can be differentiated into DA-producing cells that are morphologically, electrochemically, and biochemically similar to mature DAergic neurons after 6-7 days (154–156). LUHMES cells contain only one phenotypic population and have shown to have considerably higher expression of neuronal markers after differentiation compared to

RA-differentiated SH-SY5Y cells (156). These cells have been observed to have elevated sensitivity to common mitochondrial neurotoxins, MPP⁺ and rotenone (157, 158), and have recently been used for high-throughput screening of drugs that protect against α -synuclein-induced toxicity (159). As the LUHMES cell line is a more recent addition to my thesis, the majority of experiments detailed in subsequent chapters will involve the characterization of the SH-SY5Y cell line.

1.5. Thesis Aims

3D cell culture is a promising direction for the study of neurodegenerative diseases. These platforms offer more realistic mass transport, environmental cues, and cell-cell interactions, which can potentially uncover information previously inaccessible using standard 2D cell culture. However, many 3D cell culture techniques are not readily accessible to the general scientific community. Developing simpler 3D culture platforms may help expand the field of neural tissue engineering while improving the predictive capacity of preclinical research. The main goal of my research was to develop a Matrigel-based 3D cell culture platform that could provide an accessible foundation for high-throughput tissue and disease modelling. Initially, I pursued ATPSs to facilitate the production of thin-layer gels. However, through the development and characterization process of the ATPS-based technique, I ended up discovering an alternative 3D culture methodology. Therefore, two 3D cell culture methodologies will be detailed in this work. I eventually characterized these platforms and compared their performances to alternative culture platforms. Finally, I applied one of my 3D culture methodologies towards the

investigation of SH-SY5Y cell culture as a PD model and developed a neurotoxicity assay targeting known contributors to PD neuropathology.

1.5.1. Aim 1

Utilize ATPS techniques to facilitate the development of a simple, controllable, thin-layer, 3D cell culture platform with high-throughput capabilities in a 96-well plate format and characterize this system by assessing gel thickness and size compared to alternative methodologies.

1.5.2. Aim 2

Characterize the SH-SY5Y cell line and identify the impacts of differentiation and growth environment on SH-SY5Y morphology, viability, and behaviour using the 3D culture methodologies developed in this work and compare these platforms to standard 2D cell culture and the previously published thin-layer 3D culture protocol detailed by Kim et al. (2015) (80).

1.5.3. Aim 3

Define a high-throughput neurotoxicity assay protocol and assess the impact of growth environment on SH-SY5Y cell responses to neurotoxins previously used to model PD.

CHAPTER 2: 3D CULTURE PLATFORM DEVELOPMENT

2.1. Rationale

The first goal of my thesis was to generate a 3D cell culture methodology that would be easily accessible for laboratories already familiar with standard 2D cell culture. I wanted to take advantage of pre-existing tools such as common multi-well plates and multichannel pipettes. To do so, I selected Matrigel as my scaffolding substrate of choice. Matrigel is easy to handle, commercially available, and has a long history of use in cancer research and other fields for cell culture purposes. As Matrigel is a basement membrane extract containing ECM components, all characteristics necessary for cell growth and adherence are already available within the platform without further modification. Matrigel also does not require any additional chemical or UV crosslinking agents aside from a minor temperature change from $<10\text{ }^{\circ}\text{C}$ to $\sim 37\text{ }^{\circ}\text{C}$ to induce gelation. These features would provide familiarity and accessibility to the technique I planned to develop and potentially encourage more research groups to pursue neuroscience with 3D cell culture.

For my 3D cell culture platform, I aimed to produce a simple technique that could efficiently generate thin-layer 3D cultures using Matrigel while avoiding issues of evaporation and air-liquid interfacial tension. Thin-layer 3D cell cultures are attractive because they minimize potential oxygen, nutrient, and waste gradients that may form in standard thick layer cultures. Such techniques use less material and are ultimately more cost-effective. The commonly used ATPS polymers investigated in this work are commercially available and have been observed to have negligible negative impact on cell

viability. Numerous studies have used ATPSs for cell culture applications (57–59, 79, 92, 93).

As both the top-phase solution and the bottom-phase solution of ATPSs are water soluble, various compounds can be mixed into either phase. Matrigel could be combined with the bottom-phase solution of the ATPS, while regular medium could be used as the solvent to form the top-phase solution. In this model, Matrigel would be effectively isolated from air by the overlaying top-phase. A similar strategy was employed to produce type I collagen gels from volumes as low as 0.25 μ l (92, 93). While this group took advantage of 384-well plates, I decided to use 96-well plates for my experiments. Most of our liquid handling tools and equipment were optimized for the 96-well plate format. For these experiments, I examined the impacts of various ATPS polymers on Matrigel and selected the optimal ATPS pair for use in the 3D culture platform. I assessed the ATPS-based 3D culture platform's capacity to control gel thickness and surface area coverage in untreated 96-well plates.

NOTE: Portions of this chapter and Chapter 3 have been previously outlined in my MRS Advances publication (160). Sections stemming from experiments featured in that publication have been further explored, updated, and reproduced here with permission (see Appendix A).

2.2. Methodology

2.2.1. ATPS Polymer-Matrigel Compatibility Assessment

Poly(ethylene glycol) (PEG) 35 kDa (P35), PEG 8 kDa (P8), poly(vinyl alcohol) (PVA), Pluronic F-127 (PF-127), and poly(2-ethyl-2-oxazoline) 500 kDa (PEtOx) were obtained from Sigma-Aldrich. Dextran (DEX) 500 kDa (D500), DEX 70 kDa (D70), and DEX 10 kDa (D10) were obtained from Pharmacosmos. DEX 150 kDa (D150) was obtained from Dextran Products Ltd. Ficoll 70 kDa was obtained from GE Healthcare. Hydroxypropyl methylcellulose 4000 cps (HPMC) was obtained from Dow Chemical Co. Polymers were selected based on previous binodal characterization and application in ATPSs reported in the literature and/or identified in the Frampton lab (91). All polymers except for HPMC were dissolved in distilled water (dH₂O) to generate 10% and 20% w/v stock solutions. HPMC was dissolved in dH₂O to generate 2% and 1% stock solutions due to the high viscosity of concentrated HPMC solutions. Growth-factor reduced Matrigel (#356230; Corning) was diluted with polymer stock solutions to generate final w/v polymer concentrations of 1%, 2.5%, and 5% for all polymers except for HPMC, where final w/v HPMC concentrations were 0.1%, 0.25%, and 0.5%. All experiments used a 5 mg/ml final Matrigel concentration, and all materials were kept chilled on crushed ice to prevent premature gelation. Matrigel diluted with dH₂O-only acted as a control for standard gel formation without polymer interference.

Five microliters of each Matrigel solution were dispensed into a chilled 96-well plate. Following pipetting of all solutions, the plate was kept on ice for an additional 1 min and transferred to the 37 °C incubator for 10 min to induce gelation. Matrigel-polymer samples

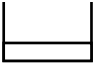
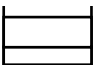

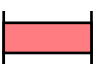
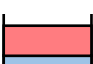
were then visualized, and images were captured under brightfield with a 2X objective lens using a Nikon Eclipse T1 Microscope. The end of a pipette tip was used to prod each droplet to confirm gelation. Polymer effects on Matrigel gelation were ranked as follows: complete gel interference, partial gel interference, and negligible gel interference. Complete gel interference involved total inhibition of typical gel formation. For some, this included the formation of condensed precipitate at the bottom of the Matrigel-polymer droplet while leaving a non-gelled liquid. For others, minimal to no precipitate was formed, but droplets remained in liquid form. Partial gel interference indicates conditions where solidified gels were formed, but the outer shell of the droplet remained a liquid as evidenced by capillary action in response to prodding with the pipette tip. In these cases, slight graininess in the gel could be observed. However, the bulk of the gel remained largely intact. Finally, negligible gel interference identified conditions that produced fully intact gels with no evidence of partial gel formation but may appear slightly altered in appearance compared to the Matrigel-dH₂O control. Based on minimal interference of D10 on gelation, observations of suspected phase separation between Matrigel and HPMC, and previous reports of HPMC/DEX phase separation (160), an ATPS comprised of 2.5% D10 (bottom-phase) and 0.5% HPMC (top-phase) was selected as the potential foundation for the ATPS-Matrigel 3D cell culture platform and used for subsequent studies.

2.2.2. Matrigel Platform Characterization

All Matrigel platform characterization solutions were prepared using Dulbecco's modified Eagle's medium (DMEM) supplemented with 10% fetal bovine serum (FBS) and 1% antibiotic antimycotic solution (ABX; Sigma-Aldrich), the most common

medium composition for SH-SY5Y cell culture, which will be referred to as complete medium henceforth (130). Stock and working solutions, respectively, of 10% D10 and 0.5% HPMC were prepared using complete medium. Five gel formation methods were evaluated: 1) Matrigel into air (M/Air), 2) Matrigel into complete medium (M/Medium), 3) Matrigel combined with 2.5% D10 into complete medium (M+D10/Medium), 4) Matrigel into 0.5% HPMC (M/HPMC), and 5) Matrigel combined with 2.5% D10 into 0.5% HPMC (M+D10/HPMC) (see Table 1 for more detailed solution compositions). Polystyrene microbeads (3.0 μm diameter; Sigma-Aldrich) were added to the bottom Matrigel solution to facilitate visualization and thickness assessment.

Table 1 Gel formation methods and corresponding bottom solution and top solution compositions.

	CONDITION	ABBREVIATION	BOTTOM	TOP
	Standard Method	M/Air	5 mg/ml Matrigel in Complete Medium + 3.0 μm microbeads	Air
	No ATPS	M/Medium	5 mg/ml Matrigel in Complete Medium + 3.0 μm microbeads	Complete Medium
	No ATPS (D10-Only)	M+D10/Medium	5 mg/ml Matrigel + 2.5% D10 in Complete Medium + 3.0 μm microbeads	Complete Medium
	“No ATPS” (HPMC-Only)	M/HPMC	5 mg/ml Matrigel in Complete Medium + 3.0 μm microbeads	0.5% HPMC in Complete Medium
	ATPS Method (HPMC+D10)	M+D10/HPMC	5 mg/ml Matrigel + 2.5% D10 in Complete Medium + 3.0 μm microbeads	0.5% HPMC in Complete Medium

Cold top solutions (i.e., complete medium or 0.5% HPMC in complete medium) were dispensed at 70 μl /well into chilled untreated 96-well plates. Matrigel volumes of 5, 7.5,

10, 15, 20, 30, and 40 μl were dispensed into the pre-filled wells for each condition, allowed 1 min to settle on ice following pipetting, and transferred to a 37 °C incubator for 15 min to induce gelation. The 1 min wait period accommodated for pipetting time and provided solutions that had been dispensed last time to settle. This session was not longer because the chosen 3D platform generated from these experiments was expected to house viable cells in the future. As cells naturally survive at 37 °C, extended periods of cold temperatures would likely be harmful to cell viability.

Following incubation at 37 °C, thickness and surface area measurements were recorded. This Matrigel characterization protocol was repeated 4 times and was replicated for another 4 iterations with a reversed order of solution dispensing where the bottom solution was dispensed first followed by the top solution (except for M/Air) to assess the impacts of dispensing order on gel formation.

2.2.3. Thickness Measurements

Following gelation, plates were taken to the Nikon Eclipse T1 Microscope to measure gel thickness and to capture 2X images of each well to assess gel shape and surface area (Figure 5). For gel thickness measurements, each well was centred under the 4X objective before switching to 20X. The microscope's coarse adjustment knob was used to focus on the bottom-most microbeads dispersed throughout the well. Using the fine adjustment knob, thickness was determined based on the number of rotations (each rotation = 100 μm) required to raise the stage until reaching the last focusable microbeads.

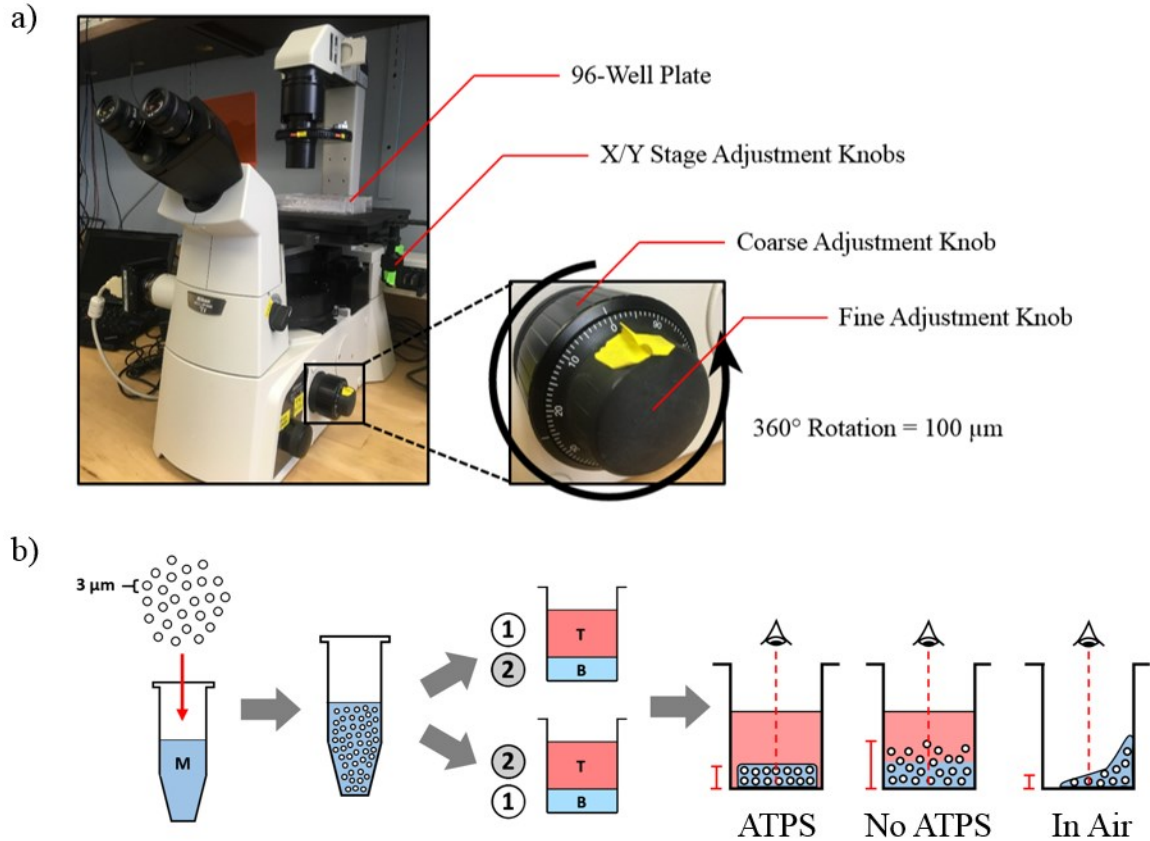


Figure 5 Schematic of thickness measurement protocol.

a) Nikon Eclipse T1 Microscope. Each 360° rotation of the fine adjustment knob equated to a 100 μm stage adjustment. **b)** The Matrigel (M) solution was combined with 3 μm microbeads and mixed thoroughly. The “top” solution (T) was either pipetted first (1) into the well followed by the “bottom” solution (B) containing Matrigel (2) or in the opposite order: (B) then (T). Dispersed microbeads were visualized using a brightfield microscope at 20X at the centre of the well. The adjustment knobs were used to focus on the bottom-most microbeads. The fine knob was rotated until focused on the top-most microbeads. The stage adjustment was recorded in μm .

A theoretical measurement of liquid thickness without consideration of interfacial tension was also calculated:

$$\textit{Theoretical Thickness} (\mu\text{m}) = \frac{DV \times 10^9 \mu\text{m}^3}{3.2 \times 10^7 \mu\text{m}^2}$$

where DV is the dispensed volume in μl divided by the estimated interior growth area of a single well (32 mm^2) of a standard 96-well plate.

2.2.4. Area Measurements

For gel surface area measurements, 2X images were stitched using the Large Image Capture function of the NIH Elements software, an imaging and editing platform associated with the Nikon microscope. Files were transferred into ImageJ, where the oval or polygon selection tools were used to trace gel boundaries and areas were measured. In cases where microbead dispersion covered the entire well, the surface area of the bottom of the well was measured and recorded. When gels could not be traced due to forming complex shapes and strands that appeared on multiple focal planes, a surface area value of 0 mm² was assigned. The theoretical surface area was assigned the value of 32 mm².

2.3. Results

2.3.1. Common ATPS Polymers Interfere with Matrigel Gelation

To produce the ATPS-Matrigel 3D cell culture platform, I originally considered using P35 and D500, a common ATPS formulation that was previously used to generate ATPS-based 3D collagen gels (92, 93). However, when D500 was introduced to Matrigel, fibrous precipitate was formed. I soon discovered that both D500 and P35 completely interfered with Matrigel gelation and left behind a dense precipitate. Therefore, I attempted to search for a suitable ATPS alternative by assessing Matrigel compatibility with a range of polymers previously used in ATPS formulations. After assessing various concentrations of ATPS polymers, I discovered that most ATPS polymers were incompatible with Matrigel (Table 2). These polymers resulted in precipitate formation and gelation interference (Figure 6). As expected of a surfactant, the PF-127 condition spread the 5 µl droplet over

a considerably wider area compared to the other conditions, and it also interfered with gel formation.

Table 2 ATPS Polymer-Matrigel Compatibility.

Polymer	w/v (%)		
	1	2.5	5
	0.1*	0.25*	0.5*
P35	■	■	■
P8	■	■	■
D500	■	■	■
D150	■	■	■
D70	□	□	□
D10	□	□	□
Ficoll	□	■	■
PVA	■	■	■
PF-127	■	■	■
PEtOx	■	■	■
HPMC*	□	□	■

Dark grey shading ■ indicates complete gel formation interference. Light grey shading □ indicates partial gel formation interference. White shading □ indicates negligible gel formation interference. * indicates corresponding w/v (%) concentration for HPMC only. Reproduced with permission (160).

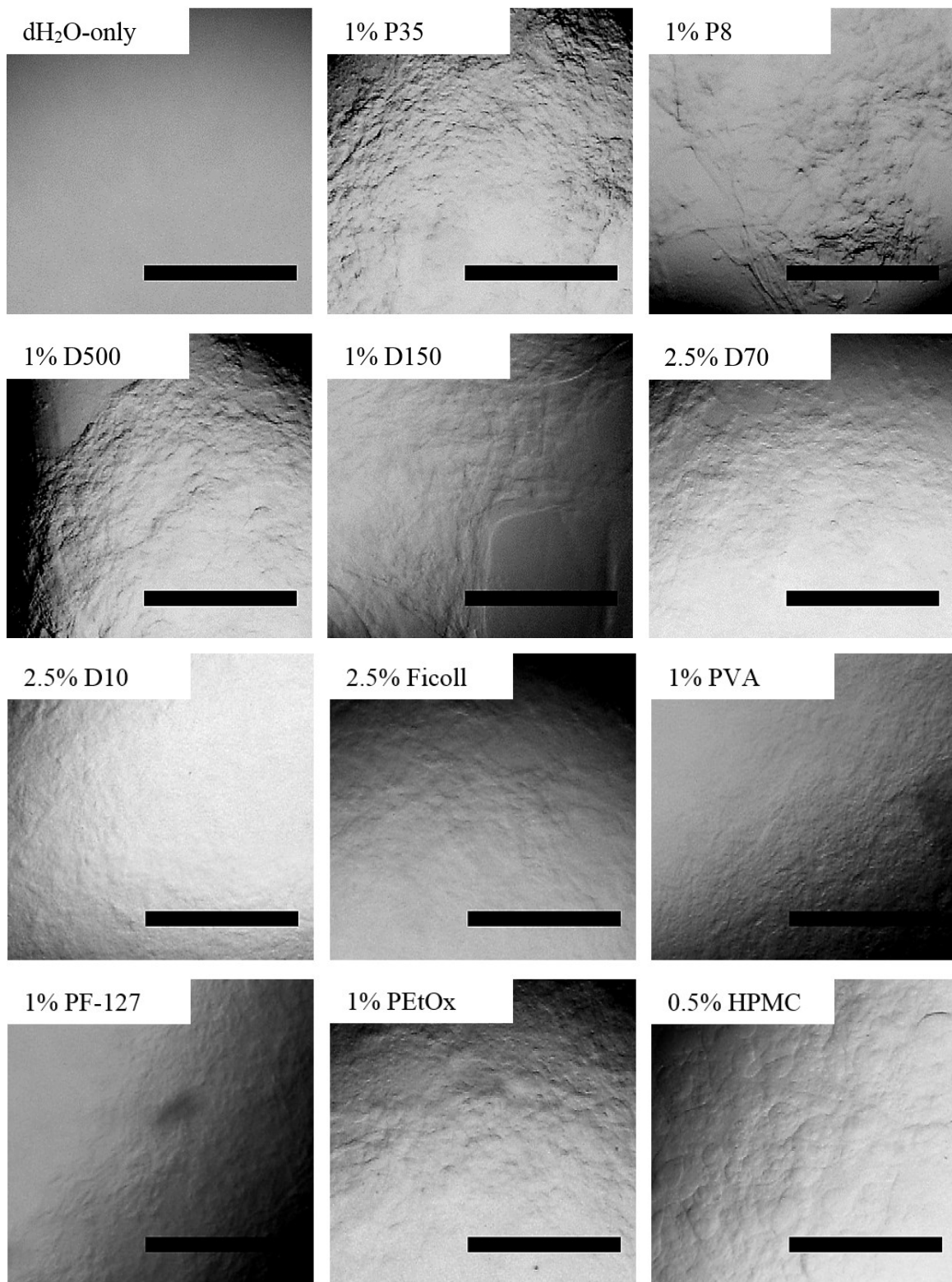


Figure 6 Representative images of ATPS polymer effects on Matrigel stability and gel formation.
Scale bar = 0.5 mm.

Only four polymers (D70, D10, Ficoll, and HPMC) were observed to retain gelation capacity following incubation at 37 °C. The only concentration of Ficoll capable of maintaining gel integrity with minimal precipitate formation was 1% w/v, which was too low for ATPS formation, as previously reported (91). Therefore, Ficoll was not considered as a potential candidate for the ATPS-Matrigel 3D cell culture method. D70 and D10 produced intact gels with slightly grainy appearances across all tested concentrations (Figure 6). Prodding with a pipette tip revealed that an outer liquid shell surrounding the underlying gel, indicating that gel formation was partially impacted by the presence of D70 and D10. D70 conditions were also observed to produce grainier gels compared to D10. Additional brief experiments not detailed in this thesis were performed assessing the impacts of D70 and D10 on precipitate formation in Matrigel, and D70 was observed to occasionally interfere with Matrigel gelation based on the length of time the Matrigel and D70 sat in solution on ice. D10 did not have a discernible impact on gelation over time.

The only ATPS polymer condition that formed fully stable gels with no liquid loss akin to the Matrigel+dH₂O control condition was 0.1% and 0.25% HPMC. The liquid shell observed in D70 and D10 was not present in 0.1% and 0.25% HPMC. However, I observed a curious phenomenon in HPMC-Matrigel pairs. In the 0.5% HPMC condition, gelation was completely inhibited, but a precipitate was not detected. Instead, the 0.5% HPMC/Matrigel solution was observed to have characteristics of an emulsion, which is a characteristic of immiscible solutions. Spherical and globular formations were observed under brightfield microscopy (Figure 6). Lower concentrations of HPMC (0.1% 0.25%)

produced similar characteristics, but were likely not at high enough concentration to interfere with gel formation when mixed into the Matrigel.

As DEX and HPMC have previously been noted to phase separate, D10 and HPMC had the potential to form the bottom- and top-phase, respectively, of an APTS (91). Since D10 was observed to be miscible with Matrigel while 0.5% HPMC showed potential phase separation with Matrigel, I sought to take advantage of these characteristics and use 2.5% D10 and 0.5% HPMC to generate the APTS-Matrigel 3D culture platform.

2.3.2. Characterization of Matrigel-based 3D Platforms

Various Matrigel 3D platforms were analysed to determine if the presence of the 2.5% D10 and 0.5% HPMC APTS was necessary to produce thin-layer gels. Bottom solutions were initially dispensed into the top solution to minimize exposure to air and avoid disturbance of the bottom solution. Qualitative observations of gel formation in Matrigel dispensed into empty wells (M/Air) confirmed the effect of high air-liquid interfacial tension on gel shape and size (Figure 7a). M/Air produced either small droplets or spread unequally across the well as evidenced by the height of microbead dispersion at the centre of the wells (Figure 7b). M/Air gels below 20 μ l were thick (>500 μ m), and a minimum of 40 μ l of undisturbed Matrigel solution was required to cover the full well (Figure 7c).

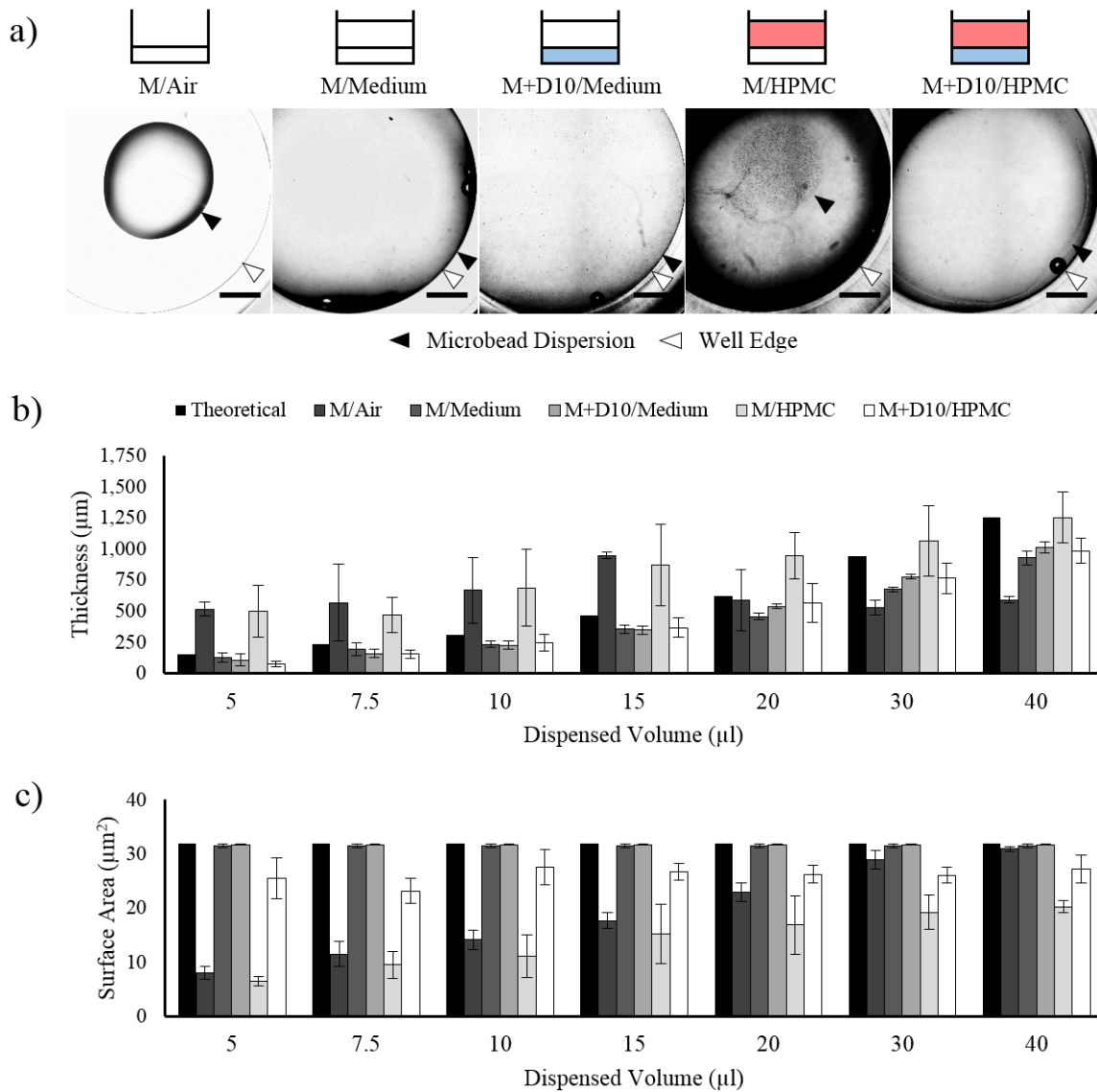


Figure 7 Characterization of bottom (B) dispensed into top (T) 3D Matrigel methods.

a) Representative images (2X) of 5 µl gels within their respective conditions. Scale bar = 1 mm. **b)** “Thickness” (microbead dispersion along z-axis) measurements of the (B) gel layers. Results are expressed as mean ± SD; n=4. **c)** Surface area (microbead dispersion along x-y-axis) measurements of (B) gel layers. Black arrowheads (▶) indicate the edge of microbead dispersion/gel. White arrowheads (▷) indicate edge of the well. Results are expressed as mean ± SD; n=4.

When Matrigel or Matrigel+2.5% D10 was dispensed into complete medium (M/Medium and M/D10, respectively), microbead distribution revealed thickness and surface area values that followed the theoretical estimates quite closely. Curiously, when plates were left at room temperature overnight and gels were checked the next day, microbeads remained in suspension within M/Medium and M/D10 conditions. This observation suggested the presence of a solid construct surrounding the microbeads that prevented sinking due to gravity. Thicknesses of microbead dispersion were not recorded following the overnight incubation and will need to be tested in future studies. The presence of D10 within the system did not appear to appreciably impact microbead dispersion or gel formation from M/Medium conditions.

In Matrigel dispensed into 0.5% HPMC conditions (M/HPMC), phase separation behaviours were once again observed. Microbeads in the M/HPMC condition were effectively isolated within the clearly visible gel constructs under brightfield microscopy. However, conditions using M/HPMC were highly variable in shape, size, and thickness. In some experiments, M/HPMC could produce gels shaped like disks while in others, gels could be highly non-uniform. Overall, the M/HPMC condition was variable depending on pipetting technique and likely needed more time on ice to settle via gravity to form more consistently shaped gels.

Finally, in conditions where both 2.5% D10 and 0.5% HPMC were present, thin gel disks were clearly formed. Under brightfield, the perimeter of flat, circular gels could be observed. Gel disks covered nearly the full surface area of the wells of 96-well plates at all

volumes (5 to 40 μl), and microbeads remained trapped within the gel. Gel thickness and surface area coverage were slightly below theoretical predictions compared to M/Medium and M+D10/Medium conditions, but gels were consistent in terms of size and shape compared to M/HPMC conditions. It should be noted that although 40 μl M/Air was capable of completely covering the surface of the well, M+D10/HPMC conditions never completely covered the surface. From 5 to 40 μl , the surface area stabilized around 26 mm^2 while the total surface area of the well is 32 mm^2 .

To confirm the ATPS behaviour of the M+D10/HPMC condition, I reversed the pipetting order. While doing so would introduce shear force to the bottom Matrigel-based solution, a strong bottom-phase solution would preferentially reside at the bottom of the well while the top-phase would preferentially reside on top. Therefore, regardless of dispensing order, the ATPS method should still form an intact gel. Without an ATPS, microbeads would disperse throughout the bottom and top solutions due to shear force mixing.

As predicted, when the pipetting order was reversed, the M+D10/HPMC condition produced thin gel disks (Figure 8a). While the thicknesses of these gel constructs were reduced (approximately half of the theoretical estimate) compared to gels formed when the bottom solution was dispensed into the top solution, this result was expected due to the elevated shear force during pipetting (Figure 8b). In addition, M+D10/HPMC conditions generated with the reversed pipetting order were observed to cover the complete surface of the well with 10 μl and above (Figure 7c, Figure 8c). Once again, M/HPMC conditions were variable. If the HPMC solution was dispensed right above a Matrigel droplet, flat gel

disks could be formed. However, in those cases, the middle of the gel was often maximally 3 μm thick because only one layer of microbeads could be observed during thickness assessment. Alternatively, if the top-phase was dispensed at an angle and/or too fast, gels could form into complex shapes displayed in Figure 8a where strands of gel are formed. Such complex shapes were difficult to measure. As the centre of the well was used as the landmark for thickness measurements, there were often no bottom-most microbeads touching the surface of the well resulting in the M/HPMC condition being unquantifiable. Surface areas were also not generally feasible to measure in cases where gels were dispersed in streaks throughout the well. These cases were counted as a 0 value and resulted in large standard deviations. However, despite the added disturbance of pipetting the top-phase onto the bottom-phase, in M/HPMC conditions, microbeads remained solely within gel constructs with very few escaping the Matrigel. Finally, as expected for conditions suspected to have no ATPS (M/Medium and M+D10/Medium), reversal of pipetting order resulted in random microbead dispersion. Resultant “thickness” values were therefore much higher than theoretical estimates because the thickness measurements took place shortly after solution dispensing.

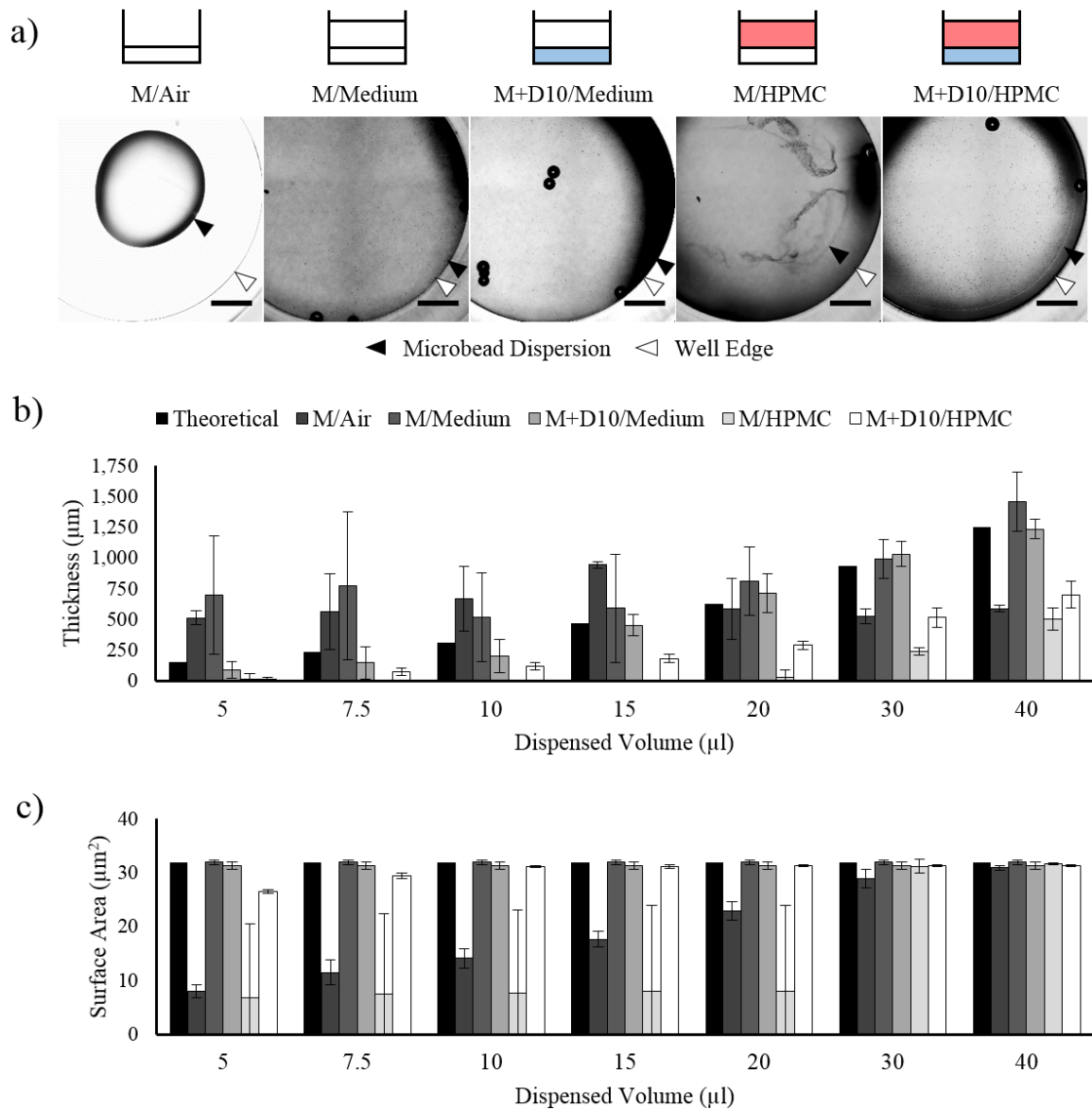


Figure 8 Characterization of top (T) dispensed onto bottom (B) 3D Matrigel methods.

a) Representative images (2X) of 5 μl gels within their respective conditions. Scale bar = 1 mm. **b)** “Thickness” (microbead dispersion along z-axis) measurements of the (B) gel layers. Results are expressed as mean \pm SD; n=4. **c)** Surface area (microbead dispersion along x-y-axis) measurements of (B) gel layers. Black arrowheads (▶) indicate the edge of microbead dispersion/gel. White arrowheads (▷) indicate edge of the well. Results are expressed as mean \pm SD; n=4.

From these results, it appeared that the D10/HPMC ATPS was necessary to consistently produce flat gel disks. If the bottom solution was dispensed into the top solution, M/Medium and M+D10/Medium conditions were also potential platforms. A preliminary experiment was conducted to measure the microbead distribution from edge-to-centre-to-edge across 20 μl gels. Gels were measured at the left-most edge, the centre, and the right-most edge of the well after microbeads were allowed to settle in the incubator for 2 h. This experiment revealed that M/Medium and M+D10/HPMC conditions resulted in relatively even gel thicknesses across the construct with M/Air producing the most deviation across each point measured on the gel ($\pm 330 \mu\text{m}$), followed by M/HPMC ($\pm 260 \mu\text{m}$), then M/Medium ($\pm 120 \mu\text{m}$), and M+D10/HPMC ($\pm 50 \mu\text{m}$).

2.4. Discussion

2.4.1. ATPS Polymers and Matrigel

P35 and D500 were previously used to manipulate type I collagen, another ECM-based hydrogel material (92, 93). I had expected this formulation to work with Matrigel as well. However, these polymers and many others interfered with gel formation and produced precipitation in Matrigel. Only the low molecular weight DEXs, D70 and D10, the lowest concentration of Ficoll tested (1%), and very low concentrations (0.1% and 0.25%) of HPMC were found to not completely interfere with Matrigel gelation. Since PF-127 is a surfactant, perhaps it may have dispersed the ECM proteins within the Matrigel and prevented their self-assembly into a gel. However, a slight graininess in the droplet indicated some precipitate formation, so it did not seem to completely inhibit protein aggregation.

Ultimately, macromolecular crowding may have had a role in disrupting gelation and inducing precipitate formation. Macromolecular crowding involves the impact of large molecules on other molecules in a system due to their size (161). The steric exclusion of other molecules in the presence of concentrated macromolecules can result in changes to molecular behaviour such as elevated protein aggregative properties (161). Common synthetic macromolecular crowding agents that have been used to study this phenomenon have included Ficoll, PEG, DEX, and PVA at concentrations equivalent to 2.5% (w/v) and higher (161). Since Matrigel contains a diverse mix of ECM proteins and other molecules, it may have been more susceptible to the impacts of macromolecular crowding than a pure solution of type I collagen. D70 may have had a greater impact on Matrigel gelation than D10 due to its higher molecular size. While not a commonly used macromolecular crowding agent, the PEtOx used in this study had a similar molecular weight to D500. Both 500 kDa polymers interfered with gelation. Finally, despite their smaller molecular weight, PEGs have additional unique interactions with proteins that go beyond steric exclusion (161). These features may have supplemented the effects of macromolecular crowding in Matrigel for PEG conditions.

HPMC likely had a very different impact on Matrigel when used at high enough concentrations. Matrigel mixed with 0.5% HPMC revealed emulsion characteristics during the compatibility assessments. Furthermore, when Matrigel was dispensed without D10 into 0.5% HPMC, the microbeads preferentially remained within the gel regardless of pipetting order. These observations suggest that Matrigel and HPMC may act as an ATPS. Additionally, gelation was not impeded with 0.1% and 0.25% HPMC. However, under

phase contrast microscopy, spherical inclusions can be observed within these gels. If the HPMC emulsion spread throughout the Matrigel construct, HPMC pores may have been produced leading to a rather unique gel structure. The characteristics that define this unique interaction between Matrigel and HPMC remain unknown and will need to be further explored.

While the M/HPMC condition offered an APTS-like platform with potential for 3D cell culture, gels were often inconsistently formed. Additional time on ice, low binding pipette tips, and consistent pipetting skill may accommodate for some of these issues. However, added steps add difficulty to the protocol. Until the M/HPMC model is further characterized and optimized, it is not an ideal 3D cell culture platform. Ultimately, both HPMC and D10 were found to be necessary to generate the APTS-Matrigel 3D culture method.

2.4.2. The APTS-Matrigel 3D Culture Method

The APTS-Matrigel 3D culture method was shown to generate consistently flat gels as thin as 76 μm using only 5 μl of a combined Matrigel/D10 solution. To minimize exposure to air and fluid shear force, dispensing the Matrigel/D10 solution into HPMC is optimal. Gel thicknesses were thinner than predicted, but these results are expected based on previous observations of fluid loss after combining Matrigel and D10. The role of D10 in the APTS-Matrigel 3D culture method is not completely clear. It may act to help spread the Matrigel ECM proteins. DEXs typically act as bottom-phase solutions when combined with

methylcellulose solutions. This feature may have contributed to promoting the formation of M+D10 gels at the bottom of the plate in the presence of HPMC (91).

Polymer concentrations were initially selected to ensure the production of a stable ATPS-Matrigel 3D platform based on preliminary investigations into polymer compatibility. Alternative concentrations of D10 and HPMC were not tested. Could lower concentrations of D10 and HPMC produce similar results? As emulsion characteristics were observed in 0.1% and 0.25% HPMC conditions during the polymer compatibility experiments, perhaps HPMC concentration could be reduced. The impact of Matrigel lot was also not examined in further detail. The characterization of gel thicknesses and surface areas were performed using only one lot of Matrigel. Some Matrigel from this lot was eventually used for early cell culture experiments, but a new batch of Matrigel had to be purchased after stocks were depleted. For the purposes of streamlining the preparation of thin-layer 3D culture platforms and testing their potential applications, differing lots of Matrigel were considered identical apart from stock concentration differences. Differences in protein concentration between Matrigel lots were accommodated for by consistently using 5 mg/ml of Matrigel rather than ratios. Ratio calculations (e.g., 1:1 Matrigel is prepared by adding 1 part Matrigel and 1 part medium solution) are surprisingly common in studies using Matrigel despite stock concentration differences between lots. This can lead to significant experimental inconsistencies.

A unique observation of the ATPS-Matrigel 3D culture method involved the curiously consistent smaller surface areas. No volume of M+D10 dispensed into HPMC formed gels

that covered the full surface of the well. Even with high interfacial tension, 40 μl of Matrigel was sufficient to cover the well surface. Subsequent repetitions of the characterization protocol to reproduce the M+D10/HPMC condition eventually revealed that the gel disks were non-adherent. Agitation of the M+D10/HPMC condition could cause gels to shift in position. Gels would only adhere to the plate when HPMC was dispensed on top of the M+D10 solution. This observation is reflected in the surface area results for that condition where a volume of 10 μl was sufficient to cover the well's surface. However, I observed that gel adherence only covered the space where the M+D10 solutions were dispensed. Any surface that touched HPMC without initial M+D10 coverage were not adherent. HPMC could be slowly dispensed onto the M+D10 droplet, but performing this task by hand with a multichannel pipette is arduous and not every laboratory owns liquid-handling robots for more precise liquid dispensing.

These results suggested that HPMC formed a barrier at the bottom of the well that prevented M+D10 gel adhesion. Exploring adhesion of Matrigel in glass capillaries revealed that simply coating the capillary with 0.5% HPMC and adding Matrigel alone was sufficient to eliminate Matrigel adherence to the glass (results not shown). Without HPMC, Matrigel readily adhered to the glass surface. Dispensing the bottom-phase first followed by the top-phase was not ideal because the initial M+D10 volume would be exposed to air resulting in evaporation.

Nonetheless, the ATPS-Matrigel 3D culture method remains a powerful technique to control gel formation using small volumes of Matrigel. Therefore, its performance as a cell

culture platform was assessed. The efficacy of this system as a cell culture platform will be discussed in Chapter 3.

2.4.3. The Matrigel-Only 3D Culture Method

The last key finding from these set of experiments was the identification that simply dispensing Matrigel alone or Matrigel combined with D10 into medium was sufficient to form gels. When dispensed under standard Matrigel-air conditions, Matrigel adheres to plastic and glass regardless of standard cell culture surface treatment (e.g., treated vs. untreated plates). Therefore, this Matrigel-only 3D culture method would be expected to produce adherent gels because HPMC is not present in the system. The addition of D10 to the system without HPMC seemed unnecessary because results were largely similar to the M/Medium condition. Removing D10 would provide the simplest method for 3D cell culture while avoiding issues of evaporation and interfacial tension. With these preliminary findings, the Matrigel-Only 3D culture method was developed and tested with cell culture to determine if the underlying gel layer was capable of supporting cell growth and differentiation. Results from these experiments will be discussed in Chapter 3.

CHAPTER 3: ASSESSMENT OF CELL CULTURE PLATFORMS

3.1. Rationale

In Chapter 2, I presented two promising 3D cell culture techniques: the ATPS-Matrigel 3D culture method and the Matrigel-only 3D culture method. The next step was to assess their performance as viable 3D cell culture platforms. As the focus of my thesis involved developing a platform that could potentially be used to model PD and play a role in future drug development applications, I selected the traditionally used SH-SY5Y cell line for subsequent cell culture experiments. As previously discussed, the SH-SY5Y cells are easy to maintain and have a long history in PD research and modelling (130). Additionally, the presence of N-type and S-type cells offered a unique opportunity to morphologically assess the impacts of growth environment in 2D vs. 3D cell culture. However, while it has been long reported that SH-SY5Y cell cultures contain DAergic neuronal characteristics, I wanted to confirm these observations in the SH-SY5Y cell line available in our lab, so I performed some preliminary assessment of these features using Western blotting and immunocytochemistry. Following these early assessments, I examined the impacts of differentiation on SH-SY5Y cell growth. Various differentiation protocols are available that produce neuronal features in SH-SY5Y cells. While I briefly examined RA-only and RA/TPA differentiation, I settled on the RA/BDNF protocol because it produced exquisitely differentiated cells with extensive branching neural processes and excellent cell viability.

After characterizing the SH-SY5Y cells, I assessed the ATPS-Matrigel 3D culture and Matrigel-only 3D culture platforms and their impacts on cell growth and viability in undifferentiated and RA/BDNF differentiated SH-SY5Y cultures. I compared these new 3D culture platforms to pre-existing cell culture techniques to determine if they were comparable or offer unique features over existing platforms. The alternative culture methods tested in this work were standard 2D cell culture and the Kim et al. (2015) thin-layer 3D culture method (80). Additionally, I considered that untreated plates would minimize cell adherence to the culture vessel, which would be ideal for the 3D cell culture platforms. Therefore, I examined the influence of untreated vs. treated cell culture vessels on SH-SY5Y cell growth across the various cell culture platforms.

3.2. Methodology

3.2.1. SH-SY5Y Cell Culture

The SH-SY5Y human neuroblastoma cell line (CRL-2266, ATCC) was cultured with complete medium (DMEM+10% FBS+1% ABX) in 100-mm culture dishes and maintained in a 37 °C, 5% CO², humidified incubator. Complete medium was changed every 4-7 days as per ATCC recommendations. Cells were passaged at ~60-90% confluence and used for experiments before 20 passages using standard passaging protocols. Briefly, culture plates were washed with 5 ml of warmed 1X filter sterilized phosphate buffered saline (PBS), and 2 ml trypsin-EDTA (0.05% Trypsin/0.53 mM EDTA; Corning) was added. Cells were incubated at 37 °C for 3 min before tapping the plate to dislodge remaining adherent cells. Complete medium (2 ml) was added, and cells were centrifuged at 0.2 rcf and 20 °C for 5 min. The supernatant was removed, and pellets were

resuspended in complete medium to be re-plated, stored in liquid nitrogen, or used for experiments.

3.2.2. PC-12 Cell Culture

The PC-12 rat pheochromocytoma cell line (ATCC, CRL-1721) was cultured as per ATCC guidelines. Briefly, PC-12 cells were cultured in PC-12 growth medium containing Roswell Park Memorial Institute (RPMI) 1640 medium, 10% horse serum (HS), 5% FBS, and 1% ABX and maintained in a 37 °C, 5% CO₂, humidified incubator. As PC-12 cells do not adhere well to plastic, light trituration was sufficient to dislodge cells for passaging. PC-12 cells were only used for initial examination of our TH antibody. As PC-12 cells are derived from the rat adrenal medulla, they are expected to have high endogenous TH expression. TH is necessary to produce DA and ultimately norepinephrine and epinephrine, the predominant neurotransmitters expressed by the adrenal medulla. Due to these qualities, PC-12 cells were used to confirm TH specificity of the primary antibody used in Western blotting and immunocytochemical analysis of TH expression.

3.2.3. SH-SY5Y Differentiation Protocols

Over the course of this work, SH-SY5Y cells were differentiated based on three established protocols previously discussed in section 1.4.3. Preliminary examination of SH-SY5Y differentiation involved RA-only treatment. SH-SY5Y cells were maintained in complete medium supplemented with 10 μM RA (44540; Alfa Aesar) over 5 days and immunocytochemistry was performed on the cultures to assess TH and neurofilament (NF) expression. RA/TPA was also briefly explored. Ultimately, the RA/BDNF differentiation

protocol was selected for subsequent experiments after comparing differentiation protocols. Additionally, RA/BDNF differentiation has not been well characterized and has limited examination in neurotoxicological research, so further investigations could lead to novel exploratory results in the field.

RA/BDNF differentiation was adapted from Encinas et al. (139) and detailed in Figure 9. SH-SY5Y cells were sub-cultured, plated in complete medium, and stored in the incubator overnight. The next day, the medium was replaced with complete medium supplemented with 10 μ M RA. Cells were grown in complete medium + 10 μ M RA for 5 days with a medium change in day 3. On day 5, the complete medium + 10 μ M RA was replaced with serum-free medium (DMEM+1% ABX) supplemented with 50 ng/ml BDNF (100-01; Shenandoah Biotechnology) for 4 days with a medium replacement on day 7. Processing/assessment occurred on day 9 of the differentiation protocol.

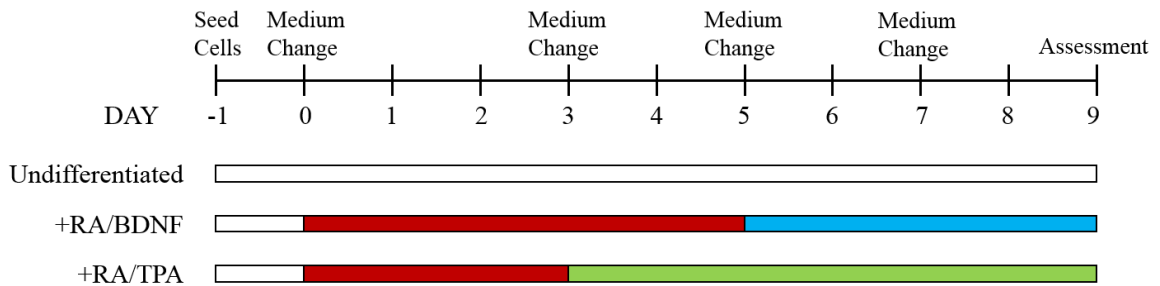


Figure 9 SH-SY5Y differentiation protocols.

White bars (□) indicate SH-SY5Y complete medium. Red bars (■) indicate RA treatment. Blue bars (■) indicate serum-free BDNF treatment. Green bars (■) indicate TPA treatment.

RA/TPA differentiation was adapted from Presgraves et al (127). SH-SY5Y cells were treated with complete medium supplemented with 10 μ M RA for 3 days (Figure 9). The

medium was then switched to complete medium supplemented with 80 nM TPA (P1585; Sigma-Aldrich) and maintained for 6 more days with medium changes every 2 days.

3.2.4. Western Blotting

Western blotting procedures are based on Novus Biological's recommended protocols with minor modifications. SH-SY5Y cells were cultured in complete medium until ~80% confluent in 100 mm dishes. PC-12 cells were cultured in PC-12 growth medium until ~80% confluent as well. Culture dishes were washed with ice-cold 1X PBS once, and 2 ml of 20 mM Tris-HCl (pH 7.5) supplemented with 1X MS-SAFE Protease and Phosphatase Inhibitor (Sigma-Aldrich) was added to each dish. Cell scrapers were used to remove remaining adhered cells. Cell lysates were transferred into centrifuge tubes, agitated for 30 min at 4 °C, centrifuged at 12,000 rpm at 4 °C for 20 min, and then transferred into new tubes on ice. Lysates were stored at -20 °C until ready for further processing and analysis.

A 5X Bradford reagent stock was prepared as follows, 50 mg Brilliant Blue G250 was added to 25 ml Methanol (Fisher Scientific) to dissolve followed by 50 ml 85% phosphoric acid. The 5X Bradford reagent stock was topped up to 100 ml with dH₂O. A 1 mg/ml bovine serum albumin (BSA; Sigma-Aldrich) protein standard in 0.15 M NaCl was prepared. The 5X Bradford reagent was diluted with dH₂O, and the 1X Bradford reagent was filtered through Whatman grade 1 filter paper. A Bradford assay was conducted to determine protein standard curves and measure unknown cell lysate samples. Absorbance was read using a FilterMax F5 microplate reader.

Sample buffer (SB) stock (2X) was prepared (4% SDS, 0.2% bromophenol blue, 20% glycerol, 200 mM dithiothreitol). Lysates were diluted to produce equivalent protein concentrations, and equal parts lysate and 2X SB were combined. SB-lysate solutions were heated at 95-100 °C for 5 min in a hot water bath. Lane spacers (dH₂O) and Precision Plus Protein™ Dual Color Standards (5 µl/lane; BioRad) were prepared in 1X SB. Each sample was loaded at 20 µg protein per lane (3 lane repeats per cell type) and separated on a 4-20% polyacrylamide gradient gel, which was prepared in advance using the Model 485 Gradient Former (BioRad) and Mini-PROTEAN 3 Multi-Casting Chamber (BioRad). Gels were run at 100 V for 1 h and 200 V for 30 min. Proteins were transferred at 100 V for 1 h 15 min onto a PVDF membrane (GE Healthcare).

The membrane was briefly washed once with 1X Tris-buffered saline with Tween 20 (TBST) and blocked with 1% BSA in 1X TBST overnight at 4 °C. The next day, the blocking solution was replaced with the primary antibody anti-TH (0.25 µg/ml; MAB7566; Novus Biologicals) prepared according to the manufacturer's recommendations with 1% BSA in 1X TBST and incubated overnight at 4 °C. The following day, the membrane was washed 3 times with 1X TBST for 10 min/wash. The membrane was incubated in goat anti-mouse HRP-conjugated secondary antibody (1:1000; HAF007; Novus Biologicals) diluted with 1% BSA in 1X TBST at room temperature for 1 h at room temperature. The membrane was washed again 3 times for 10 min/wash with 1X TBST. SuperSignal West Pico Chemiluminescent Substrate (Thermo Scientific) was added to visualize the blot. Images were captured using the Azure c600 Imaging System.

3.2.5. Immunocytochemistry

SH-SY5Y cells were passaged, resuspended in complete medium, and plated at 1.5×10^4 cells/well in a treated 96-well plate. Cells were counted using a Countess II FL Automated Cell Counter. The next day, wells were assigned to either the undifferentiated treatment group or the RA-differentiated treatment group. Medium was changed to either complete medium (undifferentiated) or complete medium with 10 μ M RA (RA-differentiated). Media was refreshed on the third day. On day 5, media from all wells were removed, and 70 μ l/well 3.7% formaldehyde (Sigma-Aldrich) in 1X PBS was added. Plates were fixed at room temperature for 10 min and washed 3 times with ice cold 1X PBS. Cells were permeabilized with 0.25% Triton X-100 (Sigma-Aldrich) diluted with 1X PBS for 10 min at room temperature and then washed 3 times with 1X PBS for 5 min/wash. A blocking solution of 1% BSA in 1X PBS with Tween 20 (PBST) was prepared and added to the samples. Cells were blocked for 30 min at room temperature. Primary antibodies, anti-TH (10 μ g/ml; MAB7566; Novus Biologicals) and anti-NF heavy 200 kDa (1:200; AB1989; Sigma-Aldrich), were prepared in accordance with manufacturers' recommendations in 1% BSA in 1X PBST. Samples were incubated in primary antibodies overnight at 4 °C. The next day, cells were washed 3 times with 1X PBS for 5 min/wash. Secondary antibodies, goat anti-mouse IgG HiLyte Fluor 488 (5 μ g /ml; NB710-40671; Novus Biologicals) and goat anti-rabbit IgG HiLyte Fluor 555 (5 μ g /ml; NB710-94951; Novus Biologicals), were prepared according to manufacturer recommendations in 1% BSA in 1X PBST. Following the addition of secondary antibodies, plates were covered in foil and incubated for 1 h at room temperature. Cells were washed for a final 3 times with 1X PBS for 5 min/wash. Images were captured under epifluorescence with the Nikon Eclipse T1 Microscope.

3.2.6. 2D Culture Method

Once SH-SY5Y cells had reached 70-90% confluence, cells were passaged and counted. Cells were split into separate labelled tubes based on their prospective growth condition prior to centrifugation. The resultant cell pellet for the 2D growth condition was resuspended in cold complete medium to simulate conditions for the 3D cultured cells. SH-SY5Y cells were plated at 1.6×10^4 cells/well on both treated and untreated ice cold 96-well plates using an automated handheld multichannel pipette. Plates were kept on ice for 1 min and transferred to the 37 °C incubator. Plates were left undisturbed overnight. 2D cultured cells were subsequently subjected to the same pipetting (multichannel pipettors), medium changes, and differentiation conditions as controls for 3D-grown cell cultures.

3.2.7. ATPS-Matrigel 3D Culture Method

Stock and working solutions of 10% D10 and 0.5% HPMC, respectively, were prepared a day in advance in complete medium and stored at 4 °C. Freshly made polymer solutions are recommended to be made a minimum of a day in advance. On the experiment day, 70 µl/well of cold 0.5% HPMC solution was dispensed into chilled treated and untreated 96-well plates. SH-SY5Y cells were passaged and resuspended in ice cold complete medium at a concentrated pre-calculated cell density. Resuspended cells, 10% D10, and Matrigel were combined to generate a 5 mg/ml Matrigel + 2.5% D10 solution with a cell density of 3.2×10^3 cells/µl. A multichannel pipette was used to dispense 5 µl of cell-laden Matrigel+2.5% D10 into the pre-filled wells containing 0.5% HPMC resulting in a total of 1.6×10^4 cells plated per well. Plates were left on ice for 1 min following pipetting and transferred to the 37 °C incubator to induce gelation. Plates were left undisturbed overnight.

The following day, the 0.5% HPMC was removed and replaced with either complete medium or complete medium with 10 μ M of RA. ATPS-Matrigel 3D cell cultures and corresponding 2D cell culture controls were grown under shorter differentiation protocols. Undifferentiated cells were grown for 7 days in complete medium while RA/BDNF-differentiated cells received 5 days of RA treatment followed by 2 days of serum-free BDNF treatment.

3.2.8. Kim et al. (2015) 3D Culture Method

This thin-layer 3D cell culture technique was adapted from Kim et al (80). Some alterations were made to the protocol. Changes included the type of cells seeded (SH-SY5Y vs. ReN cells), number of cells seeded (1.6×10^4 cells/well vs. 2×10^5 cells/well to 1×10^6 cells/well), volume dispensed per well (70 μ l/well vs. 100 μ l/well), differentiation protocol to account for cell type, time in culture (9 days vs. 2+ weeks), and tissue culture plate (untreated and treated 96-well plates vs. only treated 96-well plates).

Following passaging, the SH-SY5Y cell pellet was resuspended in ice cold complete medium. The cell suspension was combined with Matrigel at a 1:1 ratio and kept on ice. Additional cold complete medium was added to the cell suspension to generate a final 1:11 dilution. The final solution contained 1 part cells, 1 part Matrigel, and 9 parts complete medium. Note: the final Matrigel concentration for this experiment after dilution was 0.71 mg/ml based on an original protein concentration of 7.8 mg/ml. The authors recommended pre-testing 1:10, 1:15, and 1:20 dilutions of Matrigel and selecting the “best” one (80). I hypothesized that a more concentrated Matrigel solution would have a higher chance of

producing a 3D cell culture. Once the cell-laden diluted Matrigel solution was prepared and thoroughly mixed, 70 μl /well was added into room temperature treated or untreated 96-well plates. Plates were immediately stored in the 37 °C incubator and left undisturbed overnight. The next day, cells were differentiated or left undifferentiated as described in section 3.2.3.

3.2.9. Matrigel-Only 3D Culture Method

Treated and untreated 96-well plates were chilled on ice, and 70 μl of cold complete medium was added to each well. After passaging, cells were resuspended in cold complete medium and combined with Matrigel to generate a 5 mg/ml Matrigel solution with a cell density of 800 cells/ μl . Cell-laden Matrigel was kept on ice and dispensed at 20 μl /well (resulting in 1.6×10^4 cells/well) using a multichannel pipette into pre-filled wells containing complete medium. Plates were left on ice for 1 min and transferred to the 37 °C incubator to induce gelation. Plates were left undisturbed overnight. The next day, cells were differentiated or left undifferentiated as described in section 3.2.3.

3.2.10. Cell Viability Assessment

Calcein-AM (C-AM; Biotium) and propidium iodide (PI; Sigma-Aldrich) staining were used to identify living and dead cells, respectively. C-AM permeates the cell and is hydrolysed by esterases resulting in the emission of green fluorescence within the cytoplasm of cells. PI is a red fluorescent stain that binds to DNA but cannot enter living cells. Cells were also stained with Hoechst, a common UV-excitable nuclear stain that binds to DNA, to cross-reference to C-AM and PI staining. Stains (3 μM C-AM, 3 μM PI,

and 1:2000 Hoechst) were prepared together in serum-free medium (DMEM+1% ABX). At the end of the differentiation protocols, media were replaced with 70 μ l of C-AM/PI/Hoechst solution per well. Plates were stored in the incubator for 30 min. Cells were imaged under epifluorescence with the Nikon Eclipse T1 Microscope. Additional image processing was completed using ImageJ's Colour Balance feature to minimize background and brighten staining.

3.3. Results

3.3.1. Assessment of DAergic Characteristics in SH-SY5Y Cells

Since its early characterization in the late 1970s and onwards, the SH-SY5Y cell line has been known to express TH (*124, 126*). Due to these DAergic characteristics, numerous studies have used these cells as model neural cell lines for PD research (*130*). Western blotting was performed to assess TH expression in undifferentiated and RA-differentiated SH-SY5Y cells. However, TH expression could not be detected in SH-SY5Y cells across multiple attempts (results not shown). As the antibody had been previously shown to detect TH (~60-62 kDa) in adrenal gland tissue, PC-12 cells were used to assess TH specificity and compared to undifferentiated SH-SY5Y cells. Western blotting results revealed antibody specificity for the 60-62 kDa TH protein with no cross-reactivity in PC-12 samples (Figure 10a). Once again, TH expression was not detected in SH-SY5Y samples. In the presence of the stronger PC-12 TH signal, it was expected. However, I considered that perhaps SH-SY5Y cells expressed TH in quantities too low to detect using Western blotting techniques. As the PC-12 Western blotting results suggested high TH antibody specificity, I assumed the antibody would localize well in SH-SY5Y cells using

immunocytochemistry techniques. Here, I was finally able to observe TH expression in SH-SY5Y cells (Figure 10b). After differentiating the SH-SY5Y cells over 5 days with 10 μ M RA, cells extended long processes and appeared to have strong TH expression. NF, an intermediate filament present in neurons, was also detected in both undifferentiated and RA-differentiated cells.

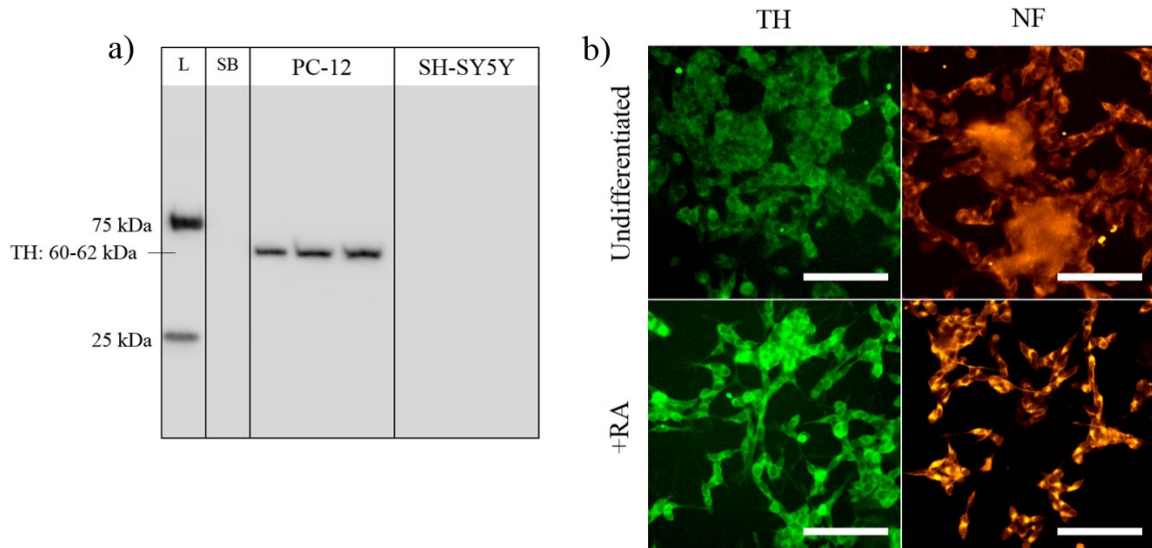


Figure 10 Preliminary assessment of DAergic and neuronal markers in SH-SY5Y cells.

a) Western blot comparison of TH expression between PC-12 and SH-SY5Y cells including a Precision Plus Protein™ Dual Color Standard (L) and sample buffer lane spacer (SB). All bands for each cell type come from the same protein sample at 20 μ g/lane. **b)** Representative (20X) immunofluorescent TH and a NF staining of undifferentiated and 5-day RA-differentiated SH-SY5Y cells grown in standard 2D cell culture conditions. Scale bar = 100 μ m.

3.3.2. ATPS-Matrigel 3D Culture of SH-SY5Y Cells

2D-grown cells were seeded onto treated plates while ATPS-Matrigel 3D conditions were grown on treated (3D-T) or untreated (3D-UT) 96-well plates. Across all conditions, cell viability, as represented by C-AM staining, was quite high (Figure 11a). PI appeared to be elevated in 3D-T and 3D-UT undifferentiated conditions compared to standard 2D culture,

but this qualitative observation may not be entirely accurate. All cells remained confined within the gel in 3D conditions including any that may have died during initial seeding or over time. In 2D culture conditions, any non-adherent cells (dead or alive) would be washed away with each medium change. Therefore, PI expression in this scenario is likely artificially reduced. RA/BDNF-differentiated conditions expressed minimal PI staining across all growth protocols suggesting good cell viability following differentiation.

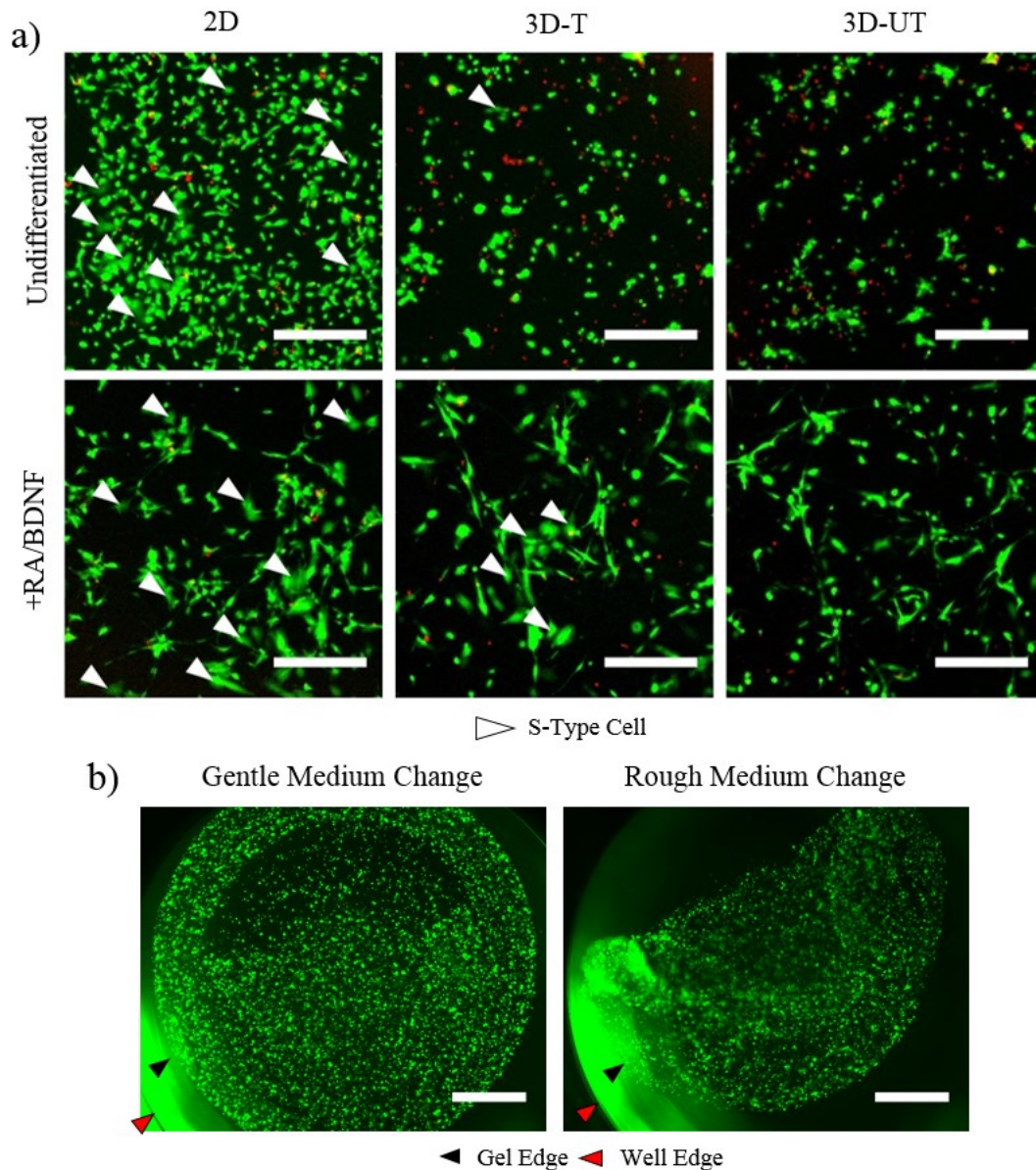


Figure 11 ATPS-Matrigel 3D SH-SY5Y cell culture.

a) Representative images (4X) of C-AM (green-live)/PI (red-dead)-stained undifferentiated and differentiated (+RA/BDNF) SH-SY5Y cultures grown under standard 2D culture conditions or using the ATPS-Matrigel 3D culture method in treated (3D-T) and untreated (3D-UT) 96-well plates. Scale bar = 300 μ m. White arrowheads (▷) indicate S-type cells. Reproduced with permission (160). **b)** Representative images (2X) of C-AM-stained SH-SY5Y cultures grown in 3D-UT after gentle (induces minor shift of gel) or rougher (gel is lifted from the well and folds over itself) perturbations during medium changes. Note the lack of C-AM expression on the plate surface indicating complete cell growth within the gel. Black arrows (▶) indicate the edge of the gel, red arrows (▶) indicate the edge of the well. Scale bar = 1 mm.

Undifferentiated cells displayed a more rounded phenotype in 3D conditions and tended to grow as aggregates over time. RA/BDNF-differentiated N-type cells grew long, extended neural processes across all growth environments (2D, 3D-T, and 3D-UT). However, differences in S-type epithelial-like cell expression could be observed between 2D, 3D-T, and 3D-UT conditions (Figure 11a). In 2D cell culture, many S-type cells can be identified in both differentiated and undifferentiated cell cultures. S-type cells have considerably larger cell bodies and lack neural processes. In 3D-T conditions, fewer S-type cells were detectable under microscope. Most SH-SY5Y cells grown in the 3D-T environment were observed to have small cell bodies with neurite extension throughout the gel. However, in the 3D-UT condition, S-type cells could not be detected at all. All cells within the 3D-UT gels appeared to have small cell bodies and neurite extension. These results suggested that the presence of an underlying, stiff, adherent substrate in a 3D hydrogel growth environment could have a significant impact on cell phenotype. Cells that sunk to the bottom and encountered the treated plastic surface were given the opportunity to attach, even if the gel itself was not adhered to the plate. Therefore, untreated plates may be necessary to promote preferential cell growth in 3D. As shown in Figure 11b, ATPS-Matrigel 3D cultures grown on untreated plates expressed no viable cell attachment to the underlying plastic surface outside of the gel.

Figure 11b also presents the non-adherent nature of ATPS-Matrigel 3D cultures. Gentle medium changes were able to shift the gel from its original position while rough medium changes could lift and fold the gel. Therefore, when handling ATPS-Matrigel 3D cultures, medium changes should be done with care. However, these features also suggest that

ATPS-Matrigel 3D cultures would be excellent platforms for contraction assessment. When SH-SY5Y cell cultures were differentiated within the ATPS-Matrigel 3D platform, contraction of the gel was observed (Figure 12).

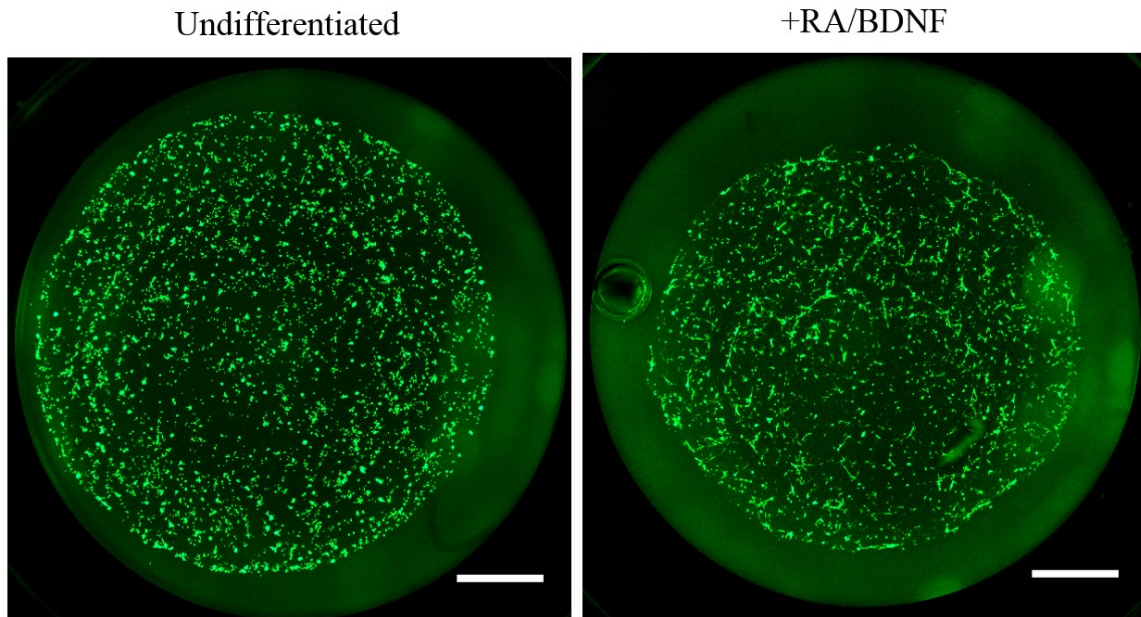


Figure 12 Representative images (2X) of differentiation-induced contraction in C-AM-stained ATPS-Matrigel 3D cell cultures. Cells were grown on untreated plates and left undifferentiated or treated with RA/BDNF to induce differentiation. Scale bar = 1 mm.

3.3.3. Comparison of Cell Culture Methodologies

A surprising discovery described in Chapter 2 revealed that simply dispensing Matrigel at the bottom of a well filled with medium was sufficient to form a gel. The Matrigel-only 3D culture technique is even simpler to perform than the ATPS-3D culture method and does not require additional polymers to form a thin-layer gel. I assessed SH-SY5Y cell growth in the Matrigel-only 3D culture method and discovered that a minimum of 20 μ l cell-laden Matrigel was required to fill the well completely. Less than 20 μ l resulted in uneven and incomplete gel coverage of the well. While this would ultimately produce

thicker gels, the Matrigel-only 3D culture protocol did not appear to significantly impact cell viability compared to 2D conditions in early assessments of the technique. Additionally, gels were adherent to the plastic. With these promising results, I used the Matrigel-Only 3D culture method for all subsequent 3D culture experiments and assessments. Here, I compared three different culture methods: standard 2D culture, the recently published Kim et al. 3D thin-layer culture method (80), and the Matrigel-Only 3D culture method. I also examined the impacts of treated vs. untreated plate surfaces and undifferentiated vs. RA/BDNF treatment on SH-SY5Y cell growth and morphology.

Undifferentiated SH-SY5Y Cells Grown on Treated Plates (Figure 13)

Undifferentiated SH-SY5Y cells grown on treated tissue culture plates in 2D tended to aggregate only after most of the available surface area in the well had been covered by cells. In the Kim et al. 3D condition, cells did not appear to have spread well over the surface compared to the 2D condition, which may have been due to presence of the diluted Matrigel. The ECM protein supplement may have prompted earlier cellular aggregation, so cells may not have been as inclined to spread across the plate. Alternatively, the cells may have been covered in a thin layer of Matrigel that encouraged aggregate growth, but 3D cell growth was difficult to identify in this model as cells could only be seen at the bottom of the well. Flat, adherent cells similar to 2D culture conditions could be identified in Kim et al. 3D culture platform. On the other hand, the Matrigel-only 3D cell culture technique clearly produced 3D cell growth. Cells were distributed throughout the gel matrix, although some S-type cells could be identified at the bottom of the well, which was to be expected in treated plates. Even the non-adherent APTS-Matrigel 3D culture method

produced the S-type phenotype when grown on treated plates. Like previous morphological observations of undifferentiated SH-SY5Y cell growth in the ATPS-Matrigel 3D culture method, cells grown in Matrigel-only 3D culture tended to grow as aggregates. Cell viability remained high across all cell culture platforms.

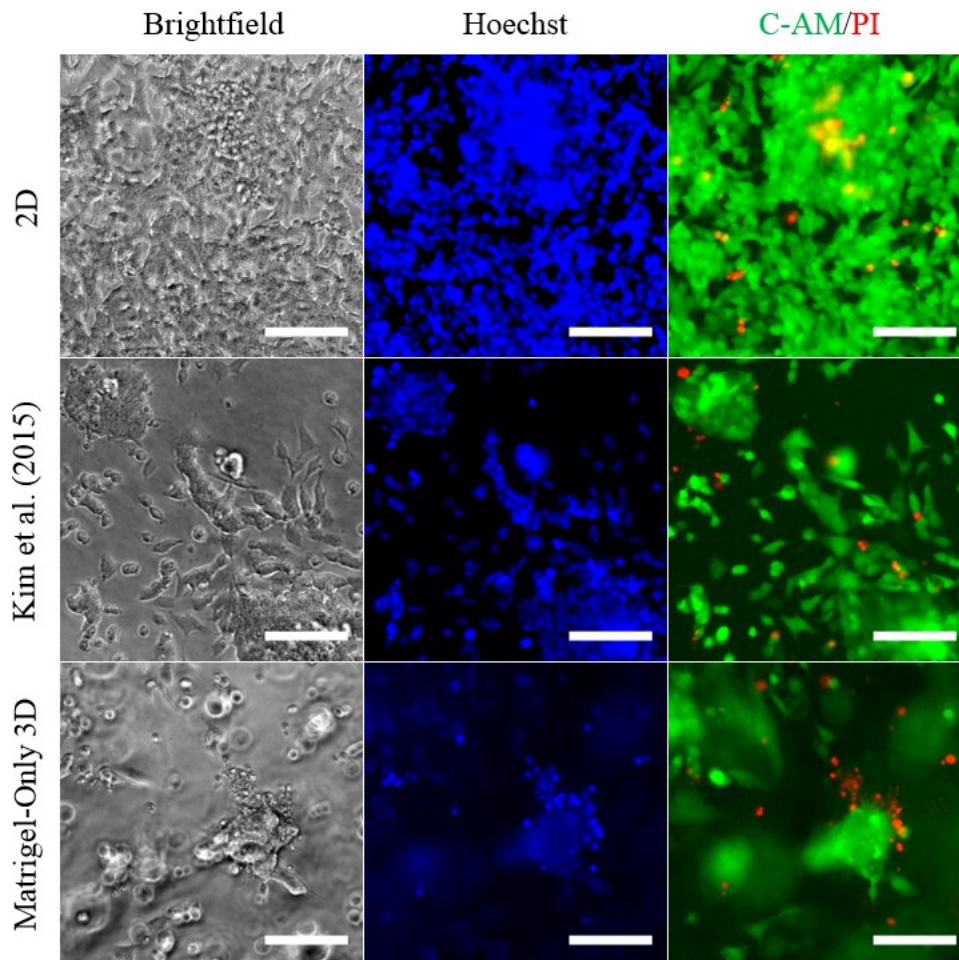


Figure 13 Representative images (10X) of undifferentiated SH-SY5Y cells grown under three growth conditions (2D, Kim et al. method, and Matrigel-only 3D method) on treated plates. Scale bar = 100 μm .

RA/BDNF-Differentiated SH-SY5Y Cells Grown on Treated Plates (Figure 14)

Hoechst staining revealed more widely spread nuclei and a reduction in cell number across all growth conditions compared to undifferentiated cells grown on treated plates (Figure 13). No discernible differences could be observed between 2D and Kim et al. 3D-grown differentiated SH-SY5Y cells. Cells appeared to grow on one plane in both platforms. In contrast, differentiated SH-SY5Y cells grew throughout the Matrigel-only 3D culture model. N-type cells grew long neurites that spread and infiltrated the gel. However, C-AM/PI staining revealed numerous S-Type cells across all growth platforms using treated plates. RA/BDNF differentiation was also observed to potentially have an impact on S-type cell morphology. In undifferentiated cultures (Figure 13), discernible S-type cells appeared smaller and rounder. Following RA/BDNF differentiation, S-type cells appeared to flatten and expand to cover a greater surface area.

Encinas et al. reported that RA treatment in complete medium followed by BDNF treatment in serum-free medium reduced S-type populations (139). Here, S-type cells remained quite prevalent. Medium changes may not have completely cleared FBS from the wells. To reduce S-type expression and select for N-type populations, reducing FBS in RA medium may be an option. However, this was discovered to be unnecessary in 3D conditions that minimize cellular adherence to the plate.

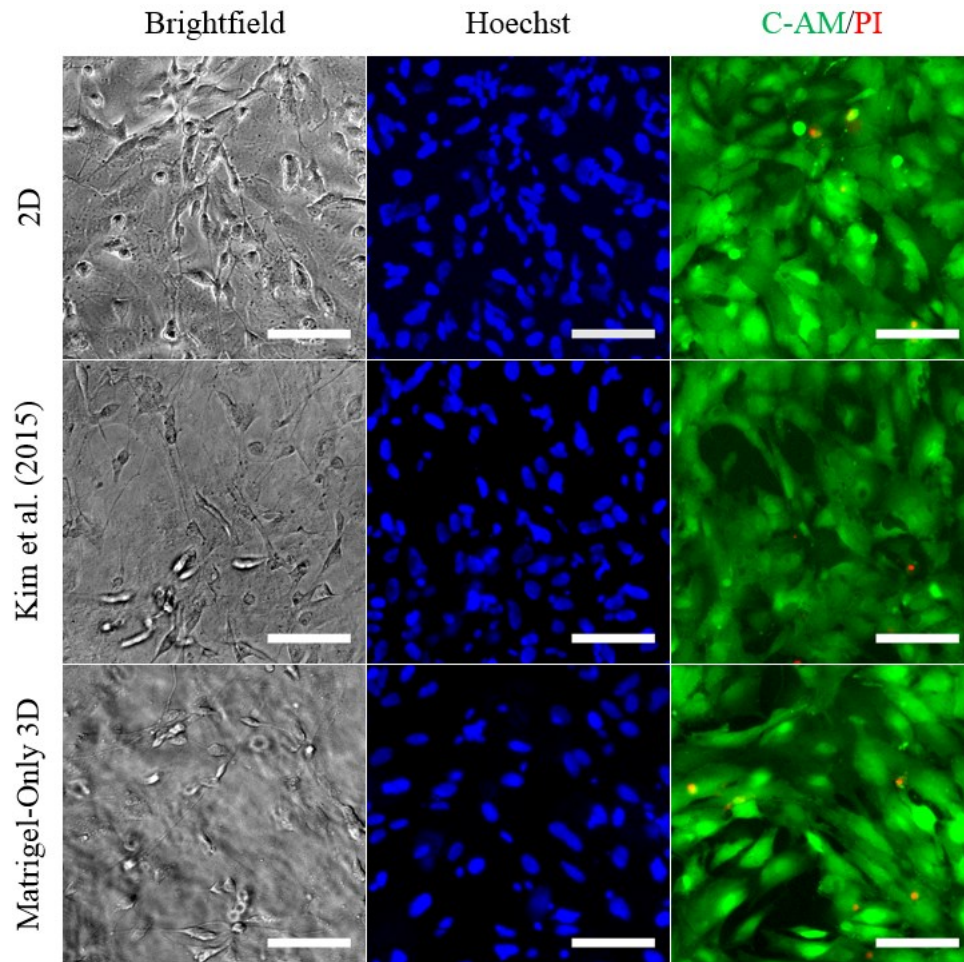


Figure 14 Representative images (10X) of RA/BDNF differentiated SH-SY5Y cells grown under three growth conditions (2D, Kim et al. method, and Matrigel-only 3D method) on treated plates. Scale bar = 100 μ m.

Undifferentiated SH-SY5Y Cells Grown on Untreated Plates (Figure 15)

Growing undifferentiated cells on untreated plates produced viable cells across all culture methods as shown by C-AM/PI staining (Figure 15). I expected poor cell adhesion in 2D cell culture, but cells survived and adhered to the untreated plate. Proteins in the FBS of the complete medium may have been sufficient to promote cell adhesion to the polystyrene despite the hydrophobicity of the plastic. However, undifferentiated cells grown in 2D culture on untreated plates were more prone to aggregating than 2D cultures grown on

treated plates suggesting poorer adhesion to the plastic surface (Figure 13). SH-SY5Y cells grown using the Kim et al. method grew similarly to their treated plate counterparts and were morphologically identical to 2D culture conditions grown on untreated plastic. S-type cells were present in both treated and untreated plates in the 2D and Kim et al. 3D platforms. The Matrigel-only 3D culture method produced similar aggregates and rounded cell morphologies between treated and untreated plates, but S-type cells were no longer detectable within these cultures.

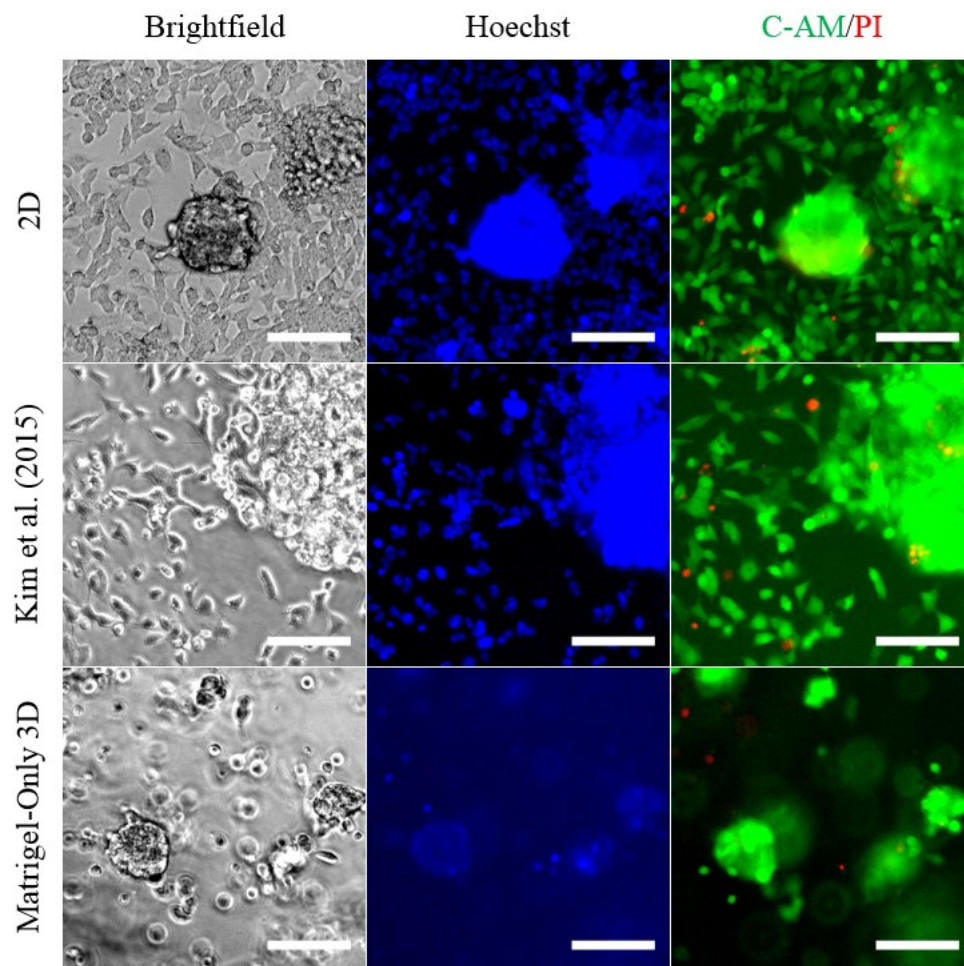


Figure 15 Representative images (10X) of undifferentiated SH-SY5Y cells grown under three growth conditions (2D, Kim et al. method, and Matrigel-only 3D method) on untreated plates. Scale bar = 100 μ m.

RA/BDNF-Differentiated SH-SY5Y Cells Grown on Untreated Plates (Figure 16)

Finally, RA/BDNF-differentiated SH-SY5Y cells grown on untreated plates using standard 2D culture and Kim et al. 3D culture appeared identical to their corresponding treated plate conditions (Figure 14). C-AM/PI showed good cell viability in 2D and Kim et al. 3D conditions but also revealed considerable S-type expression within both platforms. In contrast, S-type cells were no longer detectible in Matrigel-only 3D culture, similar to what was observed in the ATPS-Matrigel 3D culture platform grown on untreated plates. Only small N-type cells with extended neural processes could be identified throughout the gel. Using untreated plates with the Matrigel-only 3D culture method was sufficient to promote selective N-type cell growth within the gel, which could not be achieved by the Kim et al. 3D culture method.

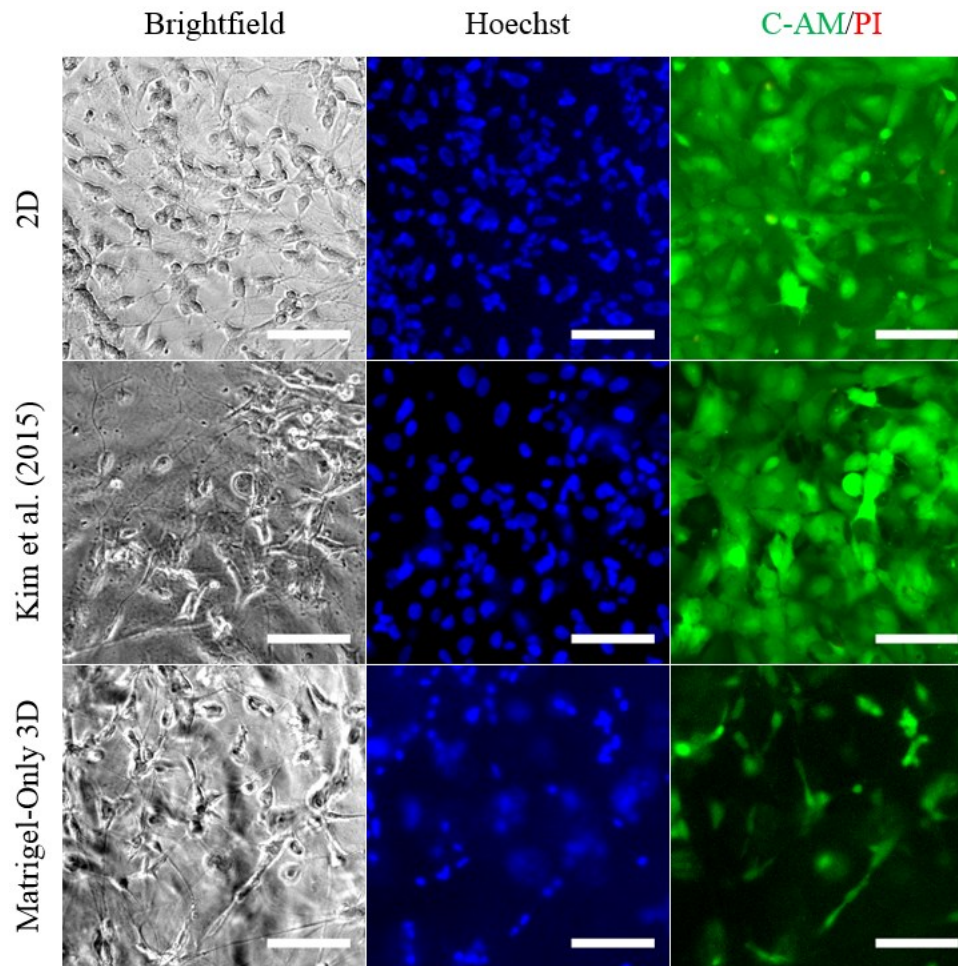


Figure 16 Representative images (10X) of RA/BDNF differentiated SH-SY5Y cells grown under three growth conditions (2D, Kim et al. method, and Matrigel-only 3D method) on untreated plates. Scale bar = 100 μ m.

3.3.4. The RA/TPA Differentiation Protocol

As previously discussed in Chapter 1, RA/TPA is the second most popular differentiation technique after RA (130). This method was reported as a way to direct SH-SY5Y cells towards the DAergic neuronal phenotype (127). However, early attempts at growing cells using this differentiation protocol under standard 2D culture conditions did not appear promising (results not shown). RA/BDNF-differentiated cells produced long extended processes and appeared more like neurons while RA/TPA-differentiated cells had shorter

projections with greater morphological similarity to undifferentiated cells. RA/TPA-differentiated cells also appeared to have poorer cell viability compared to RA/BDNF-differentiated cells. After initially shelving the RA/TPA differentiation method, I decided to return to it and test the impact of Matrigel-only 3D culture on RA/TPA-differentiated SH-SY5Y cells. RA/TPA differentiation reduced cellular aggregation and some neural processes could be observed in 2D cell culture (Figure 17). However, when RA/TPA-differentiated cells were grown under Matrigel-only 3D culture conditions, aggregates with very limited neurite extension were observed.

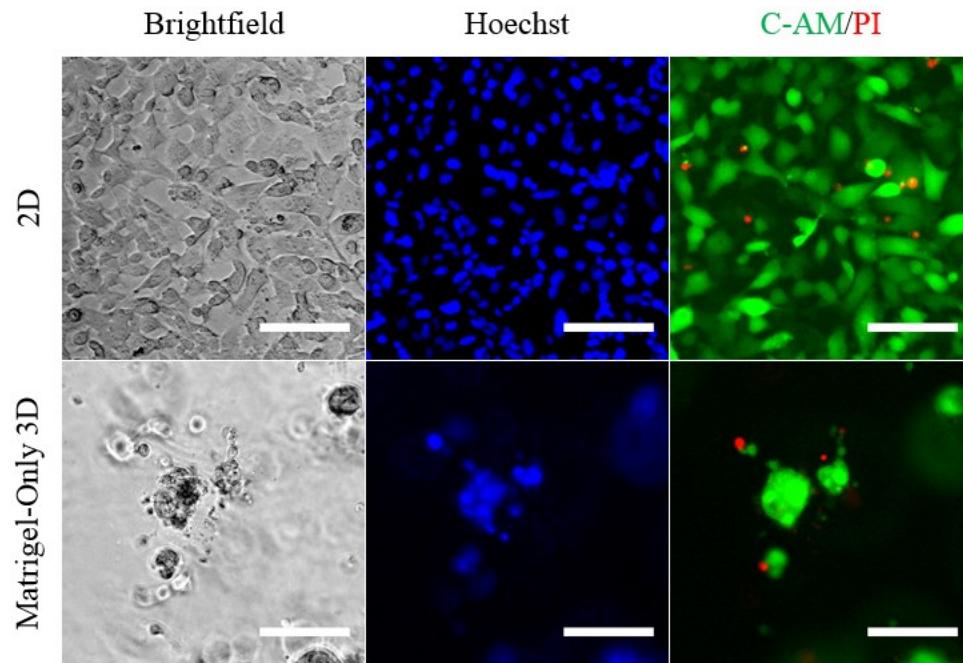


Figure 17 Representative images (10X) of RA/TPA differentiated SH-SY5Y cells grown under two growth conditions. 2D cultures were grown on treated plates and Matrigel-only 3D cultures were grown on untreated plates. Scale bar = 100 μ m.

3.4. Discussion

3.4.1. ATPS-Matrigel 3D Culture vs. Matrigel-Only 3D Culture

In this chapter, I presented two feasible and accessible methods for performing thin-layer 3D cell culture. Both methodologies showed excellent cell viability supported by strong C-AM expression and weak PI staining. Both platforms appeared to show preferential N-type cell growth within the 3D gel space when untreated plates were used. It is unknown if the S-type cells simply expressed more condensed morphologies within the 3D environment or potentially shifted towards the N-type phenotype. The dual cell populations within SH-SY5Y have not been well characterized. The 3D environment may select against S-type cells, but C-AM/PI staining did not appear to indicate loss in cell viability within 3D-UT cultures compared to the other culture platforms. Further characterization of the SH-SY5Y cell line would need to be performed to assess for biochemical differences between N- and S-type cells and potential for shifting phenotypic expression. Alternative protocols (standard 2D and Kim et al. 3D culture methods) performed on treated and untreated plates promoted cellular adherence to the plastic and both N-type and S-type cell expression. The untreated plate condition could not eliminate cellular adherence to the well surface in the Kim et al. 3D culture platform. These results suggest that growth environment and culture method have significant impacts on cell growth and morphology in undifferentiated and differentiated SH-SY5Y cultures.

The first and initially only model developed over the course of this thesis was the ATPS-Matrigel 3D culture method. This technique produced viable 3D cell cultures in a 96-well plate format. Using the ATPS-Matrigel 3D culture protocol, $76 \pm 24 \mu\text{m}$ thick cell-laden

hydrogels could be generated using merely 5 μ l of M+D10 solution. A single 10-ml bottle of Matrigel could readily produce >3300 samples in the 96-well format and far more if scaled to the 384-well format. However, the ATPS-Matrigel 3D culture method's unique non-adherent characteristic could be slightly more difficult to manage. Medium changes would shift and sometimes flip the gel if the flow of medium during aspiration or dispensing was too forceful. With practice, I eventually grew accustomed to gentler and more controlled pipetting habits when handling ATPS-Matrigel 3D cultures. Our electronic multichannel pipette that could control dispensing speed facilitated media changes throughout these experiments. Of course, liquid handling robotics would likely further improve performance and minimize gel shift. Despite the added learning curve, the non-adherent feature of this platform could be useful. Moraes et al. designed a high-throughput hydrogel system aimed at assaying contractility of microscale type I collagen gels (92). As contraction assays work best when not adhered to a surface, the investigators used shear force to dislodge the gels from the plate (92). Here, the ATPS-Matrigel 3D culture method provides naturally non-adherent gels. This technique can be readily scaled to a 384-well plate format to form microscale non-adherent gels for high-throughput contraction assessment. The Frampton lab has proceeded to move in this direction (96-well plate format for now). We will be using this platform to characterize contractility in human bronchiole smooth muscle cells (CC-2576; Lonza) for future assessment of asthma treatments in healthy and asthmatic 3D cell cultures.

The Matrigel-only 3D method provides an alternative thin-layer 3D cell culture platform. A minimum of 20 μ l of 5 mg/ml Matrigel solution was required to cover the surface of a

well in a 96-well plate. Therefore, a 10-ml bottle of Matrigel could produce >700 samples based on the 96-well plate format. This is less than the ATPS-Matrigel 3D culture method, but higher than standard Matrigel protocols where large quantities of the material are dispensed directly into air and suffer from high air-liquid interfacial tension and evaporation. Based on the Matrigel platform characterizations in Chapter 2, 20 μ l likely produces gels that are slightly thinner than $457 \pm 28 \mu\text{m}$ (microbeads may not have completely settled at the time these measurements were taken). This technique produces thicker gels than the ATPS-Matrigel 3D method. However, the Matrigel-only 3D culture protocol is much simpler to perform, does not require additional polymer compounds, and provides adherent gels that are easier to handle and feed. These features also accommodate for the lower sample yield when compared to the ATPS-Matrigel 3D culture method. While the ATPS-Matrigel 3D culture method is a very promising and powerful technique, further exploration and characterization of its features will need to be performed. Therefore, the Matrigel-only 3D culture method was ultimately selected for subsequent investigation of the application of 3D culture technologies for the field of PD research and pharmaceutical development.

3.4.2. The Kim et al. (2015) Method

During the assessment of SH-SY5Y cell growth under various culture platforms, Kim et al.'s thin-layer 3D culture method could not eliminate the S-type phenotype regardless of plate treatment. Cells likely fell to the bottom of the plate faster than the super diluted ECM protein could resolve into a stable protein layer. From there, the SH-SY5Y cells would be able to sense the stiff substrate regardless of the formation of an overlaying thin 3D gel.

Overall, the Kim et al. 3D culture method did not appear 3D. Cells grew on a single plane and were morphologically identical to 2D cell cultures.

Since the Kim et al. 3D culture method was developed only 2 years ago, limited work to replicate their thin-layer 3D culture modelling strategy outside of that group has been reported. However, I did encounter one article that took advantage of this technique while using a considerably lower cell densities (162). This group used a 1:15 Matrigel dilution in 96-well and 384-well plate formats to grow iPSCs into models of human cortical neurons that presented tau aggregation. The addition of Matrigel was included to protect against shear stress during medium changes and potential detachment and loss of cells. However, there is little discussion into the features of 3D cell culture within the bulk of the study. In fact, the word “three-dimensional” appears only four times in the full paper: once in the title, another in the key words, once in the introduction, and once in the bibliography citing the Choi et al. paper (79) that originally used the thin-layer 3D technique described by Kim et al. (80). Therefore, it is unclear if cells grew as 3D cells-embedded-in-gel cultures or were adhered to the plate with an overlaying protein coating. The coating may have promoted tau aggregation and protected the cells from shear forces during media changes. Since the main goal of that study was to generate a high-throughput tauopathy model, the 3D aspect was not a key focus and therefore not explored. Based on my observations, providing a thin Matrigel layer is not sufficient to minimize the impacts of stiff substrates on cell growth and differentiation.

As previously mentioned, primary neurons prefer growing on soft substrates and have reduced neuritic branching and slower cell growth on stiff substrates (22, 26). Alternatively, astrocytes prefer growing on stiffer substrates but also express higher levels of cellular stress and reactivity when grown on hard plastic (22, 25). Ignoring the impacts of substrate stiffness may confound or significantly influence experimental results and interpretation. I would propose that the Kim et al. technique provides a 2.5D stacked cell culture model (similar to aggregate culture except adherent to a plastic surface) rather than a cells-embedded-in-gel 3D culture model. With high enough cell densities, cells would grow on top of the adherent underlying cell layer to form a “3D” cell culture. An overlaying thin gel may be present that may promote some neurite infiltration over time, but it is difficult to identify. Nonetheless, the increased dimensionality in the Kim et al. 3D culture platform would certainly provide additional complexity and perhaps better mimic neuropathology in AD than a simple monolayer.

CHAPTER 4: HIGH-THROUGHPUT NEUROTOXICITY ASSAYS

4.1. Rationale

Various factors are involved in PD neuropathology and disease progression. Attempts to model these features in the laboratory have involved manipulating genetic expression and/or inducing DAergic cell death using neurotoxins and pesticides. Neurotoxin models are very common because DAergic cell death and subsequent motor symptoms associated with PD appear quite rapidly compared to genetic models, which can take longer and are costlier to produce. Here, I will be presenting three toxins that have been previously used in PD research to investigate the impacts of mitochondrial dysfunction, ER stress, and proteasome inhibition on DAergic cells. MPP⁺, as previously described in Chapter 1, is a neurotoxin that selectively targets DAergic neurons and impairs ATP production, resulting in cell death. It is one of the most common neurotoxins used to emulate PD features in animal models and cell culture. Tunicamycin (Tn) is a well-known ER stress inducer. The toxin functions by blocking N-linked glycosylation leading to the unfolded protein response and subsequent cell death. In recent years, Tn has been used to model PD in medaka fish and rats (*163, 164*). In both species, selective DAergic cell death and locomotor impairment were observed (*163, 164*). In the medaka fish model, α -synuclein-rich aggregation could be observed (*163*) while the rat model revealed increased α -synuclein oligomer formation (*164*). Both features are commonly associated with Lewy body formation in PD. Finally, epoxomicin (Epo), is a potent proteasome inhibitor. In 2004, McNaught et al. observed that Epo treatment over the span of 2 weeks was sufficient to induce significant locomotor dysfunction, generate α -synuclein-containing

aggregates, and promote selective DAergic cell death in the substantia nigra of rats (165). These findings were eventually replicated in medaka fish with similar results (166). However, attempts by Kordower et al. to replicate PD neuropathological symptoms in rats and monkeys failed using identical methodologies, so there is controversy regarding the use of Epox as a reliable PD modelling technique (167). Nonetheless, I decided to assess MPP+, Tn, and Epox to determine if each targeted system would have differential impacts on undifferentiated vs. RA/BDNF-differentiated SH-SY5Y cells cultured in 2D and 3D growth environments. Here, I wanted to assess the application of the Matrigel-only 3D culture method as a high-throughput screening device for PD research.

4.2. Methodology

4.2.1. SH-SY5Y Neurotoxicity Assay

SH-SY5Y cells were divided into three growth conditions (Figure 18). Cells were grown under standard 2D cell culture conditions (2D), grown in 2D cell culture but with a layer of Matrigel coated above the cells (2D-M) to simulate mass transport experienced by cells in the 3D growth condition, or grown embedded in a gel using the Matrigel-only 3D culture platform (3D). Both 2D cell culture conditions (2D and 2D-M) were grown on treated plates to promote cell adherence to the plastic while the 3D cell culture condition used untreated plates to minimize cellular adherence to the stiff substrate.

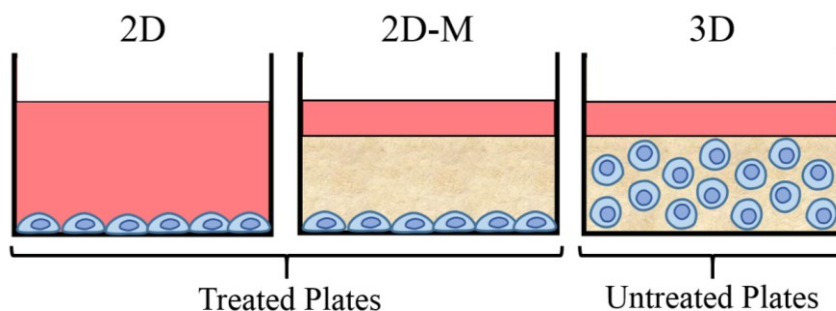


Figure 18 Growth environment conditions for neurotoxicity assays.

Standard 2D cell cultures (2D) and 2D cell cultures covered with a layer of Matrigel (2D-M) were grown on treated plates to promote cell adherence to the plate. Matrigel-only 3D-grown cells were seeded in untreated plates (3D) to promote selective cell growth within the gel.

The 2D cell culture condition experienced some slight modifications to its original protocol (section 3.2.6.) because it was used as a control for the new 2D-M condition. SH-SY5Y cells were passaged and divided into two separate tubes for 2D-based (2D and 2D-M) and 3D conditions. Once cells were pelleted, cells assigned to the 2D and 2D-M conditions were resuspended in warm complete medium. SH-SY5Y cells were dispensed at 70 μl /well into room temperature treated 96-well plates and stored in the 37 °C incubator overnight. Cells assigned to the 3D condition followed the Matrigel-only 3D culture protocol described in section 3.2.9. Briefly, ice cold cell-laden Matrigel was dispensed into chilled untreated 96-well plates containing 70 μl /well of complete medium. Plates were left on ice for 1 min followed by overnight incubation at 37 °C. SH-SY5Y cells were seeded at 1.6×10^4 cells/well for all growth conditions.

The following day, a 5 mg/ml Matrigel solution was prepared with complete medium. 2D-grown cells were removed from the incubator and placed on ice. The warmed complete medium was replaced with 70 μl /well chilled complete medium for both 2D and future 2D-

M conditions. The 5 mg/ml Matrigel solution was dispensed at 20 μ l/well onto 2D-M conditions. The 2D and 2D-M plates were left on ice for 1 min and then transferred to the incubator. 2D and 2D-M conditions were incubated at 37 $^{\circ}$ C for 30 min to induce gel formation. Complete medium was replaced for all plates (2D, 2D-M, and 3D) with the assigned medium for each differentiation condition (undifferentiated or RA/BDNF-differentiated) (Figure 19). Medium was replaced every 2-3 days for both differentiation protocols.

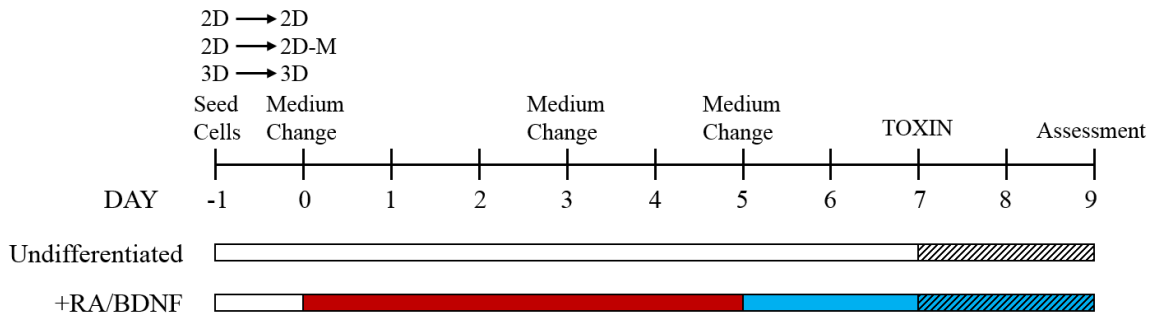


Figure 19 SH-SY5Y growth and differentiation protocols for neurotoxicity assays.

Matrigel (M) is added to one of the 2D cultures to produce the 2D-M growth condition. White bars (\square) indicate SH-SY5Y complete medium. Red bars (\blacksquare) indicate RA treatment. Blue bars (\blacksquare) indicate serum-free BDNF treatment. Hatched lines (///) indicate the addition of a toxin to the medium of each differentiation protocol.

Stock toxin solutions of 100 mM MPP⁺ in dH₂O, 1 mg/ml Tn (Sigma-Aldrich) in ultra-pure grade dimethyl sulfoxide (DMSO; Amresco), and 1 mM Epox (Millipore Sigma) in DMSO were prepared in advance. To assess MPP⁺, 0.1 mM, 1 mM, and 5 mM MPP⁺ working toxin solutions were prepared in either complete medium or differentiation medium. On day 7, SH-SY5Y cell culture media for all samples were replaced with MPP⁺ working toxin solutions as depicted in Figure 19. One row of undifferentiated cells and one row of RA/BDNF differentiated cells were provided with their corresponding media without MPP⁺ as control conditions. Cells were left in their corresponding treatment

conditions for 48 h. The 2-day incubation period was performed to accommodate for potentially slower mass transport in 2D-M and 3D cell cultures. On the final day, cell viability was assessed and is described below. Each unique combination of growth condition, differentiation protocol, and toxin concentration contained 6 well repeats (Figure 20). This neurotoxin assay protocol was replicated three times for MPP+.

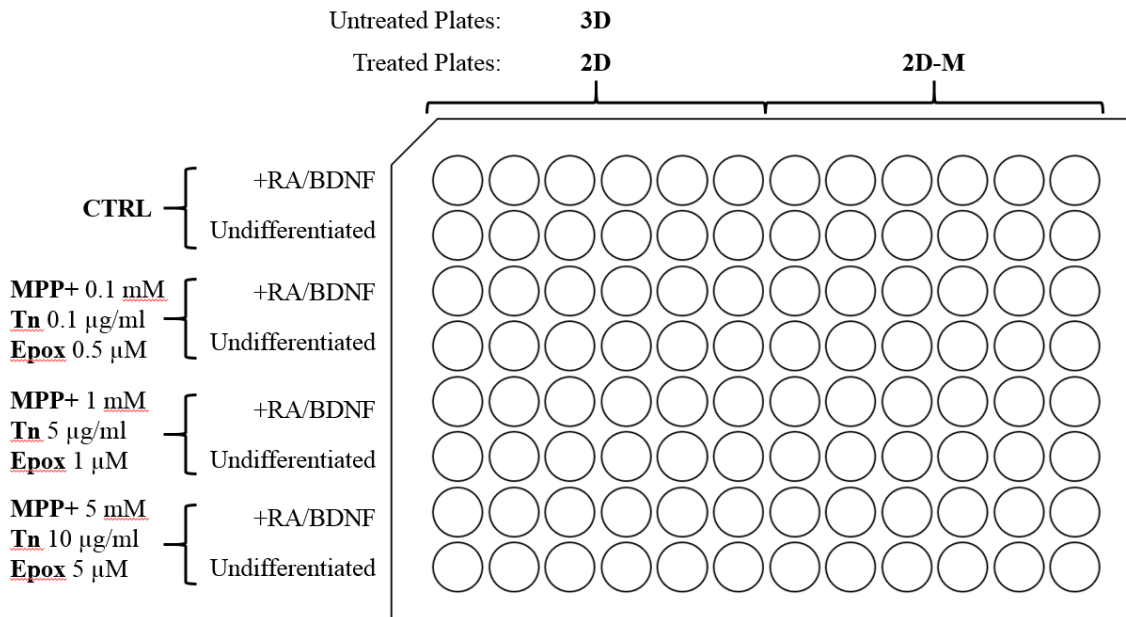


Figure 20 Schematic of 96-well plate neurotoxin assay layout.

Three growth conditions (2D, 2D-M, and 3D), two differentiation protocols (RA/BDNF differentiated vs. undifferentiated), and three toxins (MPP+, Tn, and Epox) with three concentrations for each toxin were assessed. Control (CTRL) conditions did not receive toxin treatment.

The neurotoxin assay protocol used for MPP+ was repeated with Tn and Epox separately. To assess Tn, 0.1 µg/ml, 5 µg/ml, and 10 µg/ml Tn were prepared in either complete medium or differentiation medium. Likewise, to assess Epox, 0.5 µM, 1 µM, and 5 µM Epox were prepared in complete medium or differentiation medium. A minor adjustment to the MPP+ neurotoxin protocol involved the addition of DMSO to lower concentrated Tn

and Epox solutions and control media to accommodate for differences in DMSO levels across prepared working solutions. The most concentrated Tn and Epox solutions contained the highest amounts of DMSO. While these levels were considered to have negligible impact on cell viability, I decided to control for their potential impact by equalizing DMSO amounts across all conditions. Once all Tn or Epox treatments were prepared, media was replaced with toxin solutions and maintained for 2 days before cell viability assessment. Three experimental replicates were completed for Tn and Epox each.

4.2.2. Cell Viability Assessment

To assess cell viability, cells were subjected to C-AM, PI, and Hoechst staining as detailed in section 3.2.10. Briefly, 3 μ M C-AM, 3 μ M PI, and 1:2000 Hoechst (C-AM/PI/Hoechst) were prepared in warm serum-free medium (DMEM+1% ABX). Toxin working solutions and control media were removed from all samples, and 70 μ l/well of C-AM/PI/Hoechst solution was added. Cells were incubated in a humidified, 37 °C, 5% CO₂ environment for 30 min. Representative images of all unique condition combinations were captured using a Nikon Eclipse T1 Epifluorescence Microscope. Following imaging, 50 μ l of solution was removed from each well using a standard multichannel pipette. Defrosted room temperature CellTiter-Glo® 2.0 Assay (Promega) solution was dispensed into each well at 50 μ l/well. Plates were initially agitated by hand and transferred to a FilterMax F5 plate reader. Five seconds of vigorous orbital shaking was pre-programmed into the read settings of the plate reader to lyse the cells. Plates were read three times (three sessions of vigorous orbital shaking) with the final luminescent reading taken for quantification. The third reading was taken following >10 min room temperature incubation in CellTiter-Glo.

4.2.3. LUHMES Cell Culture

LUHMES cells (CRL-2927; ATCC) were cultured as per ATCC guidelines. Briefly, frozen LUHMES cells were thawed and plated on vented T-75 cm² culture flasks pre-coated with 50 µg/ml poly-L-ornithine (PLO; Sigma-Aldrich) and 1 µg/ml fibronectin (FIB) from human plasma (Sigma-Aldrich). Cells were maintained in LUHMES complete medium containing DMEM/F12 (ATCC) supplemented with 1% N-2 Supplement (Gibco), 40 ng/ml human recombinant basic fibroblast growth factor (bFGF; Z101456; ABM), and 1% ABX. The LUHMES complete medium was filter sterilized through a 0.2 µm syringe filter as recommended by ABM after addition of bFGF. Medium was changed every 2-3 days. Cells were sub-cultured every 3-4 days. To passage the cells, cultures were washed with 10 ml 1X sterile PBS and 4 ml diluted trypsin-EDTA (0.025% Trypsin/0.26 mM EDTA in 1X PBS) was added to detach the cells. Cells were incubated at 37 °C for 3 min. The flask was tapped to dislodge remaining adherent cells, and 6 ml LUHMES wash medium (DMEM/F12+1% N-2+1% ABX) was added. Cells were centrifuged at 0.2 rcf at 20 °C for 5 min to generate a pellet. Pellets were resuspended in warm LUHMES complete medium, triturated, and re-plated. To differentiate the cells, a separate LUHMES differentiation medium was prepared containing DMEM/F12, 1% N-2, 1 mM dibutyryl-cAMP (dbcAMP; Enzo Life Sciences), 2 ng/ml human recombinant glial cell line-derived neurotrophic factor (GDNF; Z101055; ABM), 1 µg/ml tetracycline hydrochloride (Sigma-Aldrich), and 1% ABX.

4.2.4. LUHMES Neurotoxicity Assay

Similar to the SH-SY5Y neurotoxicity assay described in section 4.2.1., three growth conditions (Figure 18) were assessed: 2D, 2D-M, and 3D. Here, cell density was also assessed. LUHMES cells have been previously plated between 2×10^4 cells/cm³ (154) and 2×10^5 cells/cm³ (157) for differentiation purposes. Therefore, I selected 1.6×10^4 cells/well (5×10^4 cells/cm³) and 5×10^4 cells/well (1.5×10^5 cells/cm³) as lower and higher cell seeding densities, respectively.

LUHMES cells were passaged and counted using the Countess II FL Automated Cell Counter. 2D and 2D-M cells were resuspended in warm LUHMES complete medium, and 70 μ l/well was dispensed into treated 96-well plates pre-coated with 50 μ g/ml PLO and 1 μ g/ml FIB at 1.6×10^4 cells/well or 5×10^4 cells/well. 2D and 2D-M plates (each growth condition was seeded on separate plates) were stored in the incubator. Chilled untreated 96-well plates were pre-filled with 70 μ l/well of LUHMES complete medium. 3D-grown cells were resuspended in ice cold LUHMES complete medium and mixed with Matrigel to form a cell-laden 5 mg/ml Matrigel solution. A handheld microchannel pipette was used to dispense 20 μ l/well of cell-laden Matrigel solution into the prepared untreated plates and incubated on ice for 1 min. The plate was then transferred to the incubator and stored at 37 °C overnight. The next day, 2D-M cells were prepared as previously described (section 4.2.1.). For 2D and 2D-M conditions, warm LUHMES complete medium was replaced with 70 μ l/well chilled LUHMES complete medium, and 20 μ l/well of 5 mg/ml Matrigel diluted with LUHMES complete medium was added to 2D-M conditions. Plates were kept on ice for 1 min and then incubated at 37 °C for 30 min. LUHMES complete medium was

then replaced with LUHMES differentiation medium for all growth conditions. The undifferentiated condition was not assessed in these set of experiments. The timeline of the differentiation protocol is displayed in Figure 21.

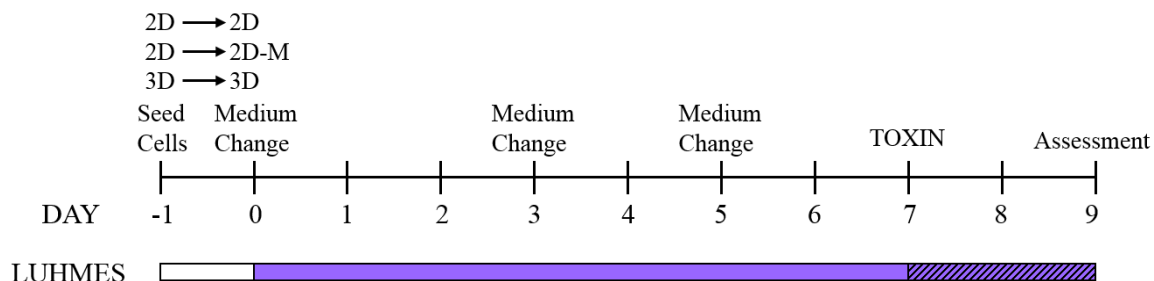


Figure 21 LUHMES differentiation protocol for neurotoxicity assays.

Matrigel (M) is added to one of the 2D cultures to produce the 2D-M growth condition. White bars (□) indicate LUHMES complete medium. Purple bars (■) indicate LUHMES differentiation medium. Hatched lines (▨) indicate the addition of a toxin to the differentiation medium.

On day 7 of the LUHMES differentiation protocol, MPP⁺ (0.1 mM and 5 mM), Tn (0.1 μg/ml and 5 μg/ml), and Epox (0.5 μM and 5 μM) toxin working solutions were prepared using LUHMES differentiation medium. Regular LUHMES differentiation medium was used as a control. Toxin working solutions were added (70 μl/well) and incubated for 2 days at 37 °C (Figure 22). On day 9, cell viability was assessed using the same protocol described in section 4.2.2. Here, each unique combination of conditions contained 4 well repeats. Due to time constraints, experimental replicates were not completed, so quantitative data remains to be assessed. Qualitative representative images will be shown here instead.

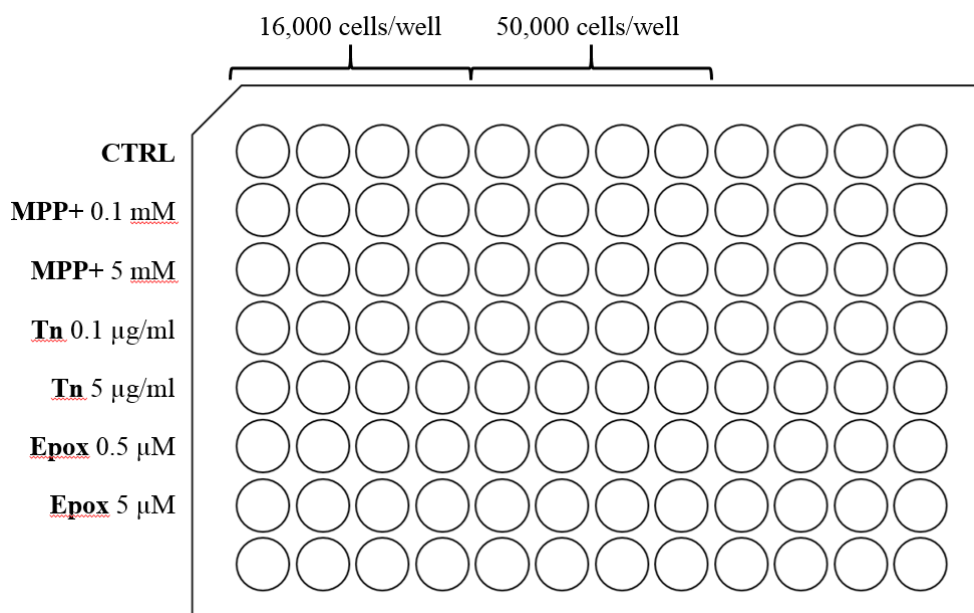


Figure 22 Schematic of 96-well plate neurotoxin assay layout for differentiated LUHMES cells.

Three growth conditions (2D, 2D-M, and 3D), two seeding densities (1.6×10^4 cells/well and 5×10^4 cells/well) and three toxins (MPP+, Tn, and Epox) with two concentrations for each toxin were assessed. Control (CTRL) conditions received regular LUHMES differentiation medium. Each growth condition was grown on a separate 96-well plate.

4.2.5. Statistical Analysis

Kruskal-Wallis analysis of variance (ANOVA) on ranks was conducted to compare the impacts of growth environment on toxin response for each differentiation protocol, toxin (MPP+, Tn, and Epox), and toxin concentration assessed followed by Tukey multiple comparison test using SigmaPlot statistical software. Quantitative data are represented as mean \pm SD. Statistical significance was defined as $*p < 0.05$.

4.3. Results

4.3.1. SH-SY5Y MPP+ Assay

MPP+ treatment was assessed across three growth environments (2D, 2D-M, and 3D) in undifferentiated and RA/BDNF-differentiated SH-SY5Y cultures. In control cultures that did not receive MPP+ treatment, all conditions appeared to generate healthy, viable cells as evidenced by C-AM/PI staining (Figure 23a). 2D-M-grown cells appeared similar to their 2D counterparts with mixed populations of adherent S-type and N-type cells at the bottom of the plate, but some cellular and neuritic infiltration into the overlaying gel could be observed in both undifferentiated and differentiated cells. This observation indicated that the 2D-M model was closer to the 2.5D Kim et al. (2015) culture method and was not an exclusively 2D cell culture. However, most cells adhered to the plastic, so the stiff underlying substrate would be expected to have an impact on cell behaviour and responsiveness to the toxin treatments akin to 2D culture conditions.

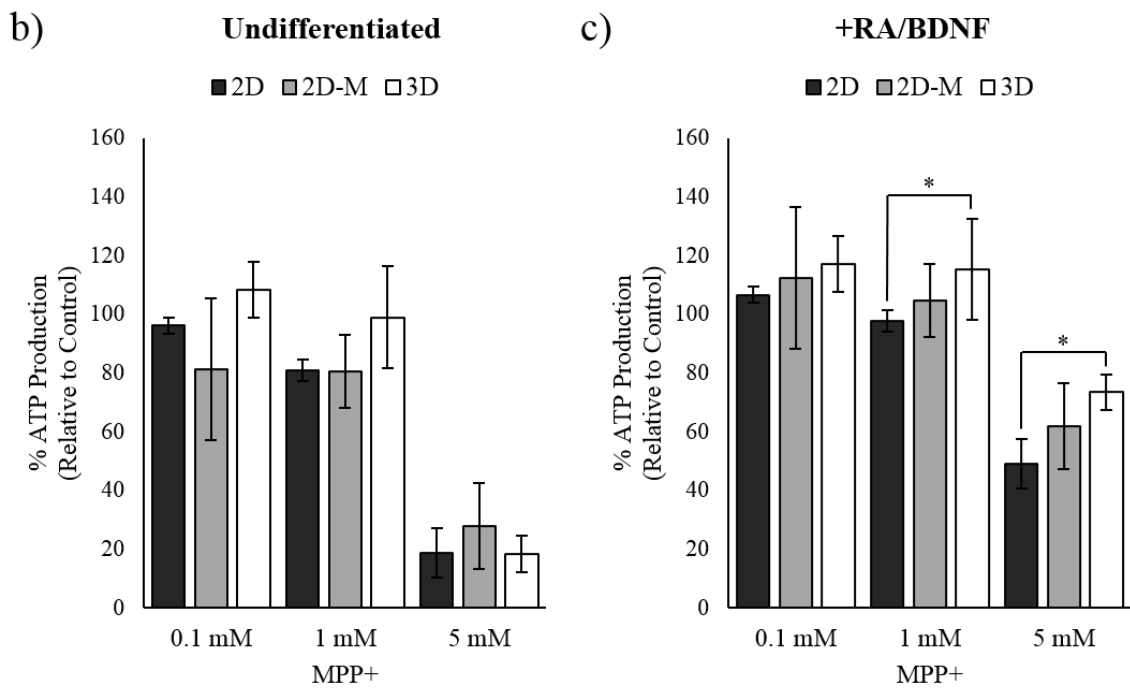
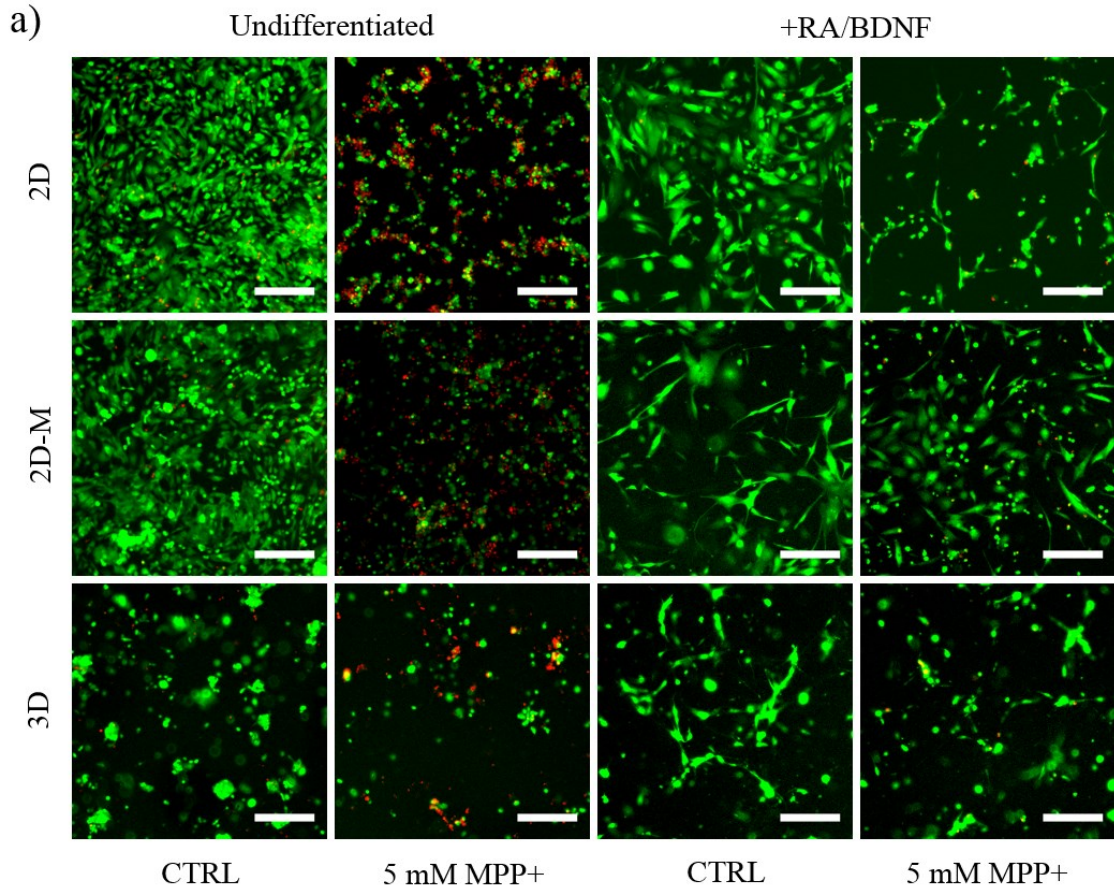


Figure 23 MPP⁺ toxicity in undifferentiated and RA/BDNF differentiated SH-SY5Y cells grown under three growth conditions (2D, 2D-M, and 3D) after 48 h treatment.

a) Representative images (4X) of C-AM (green-live)/PI (red-dead)-stained cells grown in control media or 5 mM MPP⁺. Scale bar = 200 μ m. **b)** ATP production of undifferentiated SH-SY5Y cells treated with MPP⁺. **c)** ATP production of RA/BDNF differentiated SH-SY5Y cells treated with MPP⁺. Data were normalized to their respective control conditions (no toxin media) and are expressed as mean \pm SD (n = 3; *p<0.05).

When cells were treated with 5 mM MPP⁺, undifferentiated cells showed greater PI expression across the different growth environments compared to differentiated cells. However, this could have been misleading due to inequivalent cell densities. Since undifferentiated cells continued to proliferate during the 9-day growth protocol, it was difficult to compare ratios of living to dead cells in undifferentiated vs. differentiated cells using qualitative C-AM/PI staining. Nonetheless, PI staining was quite low in differentiated cultures. However, differentiated SH-SY5Y cells appeared to shrink in size and retract their neural processes in response to 5 mM MPP⁺ treatment.

To quantitatively assess cell viability, CellTiter Glo was used to detect ATP production. Following chemiluminescent detection using the plate reader, results were initially expressed as relative light units (RLU). RLU's were normalized to each unique condition's respective control. For example, all 3D-grown, MPP⁺ treated, RA/BDNF-differentiated samples were represented as a percentage of the 3D-grown, non-MPP⁺ treated, RA/BDNF-differentiated, control condition within each experimental replicate. These results would therefore reflect the percentage of viable cells with respect to controls. The control conditions were assumed to have 100% cell viability. This was done to accommodate for

differences in cell number between undifferentiated and differentiated cell cultures and between growth environments as well.

In undifferentiated cells treated with MPP⁺, 0.1 mM and 1 mM (Figure 23b) MPP⁺ did not appear to induce a substantial decline in ATP production. While 3D cultures appeared to have higher cell viability than 2D and 2D-M conditions, this trend was not statistically significant. Overall, a range of 0-20% decline in cell viability was observed in undifferentiated cells treated with 0.1 mM and 1 mM MPP⁺ across 2D, 2D-M, and 3D growth environments. Only after administering 5 mM MPP⁺ was cell viability significantly reduced to ~20% relative to the control (~80% loss in ATP production).

Differentiated cells, however, displayed increased robustness against MPP⁺ toxicity (Figure 23c). With 5 mM MPP⁺ treatment, only ~20% of undifferentiated cells remained viable while cell viability was more than double (>40%) in differentiated cells. C-AM/PI-staining appeared to reflect these quantitative results. Very little visible red PI staining of dead cells can be observed at 5 mM MPP⁺ in RA/BDNF-differentiated cells. Lower concentrations of MPP⁺ did not appear to contribute to a reduction in ATP production and cell death across all growth environments. Rather, 0.1 mM and 1 mM MPP⁺ seemed to produce >100% cell viability, in some cases. This is likely evidence for the edge-effect where wells at the periphery of a well plate are exposed to greater thermal and evaporation gradients (168). Due to the layout of the high-throughput neurotoxicity assays (Figure 22), controls at the periphery of the plate were potentially influenced by these factors. C-AM and PI staining suggested control conditions remained highly viable, but future assessments

will benefit from assessing and accommodating for these potentially confounding factors. These experiments will likely need to be replicated with either randomized condition placements on plates and/or by filling the peripheral wells with sterile dH₂O to combat differential evaporative effects around the edges.

While growth environment appeared to have no discernible impact at the 0.1 mM concentration, 1 mM and 5 mM MPP⁺ revealed significant differences between 3D-grown and 2D-grown cells. RA/BDNF-differentiated 2D-grown cells displayed lower cell viability compared to 3D-grown cells suggesting that 3D growth conditions provided additional robustness to RA/BDNF-differentiated cells against MPP⁺. However, cell viabilities of 3D and 2D-M growth conditions treated with 1 mM and 5 mM MPP⁺ were not statistically different. 2D and 2D-M conditions treated with 1 mM and 5 mM MPP⁺ were also not statistically different. 2D-M culture was introduced to accommodate for potential mass transport differences in 3D culture. However, adding a layer of Matrigel to originally 2D-grown cells was observed to promote some 3D characteristics (cellular and neuritic infiltration into the gel). As a result, this 2.5D characteristic may have been reflected in 2D-M culture's middling tolerance to MPP⁺. Additionally, both undifferentiated and RA/BDNF-differentiated SH-SY5Y cells did not appear to be sensitive to MPP⁺ treatment, so small differences in cell viability between growth environments were not easily discernible with this toxin.

4.3.2. SH-SY5Y Tn Assay

Tn appeared to be quite potent in undifferentiated and differentiated SH-SY5Y cultures. Following 5 $\mu\text{g/ml}$ Tn, considerable PI staining was observed in both undifferentiated and differentiated conditions (with the exception of 3D-grown differentiated cells) (Figure 24a). Quantitative analysis of cell viability in undifferentiated cell cultures showed that 0.1 $\mu\text{g/ml}$ Tn was sufficient to decrease % ATP production to $\sim 80\%$ relative to control (Figure 24b). No statistically significant differences in cell viability between growth environments (2D vs. 2D-M vs. 3D) within each tested concentration of Tn (0.1 $\mu\text{g/ml}$, 5 $\mu\text{g/ml}$, and 10 $\mu\text{g/ml}$) could be identified in undifferentiated cell cultures.

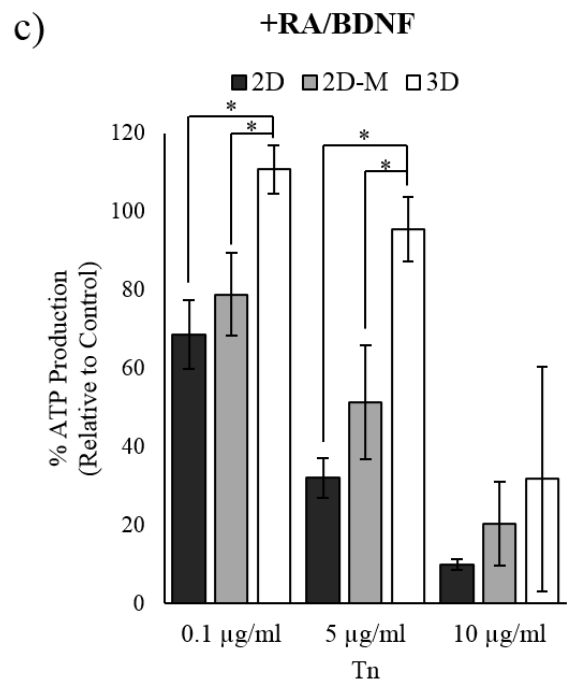
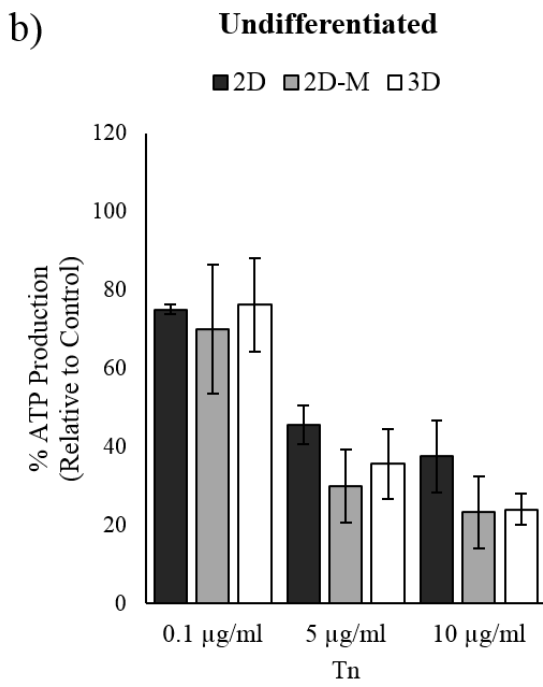
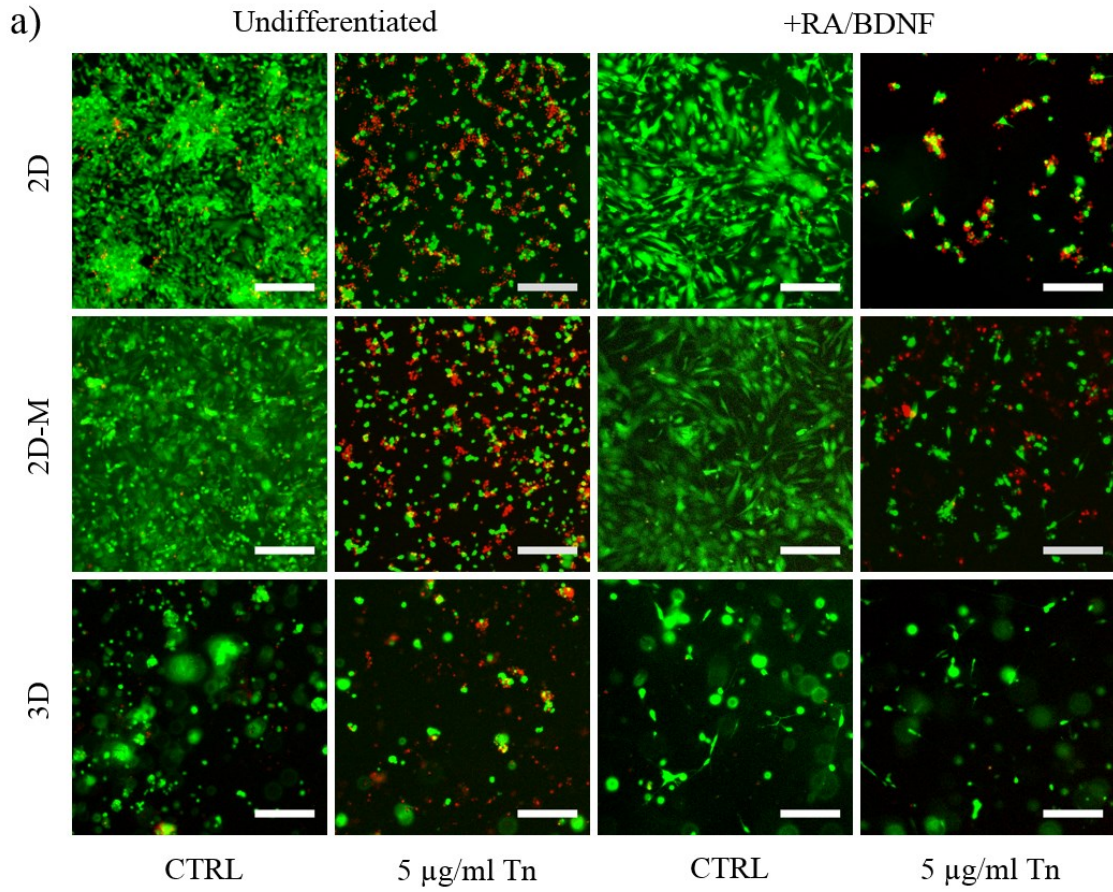


Figure 24 Tn toxicity in undifferentiated and RA/BDNF differentiated SH-SY5Y cells grown under three growth conditions (2D, 2D-M, and 3D) after 48 h treatment.

a) Representative images (4X) of C-AM (green-live)/PI (red-dead)-stained cells grown in DMSO control media (CTRL) or 5 $\mu\text{g/ml}$ Tn. Scale bar = 200 μm . **b)** ATP production of undifferentiated SH-SY5Y cells treated with Tn. **c)** ATP production of RA/BDNF differentiated SH-SY5Y cells treated with Tn. Data were normalized to their respective control conditions (no toxin media with vehicle DMSO) and are expressed as mean \pm SD (n = 3; *p<0.05).

In RA/BDNF-differentiated cultures, clear differences between growth environments can be observed (Figure 24c). When cultures were treated with 0.1 $\mu\text{g/ml}$ and 5 $\mu\text{g/ml}$ Tn, 3D-grown differentiated cells were significantly more robust against Tn toxicity compared to 2D and 2D-M conditions. No statistically significant differences between growth environments could be discerned at 10 $\mu\text{g/ml}$ Tn treatment possibly due to oversaturation of the toxin overriding the impacts of growth protocol. Curiously, 3D conditions appeared to follow an opposing trend to 2D conditions between undifferentiated and RA/BDNF-differentiated cultures. 2D undifferentiated conditions appeared more robust in response to Tn treatments compared to their differentiated counterparts. In contrast, 3D undifferentiated conditions appeared less robust in response to Tn treatment compared to their differentiated counterparts. 2D-M conditions, on the other hand, appeared to follow trends that lay between 2D and 3D (lower cell viability in undifferentiated conditions and higher cell viability in differentiated conditions compared to 2D-grown cultures).

4.3.3. SH-SY5Y Epox Assay

Finally, effects of Epox toxicity were examined. Similar C-AM/PI profiles to Tn treatment can be observed in Epox-treated culture platforms (Figure 25a). Epox induced nearly equivalent cell death across all growth environments and Epox concentrations in

undifferentiated SH-SY5Y cell cultures (Figure 25b). Lower Epox concentrations (0.5 μ M and 1 μ M) displayed statistically equivalent cell viabilities. A concentration of 5 μ M was required to significantly decrease undifferentiated cell viability across all growth environments. In contrast, RA/BDNF differentiation appeared to reduce sensitivity to the Epox toxin across all samples compared to their undifferentiated counterparts (Figure 25c). Here, 3D-grown differentiated cells expressed significantly greater tolerance to Epox at all tested concentrations compared to corresponding 2D and 2D-M conditions. No discernible differences between 2D and 2D-M conditions could be identified.

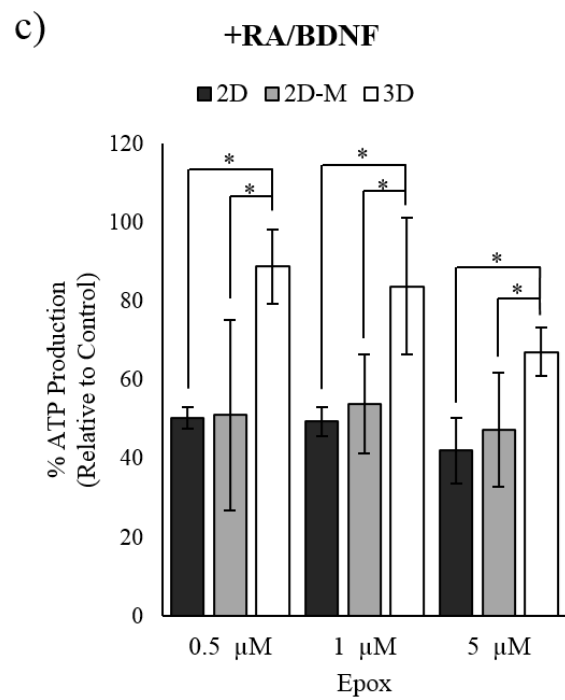
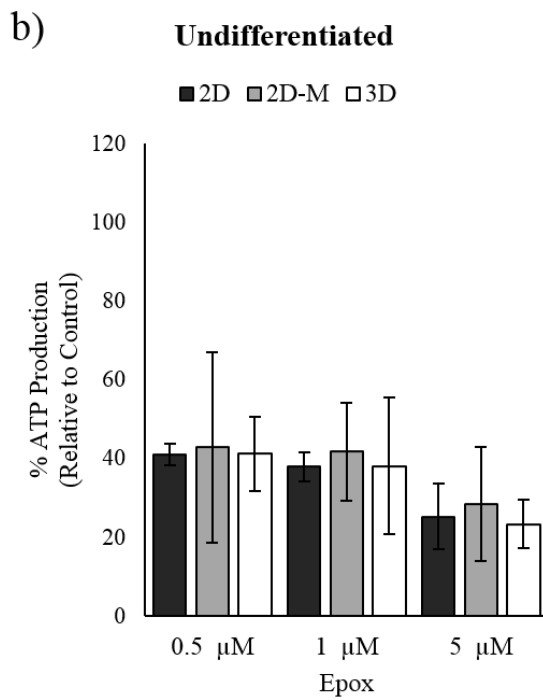
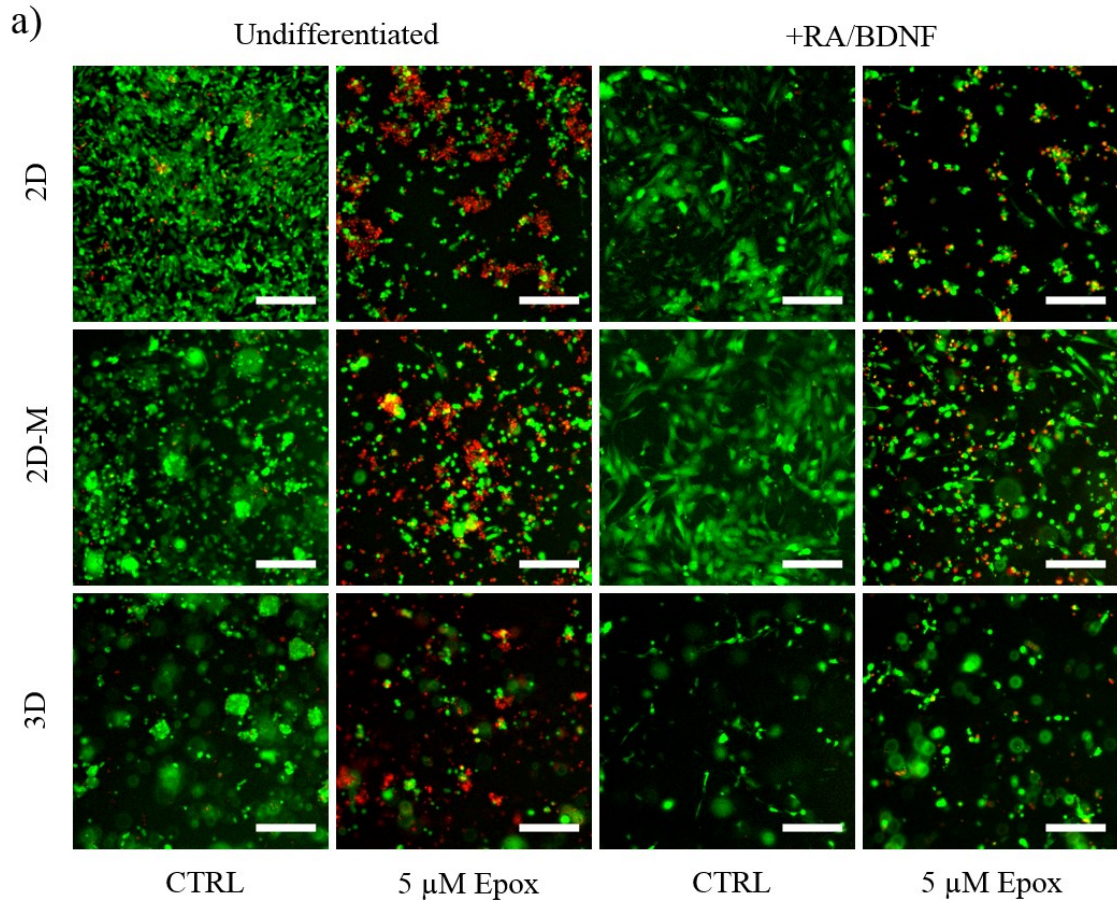


Figure 25 Epox toxicity in undifferentiated and RA/BDNF differentiated SH-SY5Y cells grown under three growth conditions (2D, 2D-M, and 3D) after 48 h treatment.

a) Representative images (4X) of C-AM (green-live)/PI (red-dead)-stained cells grown in DMSO control media (CTRL) or 5 μ M Epox. Scale bar = 200 μ m. **b)** ATP production of undifferentiated SH-SY5Y cells treated with Epox. **c)** ATP production of RA/BDNF differentiated SH-SY5Y cells treated with Epox. Data were normalized to their respective control conditions (no toxin media with vehicle DMSO) and are expressed as mean \pm SD (n = 3; *p<0.05).

4.3.4. LUHMES Cell Growth and Differentiation

Following the SH-SY5Y neurotoxin assay results, I recognized that the RA/BDNF-differentiated SH-SY5Y cell culture platform was not ideal for mimicking DAergic neuronal characteristics and modelling PD neuropathology *in vitro* using neurotoxin methodologies. The platform was too robust to perform as an accurate representation of the considerably more sensitive DAergic neurons. Therefore, I decided to pursue alternative DAergic neural models and assess if the Matrigel-only 3D culture platform could sustain other cell types and cell lines. The LUHMES cell line was selected for its DAergic qualities, human source, indefinite subculture, and its single neuronal phenotype. While these cells have previously been grown as 3D aggregate cultures (158), they have not yet been applied to hydrogel technologies.

Interestingly, growing LUHMES cells under 2D, 2D-M and 3D conditions produced fascinating gross morphological differences (Figure 26). Using standard 2D culture practices defined for LUHMES cells (PLO and FIB coating on plastic culture vessels), differentiated cells grew long extended neural processes but appeared quite condensed on the plate. When cell density was increased, cells seemed to retract from the plate to form aggregated cell bodies with extended neural processes attached to the walls of the well. In

2D-M cultures, cells spread throughout the well in a more web-like arrangement. At higher cell densities, 2D-M-grown cultures appeared to recognize the sides of the plate and curved around it rather than contracting into themselves. Under closer inspection, 2D-M conditions in both low and high cell densities contained long neuritic extensions that infiltrated profusely throughout the gel. Finally, 3D-grown cells were embedded within the gel and extended long, branching neural processes throughout the 3D construct. Only one neuronal phenotype was observed across all growth conditions.

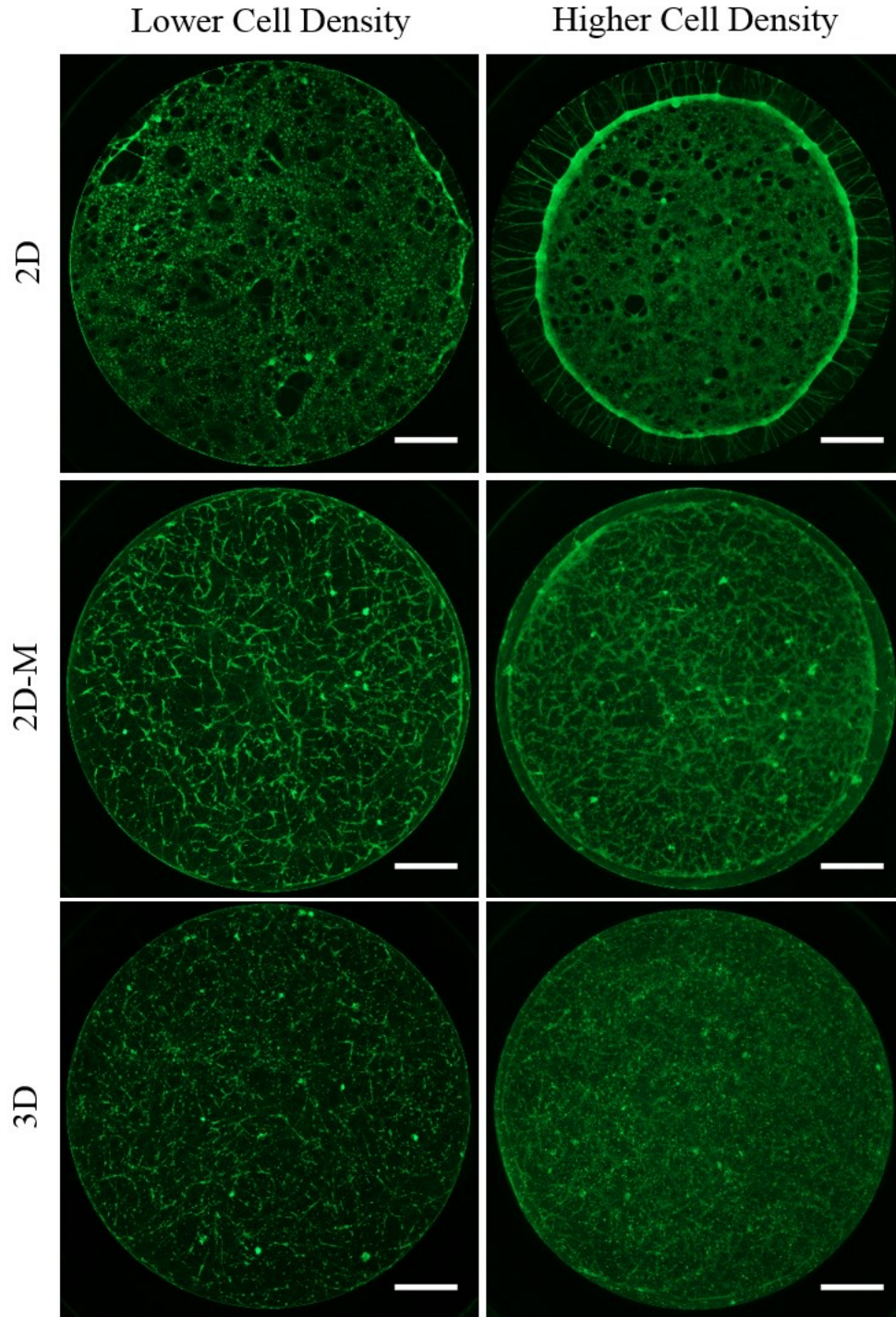


Figure 26 Gross morphological changes (2X) of C-AM-stained differentiated LUHMES cells in response to various growth conditions (2D, 2D-M, and 3D) and lower (initial seeding density: 1.6×10^4 cells/well) vs. higher (initial seeding density: 5×10^4 cells/well) cell densities. Scale bar = 1 mm.

4.3.5. Preliminary Responses of Differentiated LUHMES Cells to Neurotoxins

As quantitative exploration into assessing neurotoxin response in differentiated LUHMES cell cultures could not be completed, qualitative representative C-AM/PI images will be presented here instead. Compared to past RA/BDNF-differentiated SH-SY5Y cells, LUHMES cells displayed slightly more dead cells across all growth environments, as represented by PI staining. The addition of 0.1 mM MPP⁺ appeared to have an impact on LUHMES cell viability and morphology most evidently under 3D-grown conditions. The formerly long, smooth neurites faded in C-AM expression, retracted, and appeared kinked and rough following MPP⁺ treatment. Concentrations of 0.1 mM and 5 mM MPP⁺ increased PI staining in 3D culture conditions. In 2D and 2D-M conditions, it was difficult to identify changes to neurite characteristics at 0.1 mM due to the density of the neural projections. At 5 mM MPP⁺, neurite degradation and cell death in response to the toxin could be more clearly identified. In 2D conditions, the neurites appeared to disintegrate in response to 5 mM MPP⁺ while 2D-M and 3D conditions appeared unhealthy but intact.

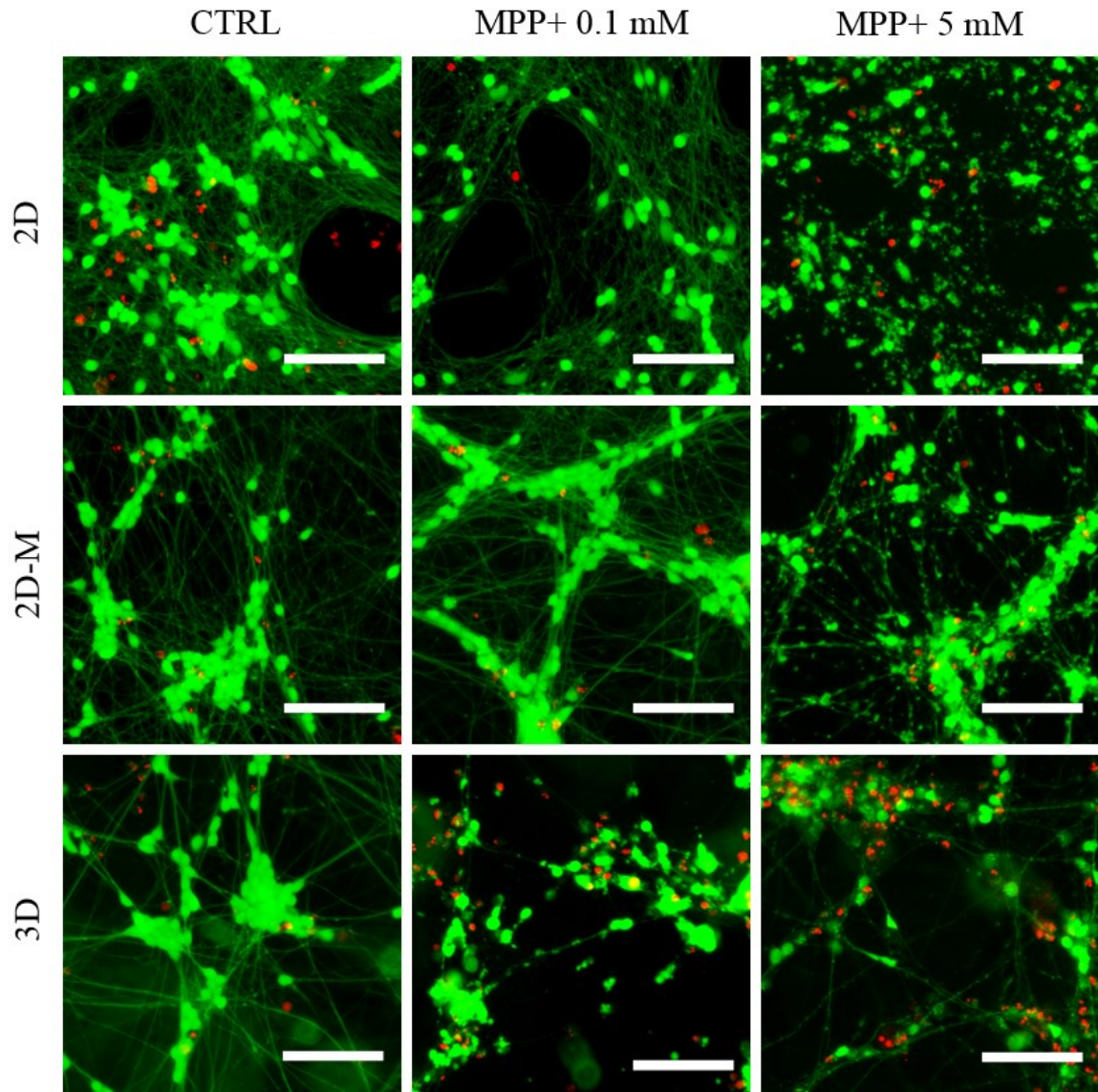


Figure 27 Representative images (10X) of C-AM (green-live)/PI (red-dead)-stained differentiated LUHMES cells grown at an initial seeding density of 1.6×10^4 cells/well in response to LUHMES differentiation medium (CTRL) and MPP+ treatment. Scale bar = 1 mm.

Epox and Tn also produced considerable cell death. Epox treatment was severely toxic to differentiated LUHMES cells. Most cells completely lost all neural processes across all growth environments at the lowest tested Epox concentration (Figure 28). Epox concentrations will likely need to be significantly reduced to identify effects of growth environment on cellular responses to toxins. Low concentration Tn (0.1 $\mu\text{g/ml}$) produced neurite degradation similar to MPP⁺-treated cells and substantial cell death most evidently in 3D cultures than 2D and 2D-M cultures. Overall, differentiated LUHMES cells appeared considerably more sensitive to MPP⁺, Tn, and Epox compared to RA/BDNF-differentiated SH-SY5Y cells. Additionally, 3D growth conditions appeared to increase sensitivity to toxins in differentiated LUHMES cells. However, these experiments would have to be quantified and replicated to confirm these qualitative observations.

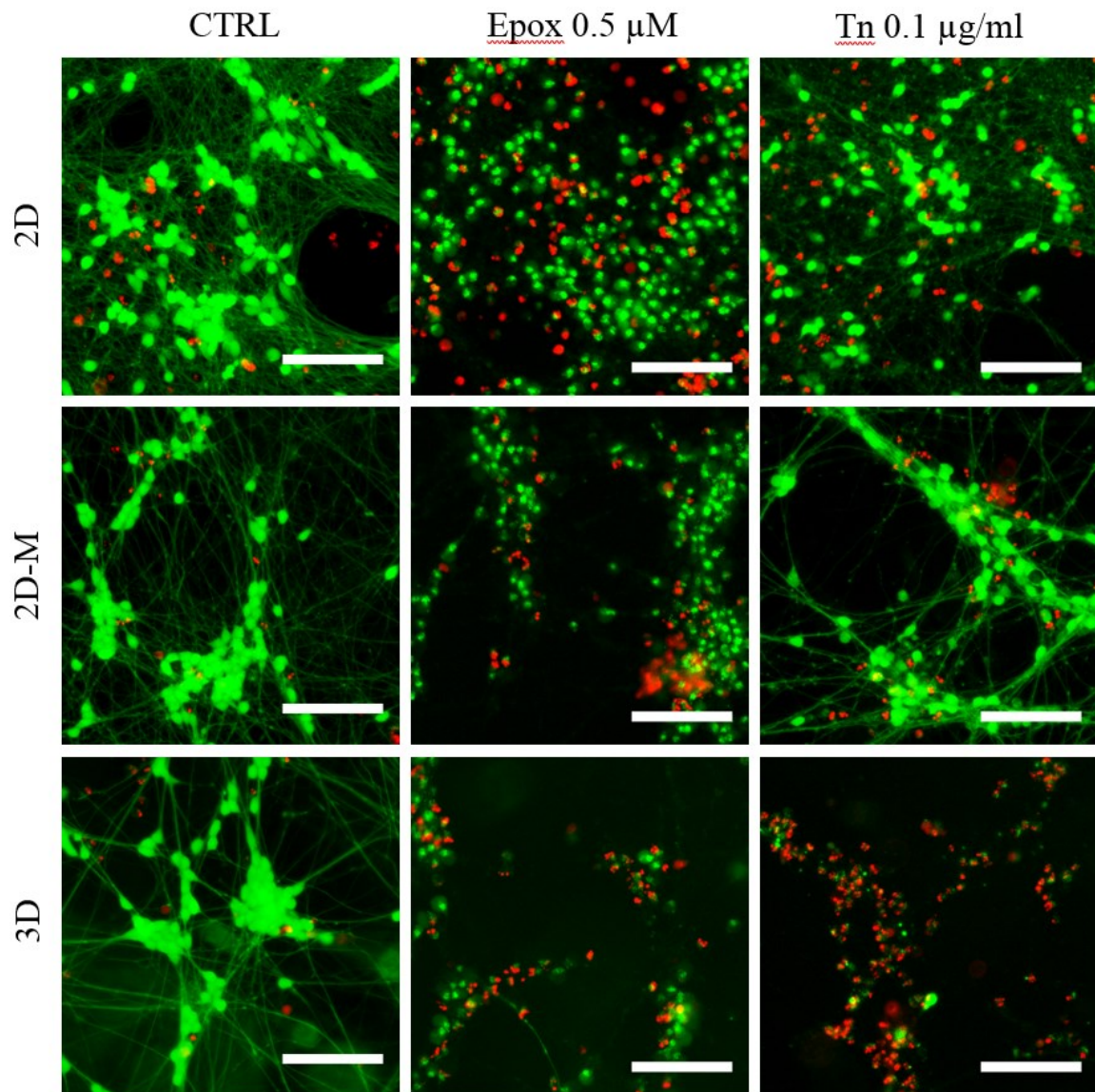


Figure 28 Representative images (10X) of C-AM (green-live)/PI (red-dead)-stained differentiated LUHMES cells grown at an initial seeding density of 1.6×10^4 cells/well in response to LUHMES differentiation medium (CTRL) and Epoxy (0.5 μ M) and Tn (0.1 μ g/ml) treatment. Scale bar = 1 mm.

4.4. Discussion

4.4.1. Impact of Growth Environment on SH-SY5Y Responses to Neurotoxins

For decades, SH-SY5Y cells have been used as neural cell culture models for the investigation of PD (*130, 131*). To generate SH-SY5Y culture PD models, >80% of studies used undifferentiated cells grown in 2D environments (*130*). Undifferentiated cells continue to proliferate, aggregate over time, and shift between adherent and non-adherent phenotypes, which can impact cell number with each medium change. Despite these dynamic characteristics, SH-SY5Y cell models are often treated as single cell adherent populations for general drug and toxicology analysis (*169–172*). 3D cell culture offered the opportunity to capture both adherent and non-adherent cell populations in the gel and minimize S-type expression by eliminating cell adhesion to the plate. I considered that 3D cell culture could potentially impact undifferentiated cell responses to neurotoxin assays. This was not the case, however. Growth environment did not significantly alter cell viability in undifferentiated SH-SY5Y cell cultures across all tested neurotoxins. Undifferentiated SH-SY5Y cells may have contained more uniform immature genetic profiles across differing phenotypes resulting in equivalent sensitivities to MPP+, Tn, and Epox.

Cell viability was slightly higher than expected after 48 h incubation in MPP+ across all undifferentiated conditions compared to previous observations in literature, which may have been a result of the edge effect impacting experimental results (*122, 172*). Nonetheless, undifferentiated SH-SY5Y cells were more robust against MPP+ compared

to previously published reports using 5-10 μM MPP⁺ to kill primary DAergic neurons (143). Tn generated lower cell viability levels than previously reported in the literature, but these results were expected because standard incubation times were approximately 24 h rather than 48 h (173). Epox concentrations used in this study were higher than average for use with SH-SY5Y cells. Cheng et al. observed a gradual tapering of Epox toxicity in undifferentiated SH-SY5Y cells and nearly complete proteasome inhibition above 0.1 μM after 24 h (174). This finding matches the Epox data presented here, where 0.5 μM , 1 μM , and 5 μM concentrations produced relatively equivalent effects after 48 h. Epox concentrations should be reduced for future assessment with this toxin in SH-SY5Y cultures to assess varying levels of proteasome inhibition. As MPP⁺, Tn, and Epox toxicity have never been previously assessed in RA/BDNF-differentiated SH-SY5Y cell cultures, these results provide a novel report on the impacts of RA/BDNF differentiation on toxin tolerance.

In contrast to undifferentiated SH-SY5Y cultures, RA/BDNF differentiation appears to promote significantly greater tolerance to MPP⁺, Tn, and Epox in 3D cultures compared to their 2D and 2D-M counterparts. I included the 2D-M condition to control for diffusion characteristics in 3D cell cultures. 2D-M conditions were not significantly different from 2D culture conditions across all toxins and concentrations in both undifferentiated and differentiated cultures suggesting minimal impact of mass transport on SH-SY5Y cell responses to toxins. These results suggested that adherence to stiff substrates significantly impacted cellular behaviour, morphology, differentiation, and responsivity to toxins in SH-SY5Y cell cultures. However, the mechanisms behind these effects are unknown.

It has been previously reported that RA-only differentiation SH-SY5Y cells imbue greater tolerance to MPP+ (122). Another report identified that following RA treatment, TrkB was upregulated and phosphorylated PKC was downregulated in SH-SY5Y cultures (139). As previously discussed in Chapter 1, TrkB is the neurotrophic receptor for BDNF that promotes cell survival and differentiation. Increases in TrkB expression would allow for BDNF-mediated differentiation but also promote downstream survivability mediated by the PI3K-Akt pathway. On the other hand, phosphorylated (i.e., activated) PKC has been observed to inhibit the PI3K-Akt pathway (175). Reductions in phosphorylated PKC and increases in TrkB would ultimately result in increased survival in the presence of BDNF.

Based on these observations and those identified in this work, elevated survivability in 3D conditions may involve the influence of 3D growth environments on RA/BDNF differentiation. For example, in 2D cell cultures, the stiff substrate may combat RA-mediated increases in TrkB during the initial 5 days of RA treatment (Figure 29). Therefore, 2D-grown cells would express lower TrkB per cell compared to 3D-grown cells. Additionally, the predominance of N-type cells over S-type cells in 3D culture due to the lack of a stiff substrate may impact TrkB expression at the macroscale level. RA differentiation may increase TrkB levels in N-type cells but not S-type cells due to their differing initial phenotypes. Due to minimal TrkB levels and perhaps even an alternative differentiation path induced by RA, S-type cells may be more susceptible to general toxic assaults such as Tn and Epox. Furthermore, it has previously been reported that C/EBP homologous protein (CHOP), a pro-apoptotic protein, is upregulated in response to ER

stressors such as Tn (176). However, when undifferentiated SH-SY5Y cells were provided with Tn and BDNF concurrently, CHOP expression was reduced (176). Therefore, elevated expression of TrkB in 3D SH-SY5Y cultures would account for increased tolerance towards Tn. Pro-survival effects of BDNF would also extend to Epox-treated differentiated cells. RA treatment has been associated with protecting SH-SY5Y cells from Epox-mediated cell death via PI3K-Akt pathway activation (177). MPP+ likely did not present large differences in cell viabilities between 3D and 2D conditions due to minimal DAT expression in SH-SY5Y cells (127). DAT has been reported to have low expression in both undifferentiated and RA-only differentiated cultures (127).

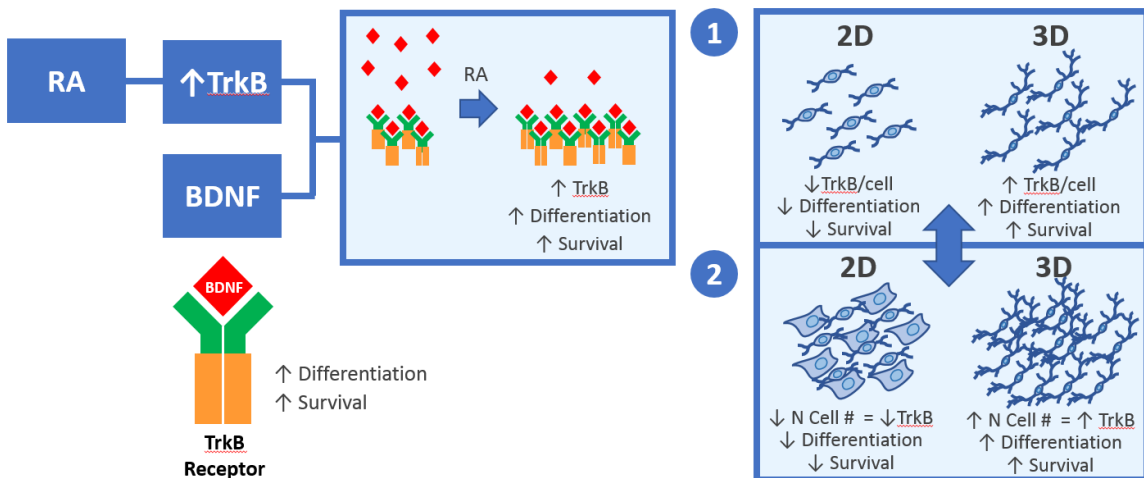


Figure 29 Cartoon depiction of hypothetical RA/BDNF effects on TrkB expression in 2D- vs. 3D-grown SH-SY5Y cells.

RA is expected to increase levels of TrkB resulting in the promotion of differentiation as well as survival. The 3D growth environment may play a role in regulating TrkB expression by 1) promoting N-type differentiation towards higher levels of TrkB compared to 2D grown conditions and 2) promoting a more uniform population of N-type cells.

Additional biochemical analyses will need to be done to elucidate the mechanisms behind these observed differences between 2D and 3D cell culture. We are currently performing PCR measurements of TH, SLC6A3 (DAT), NTRK2 (TrkB), and other interesting markers

such as nerve growth factor receptor (NGFR), which produces the p75 neurotrophic receptor that can promote apoptosis when activated by BDNF to assess changes to genetic expression between 2D- and 3D-grown SH-SY5Y cells. Ultimately, these early results seem to indicate that the current RA/BDNF differentiation protocol for SH-SY5Y cells provides a poor model of native DAergic neurons, which are considerably more sensitive to systemic dysfunction and toxic assaults. The impacts of RA and BDNF can be significant confounding factors in mimicking PD neuropathology. Considering BDNF has been reported to decrease within DAergic neurons in PD patients, adding BDNF as a long-term differentiation and survival agent may mask important cellular behaviours and responses involved in PD (178). Undifferentiated SH-SY5Y cells also require >1 mM concentrations of MPP+ to induce cell death, suggesting that this cell line may not provide an ideal foundation for PD research.

4.4.2. The Future with LUHMES Cells

Work completed with LUHMES cells remains incomplete but promising. The LUHMES cell line contained only one viable cell type and grew long, extensive, neural processes following differentiation, which would be expected in DAergic neurons. Early preliminary qualitative toxin assessments appeared to reflect the sensitivity of DAergic neurons to neurotoxic assaults targeting mitochondrial dysfunction, ER stress, and proteasome inhibition. Quantitative assessments (after reducing Epox and Tn concentrations) will be performed in the future. Overall, protocols for the maintenance, subculture, and storage of these cells are relatively simple and accessible. Only one differentiation protocol currently exists for these cells, which appears to work quite well. Ultimately, LUHMES cells grow

quite well in the Matrigel-only 3D culture platform, suggesting that this methodology is readily applicable to various cell types and cell lines.

CHAPTER 5: CONCLUSION

Despite the growing popularity of 3D cell culture techniques, 2D cell culture remains the predominant method for *in vitro* modelling of neurodegenerative disease and therapeutic development. This can be explained by multiple factors. Firstly, monolayer cultures are considerably easier to produce, process, and analyse. Techniques are readily accessible. Most laboratory equipment and *in vitro* assays have been optimized for 2D cell culture. As 3D cell culture is an emerging field, there are multiple ways to generate these models. Optimization of any one methodology is limited, and 3D cell culture remains largely unfamiliar to the general neuroscience community outside of neural tissue engineering. However, promising results mimicking AD neuropathology in Matrigel-based 3D cell culture suggested that Matrigel could be a useful, accessible platform for 3D modelling of neurodegenerative disease (79, 80). I ultimately chose to focus on PD, where most research revolved around the study of a single cell type: DAergic neurons. The SH-SY5Y cell line was selected as a model for DAergic neurons due to their historical application in PD research as catecholaminergic cells and simple maintenance protocols. However, some questions were raised concerning the efficacy of the thin-layer 3D culture methodology detailed by Kim et al. Producing 2×10^5 to 1×10^6 cells per well can be unfeasible and costly for certain cell types such as primary cells with limited proliferation cycles. Differentiating cells for 2-12 weeks per experiment can also be impractical. Additionally, the SH-SY5Y cell line contained both N-type and S-type cells. I wanted to investigate if removing substrate stiffness by providing a 3D growth environment could select for N-type cells over S-type cells. As SH-SY5Y cells were free to adhere to the treated plate in the Kim et al. 3D culture method, this hypothesis could not be tested using this model.

These factors led me to pursue my own thin-layer 3D cell culture protocols. Since ATPS methods offered a unique and accessible platform by which to manipulate liquids such as Matrigel, I pursued this option and tested its efficacy in producing thin gels. The ATPS-Matrigel 3D culture platform ultimately provided a promising, relatively simple, and accessible methodology where gel thickness could be effectively and reliably controlled using small volumes. Through the development and characterization process, I also discovered an alternative, simpler methodology for 3D cell culture that involved dispensing Matrigel directly into medium to produce an underlying gel protected from evaporation and air-liquid interfacial tension. I eventually applied this Matrigel-only 3D culture method to assess the impact of 3D growth environment on SH-SY5Y cell differentiation and responses to various neurotoxins previously used in PD research. Neurotoxin assay results appeared to indicate that growth environment has a significant impact on SH-SY5Y differentiation and suggested that RA/BDNF treatment increases tolerance to toxic assaults. Therefore, RA/BDNF-differentiated SH-SY5Y cells are likely not appropriate models for PD neuropathology. LUHMES cells may be more likely to fill this role, but additional quantitative experiments will need to be done to assess their DAergic characteristics. Overall, I have provided two simple, high-throughput, 3D neural cell culture platforms that are compatible with various cell types, standard lab equipment, and commercially available materials. These accessible platforms may promote greater exploration into the field of 3D cell culture in the neurosciences and beyond.

5.1. Statement of Contributions

- 1) Developed, optimized, and characterized a novel, ATPS-based, thin-layer, 3D cell culture technique that offers excellent control over Matrigel thickness using small volumes. Presented the potential of the ATPS-Matrigel 3D culture method as a high-throughput contraction assay platform.
- 2) Developed, optimized, and characterized a novel, simpler, Matrigel-only 3D cell culture method that required slightly more Matrigel than the ATPS-Matrigel 3D culture method but was compatible with both SH-SY5Y and LUHMES cell culture and capable of providing viable, thin-layer, 3D cell cultures shown to be effective platforms for high-throughput screening of neurotoxins.
- 3) Discovered a novel ATPS formulation: HPMC and Matrigel.
- 4) Demonstrated potential macromolecular crowding effects of large molecular weight polymers on protein aggregation in Matrigel.
- 5) Demonstrated the limitations of the Kim et al. (2015) 3D culture protocol as a 3D modelling system.
- 6) Revealed the influence of stiff substrates on SH-SY5Y N-type and S-type expression in 2D, 2D-M, and 3D cultures.
- 7) Demonstrated the effects of 3D growth environment on SH-SY5Y cell differentiation, growth, and responses to common neurotoxins used to study PD. Results appeared to indicate that RA/BDNF differentiated cells would perform poorly as models of DAergic neurons for PD research.
- 8) Revealed the compact, non-neuron-like morphology of RA/TPA differentiation on SH-SY-5Y cells grown in a 3D environment.

5.2. Future Directions

- 1) Matrigel has been reported to have batch-to-batch differences (179). For this work, Matrigel lots were considered equivalent in protein composition, and 5 mg/ml concentration was consistently maintained to control for lot differences. Therefore, it may be prudent to examine batch-to-batch differences in subsequent analyses of gel formation, thickness, and size to determine if characterization changes with lot. Cell viability may also be assessed to confirm minimal impact of lot on cell growth.
- 2) Characterization of gel thickness in the Matrigel-only 3D culture method will need to be appropriately assessed by allowing microbeads to settle overnight. Further analysis of gel distribution across the well in the Matrigel-only 3D culture and ATPS-Matrigel 3D culture platforms will need to be performed.
- 3) ATPS polymer interference with Matrigel gelation suggested a potential impact of macromolecular crowding on accelerating protein aggregation in Matrigel. 3D cell culture offers the opportunity to assess impacts of macromolecular crowding on cell behaviour and protein aggregation in a 3D environment. In neurodegenerative diseases, protein aggregation is often a key hallmark of disease progression. Macromolecular crowding and 3D environments may shorten experimental timeframes in modelling α -synuclein oligomerization and aggregation in PD, for example. However, assessing whether compounds (e.g., Ficoll) have impacts on Matrigel stability after it has already gelled will need to be the first step.
- 4) In this work, Matrigel and HPMC were observed to have ATPS characteristics. Determining the binodal curve for this pair will be useful for future applications of this system. Our lab has previously defined a rapid microscale binodal determination

- methodology (180). This technique could easily be adapted to 384-well plates to use less material and assess the ATPS behaviour of Matrigel and HPMC.
- 5) Due to the non-adherent features of the ATPS-Matrigel 3D culture technique, our lab will be using this platform to design a 3D contraction assay to measure responsiveness of healthy and asthmatic cells to various asthma treatments. The human bronchiole smooth muscle cells were observed to grow excellently within Matrigel and induced significant gel contraction in untreated conditions across various cell seeding densities.
 - 6) Biochemical analyses of 3D-grown cultures were not discussed in this work (aside from cell viability assessment). Early immunocytochemical analyses of 3D-grown cultures revealed that much longer incubation times were required for all steps (e.g., permeabilization, antibody incubation, etc.) compared to monolayer cultures. Western blotting protocols and immunocytochemical analyses will need to be optimized for assessment of the 3D pseudo-tissue.
 - 7) RA/TPA differentiation was only assessed morphologically and did not undergo additional biochemical analyses or high-throughput neurotoxin assay assessment. Performing these analyses may provide novel information regarding the impact of 3D environment against an alternative differentiation protocol in SH-SY5Y cells.
 - 8) Future high-throughput neurotoxin assays will need to accommodate for potential differences in evaporation and thermal gradients across the well plate. This can be done by adding sterile dH₂O to peripheral wells to accommodate for evaporation and/or alternating the locations of neurotoxin conditions.
 - 9) Ideally, ATP levels should be normalized to cell number or protein level to perform comparative analysis between groups and should likely be assessed in the future.

Assessing protein content across conditions would be more feasible as 3D-grown cells are difficult to count. Additionally, future neurotoxin assays will benefit from the quantification of apoptosis and necrosis to elucidate the systems of neural cell death in response to the toxic assaults under various growth environments. For example, annexin A5 and active caspase-3 activity can be measured using flow cytometry to assess levels of apoptosis. If features of apoptosis are not present, necrosis can be measured using PI or 7-aminoactinomycin D (another fluorescent DNA stain) infiltration into the nucleus of dead cells due to loss of cell membrane integrity.

- 10) We are currently performing PCR to examine the validity of the hypothesis that 3D growth environments impact gene expression of TrkB and potentially other markers compared to 2D and 2D-M grown cells. The genes we are investigating include TH, SLC6A3 (DAT), NTRK2 (TrkB), and NGFR (p75).
- 11) Considerable work remains to be done to further characterize the LUHMES cells, which showed promising behaviours in response to neurotoxin assaults. Determining maximal passaging, the impacts of long-term subculture in 2D culture environments, investigating impacts of seeding density, and assessing differential behaviours under 2D and 3D growth conditions will be useful for future applications of this cell line. Additional biochemical analyses of DAergic characteristics and changes in neuronal markers should be assessed for these cells. Investigating the influence of 2D vs. 3D growth environment on these measures and replicating neurotoxin assays in LUHMES cells will provide more solid conclusions on their applicability as a model DAergic cell line.

BIBLIOGRAPHY

1. World Health Organization, “Neurological disorders: a public health approach” (2006), , doi:10.1001/archneurol.2007.19.
2. C. P. Ferri *et al.*, Global prevalence of dementia: A Delphi consensus study. *Lancet*. **366** (2005), pp. 2112–2117.
3. G. F. Anderson, P. S. Hussey, Population aging: A comparison among industrialized countries. *Health Aff.* **19**, 191–203 (2000).
4. J. F. Kellie *et al.*, Quantitative Measurement of Intact Alpha-Synuclein Proteoforms from Post-Mortem Control and Parkinson’s Disease Brain Tissue by Intact Protein Mass Spectrometry. *Sci. Rep.* **4** (2014), doi:10.1038/srep05797.
5. R. J. Ward, F. A. Zucca, J. H. Duyn, R. R. Crichton, L. Zecca, The role of iron in brain ageing and neurodegenerative disorders. *Lancet Neurol.* **13** (2014), pp. 1045–1060.
6. D. W. Thomas *et al.*, Clinical development success rates 2006-2015. *BIO Ind. Anal.*, 1–28 (2016).
7. F. A. C. Azevedo *et al.*, Equal numbers of neuronal and nonneuronal cells make the human brain an isometrically scaled-up primate brain. *J. Comp. Neurol.* **513**, 532–541 (2009).
8. G. F. Mitchell *et al.*, Arterial stiffness, pressure and flow pulsatility and brain structure and function: The Age, Gene/Environment Susceptibility-Reykjavik Study. *Brain*. **134**, 3398–3407 (2011).
9. J. F. Cryan, T. G. Dinan, Mind-altering microorganisms: the impact of the gut microbiota on brain and behaviour. *Nat. Rev. Neurosci.* **13**, 701–712 (2012).
10. F. J. van der Staay, Animal models of behavioral dysfunctions: Basic concepts and classifications, and an evaluation strategy. *Brain Res. Rev.* **52** (2006), pp. 131–159.
11. S. Ojha, H. Javed, S. Azimullah, M. E. Haque, β -Caryophyllene, a phytocannabinoid attenuates oxidative stress, neuroinflammation, glial activation, and salvages dopaminergic neurons in a rat model of Parkinson disease. *Mol. Cell. Biochem.* **418**, 59–70 (2016).
12. E. Tronci *et al.*, Effect of memantine on L-DOPA-induced dyskinesia in the 6-OHDA-lesioned rat model of Parkinson’s disease. *Neuroscience*. **265**, 245–252 (2014).
13. Y. S. Kang, H. J. Jung, J. S. Oh, D. Y. Song, Use of PEGylated Immunoliposomes to Deliver Dopamine Across the Blood–Brain Barrier in a Rat Model of Parkinson’s Disease. *CNS Neurosci. Ther.* **22**, 817–823 (2016).

14. V. Jackson-Lewis, J. Blesa, S. Przedborski, Animal models of Parkinson's disease. *Parkinsonism Relat. Disord.* **18 Suppl 1**, S183-5 (2012).
15. S. Schmidt *et al.*, Genetic mouse models for Parkinson's disease display severe pathology in glial cell mitochondria. *Hum. Mol. Genet.* **20**, 1197–211 (2011).
16. S. T. Carmichael, Rodent models of focal stroke: Size, mechanism, and purpose. *NeuroRX.* **2**, 396–409 (2005).
17. J. a Potashkin, S. R. Blume, N. K. Runkle, Limitations of animal models of Parkinson's disease. *Parkinsons. Dis.* **2011**, 658083 (2010).
18. P. Perel *et al.*, Comparison of treatment effects between animal experiments and clinical trials: systematic review. *BMJ.* **334**, 197 (2007).
19. K. Takahashi *et al.*, Induction of Pluripotent Stem Cells from Adult Human Fibroblasts by Defined Factors. *Cell.* **131**, 861–872 (2007).
20. M. Nakagawa, N. Takizawa, M. Narita, T. Ichisaka, S. Yamanaka, Promotion of direct reprogramming by transformation-deficient Myc. *Proc. Natl. Acad. Sci. U. S. A.* **107**, 14152–14157 (2010).
21. J. Wu, J. C. Izpisua Belmonte, Stem Cells: A Renaissance in Human Biology Research. *Cell.* **165** (2016), pp. 1572–1585.
22. P. C. Georges, W. J. Miller, D. F. Meaney, E. S. Sawyer, P. A. Janmey, Matrices with Compliance Comparable to that of Brain Tissue Select Neuronal over Glial Growth in Mixed Cortical Cultures. *Biophys. J.* **90**, 3012–3018 (2006).
23. G. J. Her *et al.*, Control of three-dimensional substrate stiffness to manipulate mesenchymal stem cell fate toward neuronal or glial lineages. *Acta Biomater.* **9**, 5170–5180 (2013).
24. A. Bozza *et al.*, Neural differentiation of pluripotent cells in 3D alginate-based cultures. *Biomaterials.* **35**, 4636–4645 (2014).
25. T. B. Puschmann *et al.*, Bioactive 3D cell culture system minimizes cellular stress and maintains the in vivo-like morphological complexity of astroglial cells. *Glia.* **61**, 432–440 (2013).
26. L. a Flanagan, Y.-E. Ju, B. Marg, M. Osterfield, P. a Janmey, Neurite branching on deformable substrates. *Neuroreport.* **13**, 2411–2415 (2002).
27. M. Jorfi, C. D'Avanzo, D. Y. Kim, D. Irimia, Three-Dimensional Models of the Human Brain Development and Diseases. *Adv. Healthc. Mater.* (2017), , doi:10.1002/adhm.201700723.
28. R. Booth, H. Kim, Characterization of a microfluidic in vitro model of the blood-

- brain barrier (μ BBB). *Lab Chip*. **12**, 1784 (2012).
29. M. Ravi, V. Paramesh, S. R. Kaviya, E. Anuradha, F. D. P. Solomon, 3D cell culture systems: advantages and applications. *J. Cell. Physiol.* **230**, 16–26 (2015).
 30. K. R. Ko, J. P. Frampton, Developments in 3D neural cell culture models: the future of neurotherapeutics testing? *Expert Rev. Neurother.*, 1–3 (2016).
 31. M. Ravikumar, S. Jain, R. H. Miller, J. R. Capadona, S. M. Selkirk, An organotypic spinal cord slice culture model to quantify neurodegeneration. *J. Neurosci. Methods*. **211**, 280–288 (2012).
 32. A. De Simoni, L. M. Y. Yu, Preparation of organotypic hippocampal slice cultures: interface method. *Nat. Protoc.* **1**, 1439–45 (2006).
 33. U. V. Nägerl, N. Eberhorn, S. B. Cambridge, T. Bonhoeffer, Bidirectional activity-dependent morphological plasticity in hippocampal neurons. *Neuron*. **44**, 759–767 (2004).
 34. C. Humpel, Organotypic vibrosections from whole brain adult Alzheimer mice (overexpressing amyloid-precursor-protein with the Swedish-Dutch-Iowa mutations) as a model to study clearance of beta-amyloid plaques. *Front. Aging Neurosci.* **7**, 1–10 (2015).
 35. J. K. Leutgeb, J. U. Frey, T. Behnisch, LTP in cultured hippocampal-entorhinal cortex slices from young adult (P25-30) rats. *J. Neurosci. Methods*. **130**, 19–32 (2003).
 36. E. Eugène *et al.*, An organotypic brain slice preparation from adult patients with temporal lobe epilepsy. *J. Neurosci. Methods*. **235**, 234–244 (2014).
 37. R. S. G. Jones, A. B. da Silva, R. G. Whittaker, G. L. Woodhall, M. O. Cunningham, Human brain slices for epilepsy research: Pitfalls, solutions and future challenges. *J. Neurosci. Methods*. **260** (2016), pp. 221–232.
 38. H. S. Gwak *et al.*, Chemotherapy for malignant gliomas based on histoculture drug response assay: A pilot study. *J. Korean Neurosurg. Soc.* **50**, 426–433 (2011).
 39. Y. Huang, J. C. Williams, S. M. Johnson, Brain slice on a chip: opportunities and challenges of applying microfluidic technology to intact tissues. *Lab Chip*. **12**, 2103–17 (2012).
 40. S. Mii *et al.*, Nestin-Expressing Stem Cells Promote Nerve Growth in Long-Term 3-Dimensional Gelfoam-Supported Histoculture. *PLoS One*. **8** (2013), doi:10.1371/journal.pone.0067153.
 41. S. Mii *et al.*, The role of hair follicle nestin-expressing stem cells during whisker sensory-nerve growth in long-term 3D culture. *J. Cell. Biochem.* **114**, 1674–1684

- (2013).
42. D. Jansson *et al.*, A role for human brain pericytes in neuroinflammation. *J. Neuroinflammation*. **11**, 104 (2014).
 43. N. Sanai *et al.*, Unique astrocyte ribbon in adult human brain contains neural stem cells but lacks chain migration. *Nature*. **427**, 740–744 (2004).
 44. E. S. Maywood *et al.*, Analysis of core circadian feedback loop in suprachiasmatic nucleus of mCry1-luc transgenic reporter mouse. *Proc. Natl. Acad. Sci. U. S. A.* **110**, 9547–52 (2013).
 45. B. Bae *et al.*, Neuroscience. What are mini-brains? *Science (80-.)*. **342**, 200–1 (2013).
 46. R. Cuperus *et al.*, Pleiotropic effects of fenretinide in neuroblastoma cell lines and multicellular tumor spheroids. *Int. J. Oncol.* **32**, 1011–1019 (2008).
 47. O. G. Besançon *et al.*, Synergistic interaction between cisplatin and gemcitabine in neuroblastoma cell lines and multicellular tumor spheroids. *Cancer Lett.* **319**, 23–30 (2012).
 48. Y. J. Choi, J. S. Park, S. H. Lee, Size-controllable networked neurospheres as a 3D neuronal tissue model for Alzheimer’s disease studies. *Biomaterials*. **34**, 2938–2946 (2013).
 49. Y. L. Dingle *et al.*, Three-Dimensional Neural Spheroid Culture: An In Vitro Model for Cortical Studies. *Tissue Eng. Part C Methods*. **21**, 1274–1283 (2015).
 50. A. Sen, M. S. Kallos, L. A. Behie, Effects of Hydrodynamics on Cultures of Mammalian Neural Stem Cell Aggregates in Suspension Bioreactors. *Ind. Eng. Chem. Res.* **40**, 5350–5357 (2001).
 51. M. Denham *et al.*, Neural stem cells express non-neural markers during embryoid body coculture. *Stem Cells*. **24**, 918–27 (2006).
 52. M. Eiraku *et al.*, Self-Organized Formation of Polarized Cortical Tissues from ESCs and Its Active Manipulation by Extrinsic Signals. *Cell Stem Cell*. **3**, 519–532 (2008).
 53. M. Eiraku *et al.*, Self-organizing optic-cup morphogenesis in three-dimensional culture. *Nature*. **472**, 51–56 (2011).
 54. S. Nori *et al.*, Grafted human-induced pluripotent stem-cell-derived neurospheres promote motor functional recovery after spinal cord injury in mice. *Proc. Natl. Acad. Sci.* **108**, 16825–16830 (2011).
 55. H.-K. Lee *et al.*, Three Dimensional Human Neuro-Spheroid Model of

- Alzheimer's Disease Based on Differentiated Induced Pluripotent Stem Cells. *PLoS One*. **11**, e0163072 (2016).
56. P. R. Baraniak, T. C. McDevitt, Scaffold-free culture of mesenchymal stem cell spheroids in suspension preserves multilineage potential. *Cell Tissue Res*. **347**, 701–711 (2012).
 57. E. Atefi, S. Lemmo, D. Fyffe, G. D. Luker, H. Tavana, High throughput, polymeric aqueous two-phase printing of tumor spheroids. *Adv. Funct. Mater.* **24**, 6509–6515 (2014).
 58. C. Han, S. Takayama, J. Park, Formation and manipulation of cell spheroids using a density adjusted PEG / DEX aqueous two phase system. *Sci. Rep.* **5**, 1–12 (2015).
 59. J. P. Frampton *et al.*, Rapid Self-Assembly of Macroscale Tissue Constructs at Biphasic Aqueous Interfaces. *Adv. Funct. Mater.* **25**, 1694–1699 (2015).
 60. D. Bonne-Barkay, C. A. Wiley, Brain extracellular matrix in neurodegeneration. *Brain Pathol.* **19** (2009), pp. 573–585.
 61. A. M. Paşca *et al.*, Functional cortical neurons and astrocytes from human pluripotent stem cells in 3D culture. *Nat. Methods*. **12**, 671–678 (2015).
 62. P. P. Garcez *et al.*, Zika virus impairs growth in human neurospheres and brain organoids. *Science (80-.)*. **352**, 816–818 (2016).
 63. J. B. Jensen, M. Parmar, Strengths and Limitations of the Neurosphere Culture System. *Mol. Neurobiol.* **34**, 153–162 (2006).
 64. J. W. Haycock, 3D cell culture: a review of current approaches and techniques. *Methods Mol. Biol.* **695**, 1–15 (2011).
 65. M. J. Mahoney, K. S. Anseth, Three-dimensional growth and function of neural tissue in degradable polyethylene glycol hydrogels. *Biomaterials*. **27**, 2265–2274 (2006).
 66. K. J. Lampe, R. G. Mooney, K. B. Bjugstad, M. J. Mahoney, Effect of macromer weight percent on neural cell growth in 2D and 3D nondegradable PEG hydrogel culture. *J. Biomed. Mater. Res. - Part A*. **94**, 1162–1171 (2010).
 67. A. Meinhardt *et al.*, 3D reconstitution of the patterned neural tube from embryonic stem cells. *Stem Cell Reports*. **3**, 987–999 (2014).
 68. I. Smith *et al.*, Neuronal-glia populations form functional networks in a biocompatible 3D scaffold. *Neurosci. Lett.* **609**, 198–202 (2015).
 69. M. F. B. Daud, K. C. Pawar, F. Claeysens, A. J. Ryan, J. W. Haycock, An aligned

- 3D neuronal-glia co-culture model for peripheral nerve studies. *Biomaterials*. **33**, 5901–5913 (2012).
70. N. Li *et al.*, Three-dimensional graphene foam as a biocompatible and conductive scaffold for neural stem cells. *Sci. Rep.* **3**, 1604 (2013).
 71. J. P. Frampton, M. R. Hynd, M. L. Shuler, W. Shain, Fabrication and optimization of alginate hydrogel constructs for use in 3D neural cell culture. *Biomed. Mater.* **6**, 15002 (2011).
 72. K. E. Crompton *et al.*, Polylysine-functionalised thermoresponsive chitosan hydrogel for neural tissue engineering. *Biomaterials*. **28**, 441–449 (2007).
 73. S. M. O'Connor, D. A. Stenger, K. M. Shaffer, W. Ma, Survival and neurite outgrowth of rat cortical neurons in three-dimensional agarose and collagen gel matrices. *Neurosci. Lett.* **304**, 189–193 (2001).
 74. K. Chwalek, M. D. Tang-Schomer, F. G. Omenetto, D. L. Kaplan, In vitro bioengineered model of cortical brain tissue. *Nat. Protoc.* **10**, 1362–1373 (2015).
 75. W. M. Tian *et al.*, Hyaluronic Acid–Poly-D-Lysine-Based Three-Dimensional Hydrogel for Traumatic Brain Injury. *Tissue Eng.* **11**, 513–525 (2005).
 76. S. Suri, C. E. Schmidt, Cell-Laden Hydrogel Constructs of Hyaluronic Acid, Collagen, and Laminin for Neural Tissue Engineering. *Tissue Eng. Part A*. **16**, 1703–1716 (2010).
 77. G. Y. Liu *et al.*, Templated Assembly of Collagen Fibers Directs Cell Growth in 2D and 3D. *Sci. Rep.* **7**, 9628 (2017).
 78. A. Bozkurt *et al.*, In vitro assessment of axonal growth using dorsal root ganglia explants in a novel three-dimensional collagen matrix. *Tissue Eng.* **13**, 2971–9 (2007).
 79. S. H. Choi *et al.*, A three-dimensional human neural cell culture model of Alzheimer's disease. *Nature*. **515**, 274–278 (2014).
 80. Y. H. Kim *et al.*, A 3D human neural cell culture system for modeling Alzheimer's disease. *Nat. Protoc.* **10**, 985–1006 (2015).
 81. N. R. Wevers *et al.*, High-throughput compound evaluation on 3D networks of neurons and glia in a microfluidic platform. *Sci. Rep.* **6**, 38856 (2016).
 82. J. De Waele *et al.*, 3D culture of murine neural stem cells on decellularized mouse brain sections. *Biomaterials*. **41**, 122–131 (2015).
 83. L. J. White *et al.*, The impact of detergents on the tissue decellularization process: A ToF-SIMS study. *Acta Biomater.* **50**, 207–219 (2017).

84. Y. Yamaguchi, Lecticans: organizers of the brain extracellular matrix. *Cell. Mol. Life Sci.* **57**, 276–289 (2000).
85. S. Koutsopoulos, S. Zhang, Long-term three-dimensional neural tissue cultures in functionalized self-Assembling peptide hydrogels, Matrigel and Collagen i. *Acta Biomater.* **9**, 5162–5169 (2013).
86. S. Grefte, S. Vullings, A. M. Kuijpers-Jagtman, R. Torensma, J. W. Von den Hoff, Matrigel, but not collagen I, maintains the differentiation capacity of muscle derived cells *in vitro*. *Biomed. Mater.* **7**, 55004 (2012).
87. G. Benton, I. Arnaoutova, J. George, H. K. Kleinman, J. Koblinski, Matrigel: From discovery and ECM mimicry to assays and models for cancer research. *Adv. Drug Deliv. Rev.* **79** (2014), pp. 3–18.
88. C. S. Barros, S. J. Franco, U. Müller, Extracellular Matrix: Functions in the nervous system. *Cold Spring Harb. Perspect. Biol.* **3**, 1–24 (2011).
89. R. Derda *et al.*, Multizone paper platform for 3D cell cultures. *PLoS One.* **6** (2011), doi:10.1371/journal.pone.0018940.
90. B. Mosadegh *et al.*, Three-Dimensional Paper-Based Model for Cardiac Ischemia. *Adv. Healthc. Mater.* **3**, 1036–1043 (2014).
91. P. A. K. Albertsson, *Partition of cell particles and macromolecules : separation and purification of biomolecules, cell organelles, membranes, and cells in aqueous polymer two-phase systems and their use in biochemical analysis and biotechnology* (Wiley, New York, ed. 3, 1986).
92. C. Moraes, A. B. Simon, A. J. Putnam, S. Takayama, Aqueous two-phase printing of cell-containing contractile collagen microgels. *Biomaterials.* **34**, 9623–9631 (2013).
93. B. M. Leung *et al.*, *J. Lab. Autom.*, in press, doi:10.1177/2211068214563793.
94. T. Pringsheim, N. Jette, A. Frolikis, T. D. L. Steeves, The prevalence of Parkinson’s disease: A systematic review and meta-analysis. *Mov. Disord.* **29** (2014), pp. 1583–1590.
95. R. B. Postuma *et al.*, MDS clinical diagnostic criteria for Parkinson’s disease. *Mov. Disord.* **30** (2015), pp. 1591–1601.
96. W. Poewe *et al.*, Parkinson disease. *Nat. Rev. Dis. Prim.* **3**, 17013 (2017).
97. A. Ascherio, M. A. Schwarzschild, The epidemiology of Parkinson’s disease: risk factors and prevention. *Lancet Neurol.* **15** (2016), pp. 1257–1272.
98. A. A. Dijkstra *et al.*, Stage-dependent nigral neuronal loss in incidental Lewy body

and parkinson's disease. *Mov. Disord.* **29**, 1244–1251 (2014).

99. S. C. Daubner, T. Le, S. Wang, Tyrosine hydroxylase and regulation of dopamine synthesis. *Arch. Biochem. Biophys.* **508** (2011), pp. 1–12.
100. R. Gray *et al.*, Long-term effectiveness of dopamine agonists and monoamine oxidase B inhibitors compared with levodopa as initial treatment for Parkinson's disease (PD MED): A large, open-label, pragmatic randomised trial. *Lancet.* **384**, 1196–1205 (2014).
101. C. M. Lill, Genetics of Parkinson's disease. *Mol. Cell. Probes.* **30** (2016), pp. 386–396.
102. L. Parkkinen, T. Kauppinen, T. Pirttilä, J. M. Autere, I. Alafuzoff, Alpha-synuclein pathology does not predict extrapyramidal symptoms or dementia. *Ann. Neurol.* **57** (2005), pp. 82–91.
103. K. St. P. McNaught, R. Belizaire, O. Isacson, P. Jenner, C. W. Olanow, Altered Proteasomal Function in Sporadic Parkinson's Disease. *Exp. Neurol.* **179**, 38–46 (2003).
104. L. Narhi *et al.*, Both familial Parkinson's disease mutations accelerate α -synuclein aggregation. *J. Biol. Chem.* **274**, 9843–9846 (1999).
105. P. Ibáñez *et al.*, Causal relation between α -synuclein locus duplication as a cause of familial Parkinson's disease. *Lancet.* **364**, 1169–1171 (2004).
106. M. Xilouri, O. R. Brekk, L. Stefanis, Alpha-synuclein and Protein Degradation Systems: a Reciprocal Relationship. *Mol. Neurobiol.* **47**, 537–551 (2013).
107. J. S. Park *et al.*, Pathogenic effects of novel mutations in the P-type ATPase ATP13A2 (PARK9) causing Kufor-Rakeb syndrome, a form of early-onset parkinsonism. *Hum. Mutat.* **32**, 956–964 (2011).
108. G. Mercado, V. Castillo, P. Soto, A. Sidhu, ER stress and Parkinson's disease: Pathological inputs that converge into the secretory pathway. *Brain Res.* **1648** (2016), pp. 626–632.
109. C. Pacelli *et al.*, Elevated Mitochondrial Bioenergetics and Axonal Arborization Size Are Key Contributors to the Vulnerability of Dopamine Neurons. *Curr. Biol.* **25**, 2349–2360 (2015).
110. J. P. Bolam, E. K. Pissadaki, Living on the edge with too many mouths to feed: Why dopamine neurons die. *Mov. Disord.* **27**, 1478–1483 (2012).
111. J. Langston, P. Ballard, J. Tetrud, I. Irwin, Chronic Parkinsonism in humans due to a product of meperidine-analog synthesis. *Science (80-.).* **219**, 979–980 (1983).

112. J. W. Langston, The MPTP Story. *J. Parkinsons. Dis.* **7**, S11–S19 (2017).
113. R. R. Gainetdinov, F. Fumagalli, S. R. Jones, M. G. Caron, Dopamine Transporter Is Required for In Vivo MPTP Neurotoxicity: Evidence from Mice Lacking the Transporter. *J. Neurochem.* **69**, 1322–1325 (2002).
114. A. Bose, M. F. Beal, Mitochondrial dysfunction in Parkinson’s disease. *J. Neurochem.* (2016), pp. 216–231.
115. D. S. Cassarino *et al.*, Elevated reactive oxygen species and antioxidant enzyme activities in animal and cellular models of Parkinson’s disease. *Biochim. Biophys. Acta.* **1362**, 77–86 (1997).
116. E. V. Mosharov *et al.*, Interplay between Cytosolic Dopamine, Calcium, and α -Synuclein Causes Selective Death of Substantia Nigra Neurons. *Neuron.* **62**, 218–229 (2009).
117. S. Fahn, in *Journal of Neurology* (2005), vol. 252.
118. J. Lipski *et al.*, L-DOPA: A scapegoat for accelerated neurodegeneration in Parkinson’s disease? *Prog. Neurobiol.* **94** (2011), pp. 389–407.
119. T. M. Dawson, H. S. Ko, V. L. Dawson, Genetic Animal Models of Parkinson’s Disease. *Neuron.* **66** (2010), pp. 646–661.
120. D. Lindholm *et al.*, Current disease modifying approaches to treat Parkinson’s disease. *Cell. Mol. Life Sci.* **73** (2016), pp. 1365–1379.
121. L. M. Yshii, A. Denadai-Souza, A. R. Vasconcelos, M. C. W. Avellar, C. Scavone, Suppression of MAPK attenuates neuronal cell death induced by activated gli-conditioned medium in alpha-synuclein overexpressing SH-SY5Y cells. *J. Neuroinflammation.* **12**, 193 (2015).
122. Y. T. Cheung *et al.*, Effects of all-trans-retinoic acid on human SH-SY5Y neuroblastoma as in vitro model in neurotoxicity research. *Neurotoxicology.* **30**, 127–135 (2009).
123. A. Borrajo, A. I. Rodriguez-Perez, B. Villar-Cheda, M. J. Guerra, J. L. Labandeira-Garcia, Inhibition of the microglial response is essential for the neuroprotective effects of Rho-kinase inhibitors on MPTP-induced dopaminergic cell death. *Neuropharmacology.* **85**, 1–8 (2014).
124. J. L. Biedler, S. Roffler-Tarlov, M. Schachner, L. S. Freedman, Multiple Neurotransmitter Synthesis by Human Neuroblastoma Cell Lines and Clones. *Cancer Res.* **38**, 3751–3757 (1978).
125. J. Kovalevich, D. Langford, Considerations for the use of SH-SY5Y neuroblastoma cells in neurobiology. *Methods Mol. Biol.* **1078**, 9–21 (2013).

126. R. A. Ross, J. L. Biedler, Presence and Regulation of Tyrosinase Activity in Human Neuroblastoma Cell Variants in Vitro. *Cancer Res.* **45**, 1628–1632 (1985).
127. S. P. Presgraves, T. Ahmed, S. Borwege, J. N. Joyce, Terminally differentiated SH-SY5Y cells provide a model system for studying neuroprotective effects of dopamine agonists. *Neurotox. Res.* **5**, 579–598 (2004).
128. A. Krishna *et al.*, Systems genomics evaluation of the SH-SY5Y neuroblastoma cell line as a model for Parkinson’s disease. *BMC Genomics.* **15**, 1154 (2014).
129. A. Jämsä, K. Hasslund, R. F. Cowburn, A. Bäckström, M. Vasänge, The retinoic acid and brain-derived neurotrophic factor differentiated SH-SY5Y cell line as a model for Alzheimer’s disease-like tau phosphorylation. *Biochem. Biophys. Res. Commun.* **319**, 993–1000 (2004).
130. H. Xicoy, B. Wieringa, G. J. M. Martens, The SH-SY5Y cell line in Parkinson’s disease research: a systematic review. *Mol. Neurodegener.* **12**, 10 (2017).
131. H. Xie, L. Hu, G. Lim, SH-SY5Y human neuroblastoma cell line: in vitro cell model of dopaminergic neurons in Parkinson’s disease. *Chin. Med. J. (Engl.)*. **123**, 1086–1092 (2010).
132. M. Rhinn, P. Dolle, Retinoic acid signalling during development. *Development.* **139**, 843–858 (2012).
133. S. Meseguer, G. Mudduluru, J. M. Escamilla, H. Allgayer, D. Baretino, MicroRNAs-10a and -10b contribute to retinoic acid-induced differentiation of neuroblastoma cells and target the alternative splicing regulatory factor SFRS1 (SF2/ASF). *J. Biol. Chem.* **286**, 4150–4164 (2011).
134. S. Das *et al.*, MicroRNA mediates DNA demethylation events triggered by retinoic acid during neuroblastoma cell differentiation. *Cancer Res.* **70**, 7874–7881 (2010).
135. A. Janesick, S. C. Wu, B. Blumberg, Retinoic acid signaling and neuronal differentiation. *Cell. Mol. Life Sci.* **72** (2015), pp. 1559–1576.
136. U. Leli, A. Cataldo, T. B. Shea, R. A. Nixon, G. Hauser, Distinct Mechanisms of Differentiation of SH-SY5Y Neuroblastoma Cells by Protein Kinase C Activators and Inhibitors. *J. Neurochem.* **58**, 1191–1198 (1992).
137. G. Perez-Juste, A. Aranda, Differentiation of neuroblastoma cells by phorbol esters and insulin-like growth factor 1 is associated with induction of retinoic acid receptor beta gene expression. *Oncogene.* **18**, 5393–5402 (1999).
138. S. Cohen-Cory, A. H. Kidane, N. J. Shirkey, S. Marshak, Brain-derived neurotrophic factor and the development of structural neuronal connectivity. *Dev. Neurobiol.* **70** (2010), pp. 271–288.

139. M. Encinas *et al.*, Sequential treatment of SH-SY5Y cells with retinoic acid and brain-derived neurotrophic factor gives rise to fully differentiated, neurotrophic factor-dependent, human neuron-like cells. *J. Neurochem.* **75**, 991–1003 (2000).
140. J. A. Korecka *et al.*, Phenotypic Characterization of Retinoic Acid Differentiated SH-SY5Y Cells by Transcriptional Profiling. *PLoS One.* **8** (2013), doi:10.1371/journal.pone.0063862.
141. S. H. Hashemi, J. Y. Li, H. Ahlman, A. Dahlström, SSR2(a) receptor expression and adrenergic/cholinergic characteristics in differentiated SH-SY5Y cells. *Neurochem. Res.* **28**, 449–460 (2003).
142. F. M. Lopes *et al.*, Comparison between proliferative and neuron-like SH-SY5Y cells as an in vitro model for Parkinson disease studies. *Brain Res.* **1337**, 85–94 (2010).
143. W.-S. Choi, S. E. Kruse, R. D. Palmiter, Z. Xia, Mitochondrial complex I inhibition is not required for dopaminergic neuron death induced by rotenone, MPP+, or paraquat. *Proc. Natl. Acad. Sci. U. S. A.* **105**, 15136–41 (2008).
144. X. Zeng *et al.*, An in vitro model of human dopaminergic neurons derived from embryonic stem cells: MPP+ toxicity and GDNF neuroprotection. *Neuropsychopharmacology.* **31**, 2708–15 (2006).
145. J. Peng, Q. Liu, M. S. Rao, X. Zeng, Using Human Pluripotent Stem Cell-Derived Dopaminergic Neurons to Evaluate Candidate Parkinson's Disease Therapeutic Agents in MPP⁺ and Rotenone Models. *J. Biomol. Screen.* **18**, 522–533 (2013).
146. A. D. Spathis *et al.*, Nurr1:RXR α heterodimer activation as monotherapy for Parkinson's disease. *Proc. Natl. Acad. Sci.* **114**, 3999–4004 (2017).
147. S. P. Presgraves, S. Borwege, M. J. Millan, J. N. Joyce, Involvement of dopamine D₂/D₃ receptors and BDNF in the neuroprotective effects of S32504 and pramipexole against 1-methyl-4-phenylpyridinium in terminally differentiated SH-SY5Y cells. *Exp. Neurol.* **190**, 157–170 (2004).
148. V. H. Knaryan *et al.*, SNJ-1945, a calpain inhibitor, protects SH-SY5Y cells against MPP⁺ and rotenone. *J. Neurochem.* **130**, 280–290 (2014).
149. D. Mastroeni *et al.*, Microglial responses to dopamine in a cell culture model of Parkinson's disease. *Neurobiol. Aging.* **30**, 1805–1817 (2009).
150. A. Edsjö *et al.*, Expression of trkB in Human Neuroblastoma in Relation to MYCN Expression and Retinoic Acid Treatment. *Lab. Investig.* **83**, 813–823 (2003).
151. M. Innala *et al.*, 3D Culturing and differentiation of SH-SY5Y neuroblastoma cells on bacterial nanocellulose scaffolds. *Artif. Cells, Nanomedicine, Biotechnol.* **42**, 302–308 (2014).

152. G. N. Li, L. L. Livi, C. M. Gourd, E. S. Deweerd, D. Hoffman-Kim, Genomic and morphological changes of neuroblastoma cells in response to three-dimensional matrices. *Tissue Eng.* **13**, 1035–1047 (2007).
153. L. Agholme, T. Lindström, K. Kgedal, J. Marcusson, M. Hallbeck, An in vitro model for neuroscience: Differentiation of SH-SY5Y cells into cells with morphological and biochemical characteristics of mature neurons. *J. Alzheimer's Dis.* **20**, 1069–1082 (2010).
154. J. Lotharius *et al.*, Effect of mutant α -synuclein on dopamine homeostasis in a new human mesencephalic cell line. *J. Biol. Chem.* **277**, 38884–38894 (2002).
155. D. Scholz *et al.*, Rapid, complete and large-scale generation of post-mitotic neurons from the human LUHMES cell line. *J. Neurochem.* **119**, 957–971 (2011).
156. Z. Bin Tong *et al.*, Characterization of three human cell line models for high-throughput neuronal cytotoxicity screening. *J. Appl. Toxicol.* **37**, 167–180 (2017).
157. X. Zhang, M. Yin, M. Zhang, Cell-based assays for Parkinson's disease using differentiated human LUHMES cells. *Acta Pharmacol. Sin.* **35**, 945–956 (2014).
158. L. Smirnova *et al.*, A LUHMES 3D dopaminergic neuronal model for neurotoxicity testing allowing long-term exposure and cellular resilience analysis. *Arch. Toxicol.* **90**, 2725–2743 (2016).
159. M. Höllerhage *et al.*, Protective efficacy of phosphodiesterase-1 inhibition against alpha-synuclein toxicity revealed by compound screening in LUHMES cells. *Sci. Rep.* **7**, 11469 (2017).
160. K. R. Ko, R. Agarwal, J. P. Frampton, High-Throughput 3D Neural Cell Culture Analysis Facilitated by Aqueous Two-Phase Systems. *MRS Adv.* **2**, 2435–2441 (2017).
161. R. J. Ellis, Macromolecular crowding: Obvious but underappreciated. *Trends Biochem. Sci.* **26** (2001), pp. 597–604.
162. X. Medda *et al.*, Development of a Scalable, High-Throughput-Compatible Assay to Detect Tau Aggregates Using iPSC-Derived Cortical Neurons Maintained in a Three-Dimensional Culture Format. *J. Biomol. Screen.* **21**, 804–815 (2016).
163. H. Matsui, H. Ito, Y. Taniguchi, S. Takeda, R. Takahashi, Ammonium chloride and tunicamycin are novel toxins for dopaminergic neurons and induce Parkinson's disease-like phenotypes in medaka fish. *J. Neurochem.* **115**, 1150–1160 (2010).
164. V. Còppola-Segovia *et al.*, ER Stress Induced by Tunicamycin Triggers α -Synuclein Oligomerization, Dopaminergic Neurons Death and Locomotor Impairment: a New Model of Parkinson's Disease. *Mol. Neurobiol.* **54**, 5798–5806

- (2017).
165. K. S. P. McNaught, D. P. Perl, A. L. Brownell, C. W. Olanow, Systemic exposure to proteasome inhibitors causes a progressive model of Parkinson's disease. *Ann. Neurol.* **56**, 149–162 (2004).
 166. H. Matsui *et al.*, Proteasome inhibition in medaka brain induces the features of Parkinson's disease. *J. Neurochem.* **115**, 178–187 (2010).
 167. J. H. Kordower *et al.*, Failure of proteasome inhibitor administration to provide a model of Parkinson's disease in rats and monkeys. *Ann. Neurol.* **60**, 264–268 (2006).
 168. B. K. Lundholt, K. M. Scudder, L. Pagliaro, A Simple Technique for Reducing Edge Effect in Cell-Based Assays. *J. Biomol. Screen.* **8**, 566–570 (2003).
 169. C. van der Merwe *et al.*, Curcumin Rescues a PINK1 Knock Down SH-SY5Y Cellular Model of Parkinson's Disease from Mitochondrial Dysfunction and Cell Death. *Mol. Neurobiol.* **54**, 2752–2762 (2017).
 170. X. Jing *et al.*, Dimethyl fumarate attenuates 6-OHDA-induced neurotoxicity in SH-SY5Y cells and in animal model of Parkinson's disease by enhancing Nrf2 activity. *Neuroscience.* **286**, 131–140 (2015).
 171. X. Jin, Q. Liu, L. Jia, M. Li, X. Wang, Pinocembrin Attenuates 6-OHDA-induced Neuronal Cell Death Through Nrf2/ARE Pathway in SH-SY5Y Cells. *Cell. Mol. Neurobiol.* **35**, 323–333 (2015).
 172. D. Jantas *et al.*, Neuroprotective effects of metabotropic glutamate receptor group II and III activators against MPP(+)-induced cell death in human neuroblastoma SH-SY5Y cells: The impact of cell differentiation state. *Neuropharmacology.* **83**, 36–53 (2014).
 173. T. Oda, Y. Kosuge, M. Arakawa, K. Ishige, Y. Ito, Distinct mechanism of cell death is responsible for tunicamycin-induced ER stress in SK-N-SH and SH-SY5Y cells. *Neurosci. Res.* **60**, 29–39 (2008).
 174. B. Cheng *et al.*, Insulin-like growth factor-I mediates neuroprotection in proteasome inhibition-induced cytotoxicity in SH-SY5Y cells. *Mol. Cell. Neurosci.* **47**, 181–190 (2011).
 175. L. Li, K. Sampat, N. Hu, J. Zakari, S. H. Yuspa, Protein kinase C negatively regulates Akt activity and modifies UVC-induced apoptosis in mouse keratinocytes. *J. Biol. Chem.* **281**, 3237–3243 (2006).
 176. G. Chen *et al.*, Brain-derived neurotrophic factor suppresses tunicamycin-induced upregulation of CHOP in neurons. *J. Neurosci. Res.* **85**, 1674–1684 (2007).

177. B. Cheng *et al.*, Retinoic acid protects against proteasome inhibition associated cell death in SH-SY5Y cells via the AKT pathway. *Neurochem. Int.* **62**, 31–42 (2013).
178. D. W. Howells *et al.*, Reduced BDNF mRNA Expression in the Parkinson's Disease Substantia Nigra. *Exp. Neurol.* **166**, 127–135 (2000).
179. C. S. Hughes, L. M. Postovit, G. A. Lajoie, Matrigel: a complex protein mixture required for optimal growth of cell culture. *Proteomics.* **10**, 1886–1890 (2010).
180. M. Ruthven, K. R. Ko, R. Agarwal, J. P. Frampton, Microscopic Evaluation of Aqueous Two-Phase System Emulsion Characteristics Enables Rapid Determination of Critical Polymer Concentrations for Solution Micropatterning. *Analyst.* **142**, 1938–1945 (2017).

APPENDIX A: Cambridge University Press Copyright License

RightsLink Printable License

<https://s100.copyright.com/App/PrintableLicenseFrame.jsp?publisherID...>

CAMBRIDGE UNIVERSITY PRESS LICENSE TERMS AND CONDITIONS

Nov 16, 2017

This Agreement between Dalhousie University -- Kristin Robin Ko ("You") and Cambridge University Press ("Cambridge University Press") consists of your license details and the terms and conditions provided by Cambridge University Press and Copyright Clearance Center.

License Number	4230890855769
License date	Nov 16, 2017
Licensed Content Publisher	Cambridge University Press
Licensed Content Publication	MRS Advances
Licensed Content Title	High-Throughput 3D Neural Cell Culture Analysis Facilitated by Aqueous Two-Phase Systems
Licensed Content Author	Kristin Robin Ko, Rishima Agarwal, John Frampton
Licensed Content Date	May 8, 2017
Licensed Content Volume	2
Licensed Content Issue	45
Start page	2435
End page	2441
Type of Use	Dissertation/Thesis
Requestor type	Author
Portion	Full article
Author of this Cambridge University Press article	Yes
Author / editor of the new work	Yes
Order reference number	
Territory for reuse	North America Only
Title of your thesis / dissertation	Development Of High-throughput 3D Neural Cell Culture Platforms For Modelling Parkinson's Disease
Expected completion date	Dec 2017
Estimated size(pages)	110
Requestor Location	Dalhousie University 5981 University Avenue PO BOX 15000 Halifax, NS B3H 4R2 Canada Attn: Dalhousie University
Publisher Tax ID	123258667RT0001
Billing Type	Invoice

Billing Address Dalhousie University
5981 University Avenue
PO BOX 15000

Halifax, NS B3H 4R2
Canada
Attn: Dalhousie University

Total 0.00 USD

Terms and Conditions

TERMS & CONDITIONS

Cambridge University Press grants the Licensee permission on a non-exclusive non-transferable basis to reproduce, make available or otherwise use the Licensed content 'Content' in the named territory 'Territory' for the purpose listed 'the Use' on Page 1 of this Agreement subject to the following terms and conditions.

1. The License is limited to the permission granted and the Content detailed herein and does not extend to any other permission or content.
2. Cambridge gives no warranty or indemnity in respect of any third-party copyright material included in the Content, for which the Licensee should seek separate permission clearance.
3. The integrity of the Content must be ensured.
4. The License does extend to any edition published specifically for the use of handicapped or reading-impaired individuals.
5. The Licensee shall provide a prominent acknowledgement in the following format:
author/s, title of article, name of journal, volume number, issue number, page references,
, reproduced with permission.

Other terms and conditions:

v1.0

Questions? customer care@copyright.com or +1-855-239-3415 (toll free in the US) or +1-978-646-2777.
